INFLUENCE OF PROCESS PARAMETERS, MULTI HOLE AND MULTI GROOVE TECHNIQUES ON FABRICATION OF HYBRID SURFACE NANOCOMPOSITES BY FRICTION STIR PROCESSING

A thesis submitted in the partial fulfillment of the requirements for the award of the degree of

DOCTOR OF PHILOSOPHY

By

P. NARESH

(ROLL NO: 701306)

Under the supervision of

Dr. ADEPU KUMAR

Associate Professor

DEPARTMENT OF MECHANICAL ENGINEERING

NATIONAL INSTITUTE OF TECHNOLOGY

WARANGAL (T.S.) INDIA 506 004

October - 2017

DEDICATED

to

My Family & Friends

NATIONAL INSTITUTE OF TECHNOLOGY
WARANGAL (T.S.) INDIA 506 004

DECLARATION

This is to certify that the work presented in the thesis entitled **"Influence of Process Parameters, Multi Hole and Multi Groove Techniques on Fabrication of Hybrid Surface Nanocomposites by Friction Stir Processing"**, is a bonafide work done by me under the supervision of Dr. Adepu Kumar was not submitted elsewhere for the award of any degree.

I declare that this written submission represents my idea in my own words and where other's ideas or words have not been included. I have adequately cited and referenced the original sources. I also declare that I have adhered to all principles of academic honesty and integrity and have not misinterpreted or fabricated or falsified any idea/data/fact/source in my submission. I understand that any violation of the above will be a cause for disciplinary action by the Institute and can also evoke penal action from the sources which have thus not been properly cited or from whom proper permission has not taken when needed.

Date: **(P. Naresh)**

Place: Warangal Research Scholar,
Roll No. 701306

NATIONAL INSTITUTE OF TECHNOLOGY
WARANGAL (T.S) INDIA 506 004

CERTIFICATE

This is to certify that the thesis entitled **"Influence of Process Parameters, Multi Hole and Multi Groove Techniques on Fabrication of Hybrid Surface Nanocomposites by Friction Stir Processing"** that is being submitted by **Mr. P. Naresh** in partial fulfillment for the award of Doctor of Philosophy (**Ph.D.)** in the Department of Mechanical Engineering, National Institute of Technology, Warangal, is a record of bonafide work carried out by him under my guidance and supervision. The results of embodied in this thesis have not been submitted to any other Universities or Institutes for the award of any degree or diploma.

Dr. Adepu Kumar

Associate Professor

Department of Mechanical Engineering

National Institute of Technology, Warangal.

ACKNOWLEDGEMENT

I take the opportunity to express my heartfelt adulation and gratitude to my supervisors, **Dr. ADEPU KUMAR**, Associate Professor, Mechanical Engineering Department, National Institute of Technology, Warangal. It has been a benediction for me to spend many opportune moments under the guidance of the perfectionist at the acme of professionalism. The present work is a testimony to his alacrity, inspiration and ardent personal interest, taken by him during the course of this thesis work in its present form.

I wish to sincerely thank the authorities of the Institute, **Prof. G.R.C REDDY, DIRECTOR**, National Institute of Technology, Warangal and other top officials who gave me an opportunity to carry out research work.

I also sincerely thank **Prof. DR. BANGARUBABU POPURI,** Head, Mechanical Engineering Department, National Institute of Technology, Warangal for his continuous support towards carrying out research work.

I would like to express my sincere thanks to **Prof. C. S. P RAO**, former Head, Mechanical Engineering Department, National Institute of Technology, Warangal, for his timely suggestions, support and for providing necessary department facilities and services during successful completion of research work

I wish to express my sincere and whole-hearted thanks and gratitude to **Prof. K. V. SAI SRINADH**, **Dr. R. N. RAO** and **Dr. N. NARASAIAH** (DSC members) for their kind help, encouragement and valuable suggestions for successful completion of research work.

I would like to express my sincere thanks to **Dr. SADASHIVA RAO** and **Mr. L.R. SWAMY** Mechanical Engineering Department, National Institute of Technology, Warangal for their cooperation and the help extended during this work.

Heartfelt thanks to **Dr. A. Devaraju, Dr. L. Suvarna Raju, Dr. K. Murahari, Mr. M. Krishna Kishore, Mr. K. Kranti, Mr. Rajendra Prasad** and **Dr. Vishwanadh** for their kind help, encouragement and valuable suggestions for support during this research work.

I would like to express thanks to my dear friends **Dr. M. Srinivasa Rao, Mr. N. Shiva Kumar, Mr. M. Sandeep, Dr. Manmada Chary, Dr. Kandi Kishore, Dr. Karthikeya sharma, Dr. Rama raju** and my co-research scholars for their support and help during this work.

Words are inadequate to express my thanks to all my family members, my father Sri. **P. JANGAIAH**, and mother Smt. **P. PRAMEELA**, deserve specially mention of appreciation for exhibiting patience during this long and arduous journey.

No amount of thanks is enough, finally, for my beloved wife **URMILA** who held the key to my success. Her patience and encouragement kept my motivation up.

Finally, my thanks go to the authorities of National Institute of Technology (NIT), Warangal for providing a nice working environment for this Ph.D. work and their continuous financial support under research grant.

I want to express my sincere thanks to all those who directly or indirectly helped me at various stages of this work.

Above all, I express my indebtedness to the **"ALMIGHTY"** for all his blessing and kindness.

(P. Naresh)

ABSTRACT

Friction stir processing (FSP) is a novel surface modification technique for producing surface composites. FSP operates on the working principle of Friction stir welding (FSW) technique invented and developed by The Welding Institute (TWI), UK. In this research work, influence of the process parameters, tool shoulder diameter, volume percentage of the reinforcement particles, multi hole and multi groove techniques on the microstructural, mechanical and wear properties of the surface composites produced by Friction stir processing were studied. Nano particles such as Al_2O_3 and SiC are used as reinforcement particles and Aluminum 6061 T6 alloy was used as matrix material for fabrication of surface composites.

Various rotational speeds (900, 1150 & 1400) and traverse speeds (15, 20, 30 & 40) were used to fabricate the composites. At 1150 rpm tool rotational speed with 15 mm/min traverse speed condition the surface composites were fabricated by varying the volume percentages of the Al_2O_3 and SiC reinforcement particles by applying single groove technique. The results indicated that, at 4 volume percentage of Al/Al_2O_3 surface composites and 2 volume percentage of Al/SiC surface composites were exhibited defect free. In order to increase the amount volume percentage with in the matrix and composite area in the processed region, novel techniques were implemented such as multi hole and multi groove techniques.

The uniform distribution of the nano reinforcement particles inside the processed region has been evaluated from the macro/microstructure and microhardness distribution. Furthermore, the wear characteristics of the resulted surface composites were evaluated by applying pin-on-disk wear test at room temperature. Superior mechanical properties, microhardness and wear resistance properties were achieved in all surface composites produced with FSP. Higher microhardness values were achieved with the composites fabricated with SiC nano reinforcement and good tensile properties observed in Al/Al_2O_3 surface composites. It is found that the tensile properties of all the surface composites are reduced compared with as-received Al alloy. The Al/Al_2O_3+SiC surface hybrid composite exhibited superior wear resistance as compared to the other surface composites and unreinforced Aluminum 6061-T6 alloy.

TABLE OF CONTENTS

LIST OF FIGURES

LIST OF TABLES

LIST OF ABBREVIATIONS

Abbreviation	Description
% El	Percentage elongation
AGG	Abnormal grain growth
AISI	American Iron and Steel Institute
Al	Aluminum
Al_2O_3	Aluminum oxide
AMMCs	Aluminum metal matrix composites
AS	Advancing side
ASM	American Society for Metals
ASTM	American Society for Testing and Materials
AWS	American welding society
AZ31	Magnesium alloys with aluminum
BM	Base material
C	Carbon
CMNC	Ceramic matrix nanocomposite
Cr	Chromium
Cr_2O_3	Chromium(III) oxide
Cu	Copper
DXZ	Dynamic recrystallized zone
DXR	Dynamic recrystallized region
EBW	Electron beam welding
ECA	Equal-channel angular
EDM	Electron discharge machine
EDX	Energy dispersive x-ray spectroscopy
EL	Elongation
Fe	Iron
FSP	Friction stir processing
FSW	Friction stir welding

FSW/P	Friction stir welding/processing
FW	Friction welding
Gr	Graphite
GTAW	Gas tungsten arc welding
H13	Air hardening hot work tool steel
HAZ	Heat affected zone
HCl	Hydrochloric acid
HCP	Hexagonal close pack
HF	Hydrofluoric acid
HNO_3	Nitric acid
HP	Horse power
HV	Hardness (Vickers)
ISO	International Organization for Standardization
kN	Kilo-newton
LASER	Light Amplification by Stimulated Emission of Radiation
LBW	Laser beam welding
LCD	Liquid crystal display
Mg	Magnesium
MIG	Metal inert gas
mm	Millimeter
mm/min	Millimeter per minute
mm/s	Millimeter per second
MMCs	Metal matrix composites
MMNCs	Metal matrix nanocomposites
MMR	Mechanical mixed region
Mn	Manganic
Mo	Molybdenum
MPa	Megapascal
MWCNT	Multi walled carbon nano tube
NaCl	Sodium chloride
NC	Numerical control

Ni	Nickel
N-m	Newton- meter
NZ	Nugget zone
OM	Optical microsopy
P	Potassium
PMNC	Polymer matrix nanocomposite
rpm	Revolution per minute
RS	Retreating side
S	Sulphur
SEM	Scanning electron microscope
SFSP	Submerged friction stir processing
Si	Silica
SiC	Silicon carbide
SIPR	Severe induced plastic region
SMMCs	Surface metal matrix composites
SPD	Severe plastic deformation
SZ	Stir zone
T6	Solution heat treated and artificial aging to the peak strength
TC	Taper cylindrical or conical
Ti	Titanium
TiC	Titanium carbide
TIG	Tungsten inert gas
TMAZ	Thermo-mechanically affected zone
TWI	The Welding Institute
UFG	Ultra-fine grained
UK	United Kingdom
UMR	Un-mixed region
USA	United States of America
UTM	Universal testing machine
UTS	Ultimate tensile strength
V	Vanadium

WC	Tungsten carbid
WZ	Weld zone
XRD	X-ray diffraction
YS	Yield strength
Zn	Zinc

LIST OF SYMBOLS

List of symbols	Description	Units
D	Diameter of the hole	mm
Dg	Depth of groove	mm
Dh	Depth of hole	mm
Dp	Pin diameter	mm
Ds	Shoulder diameter	mm
F	Vertical or axial force	KN
P	Pin region	mm
P+S	Pin + shoulder	mm
W	Width of groove	mm

TERMINOLOGY

Unaffected material or parent metal – This is material remote from the weld that has not been deformed and that, although it may have experienced a thermal cycle from the weld, is not affected by the heat in terms of microstructure or mechanical properties.

Heat-affected zone (HAZ) – In this region, which lies closer to the weld-center, the material has experienced a thermal cycle that has modified the microstructure and/or the mechanical properties. However, there is no plastic deformation occurring in this area.

Thermo-mechanically affected zone (TMAZ) – In this region, the FSW tool has plastically deformed the material, and the heat from the process will also have exerted some influence on the material. In the case of Aluminum, it is possible to obtain significant plastic strain without recrystallization in this region, and there is generally a distinct boundary between the recrystallized zone (weld nugget) and the deformed zones of the TMAZ.

Weld nugget –The fully recrystallized area, sometimes called the stir zone, refers to the zone previously occupied by the tool pin. The term stir zone is commonly used in friction stir processing, where large volumes of material are processed.

Tool shoulder – the region of tool in contact with the workpiece surface. To enhance the material flow, tool shoulder can have negative or positive scrolls. A negative scroll is a depression in the shoulder surface and the workpiece material fills this. A positive scroll is a protrusion on the shoulder surface. Both types of scrolls conceptually enhance the material flow inward. The other design choice for the shoulder is concave or convex. Concave shoulders were designed to hold the workpiece material in a cup shape. The convex shoulders are relatively new and they require negative scroll spiral (or grooves) to contain the material. The advantage of convex shoulder lies in its ability to tolerate minor variability in workpiece thickness.

Tool pin – also referred to as probe in some literature, the pin of the tool is inserted in the workpiece and it influences the horizontal material flow from front to back, as well as vertical material flow from top to bottom. The most common pin profiles are cylindrical or conical. The pins can be threaded or have step spiral design. In addition, the flow can be influenced by putting flats or flutes. The overall possibilities of variations can be extremely large.

Advancing side – the tool pin surface rotation direction and the tool traverse direction have the same vectorial sense. Because of the tool's forward movement, the material wants to flow back, but the pin surface rotation opposes that flow on this side of the tool.

Retreating side – the tool pin surface rotation direction and the tool traverse direction have the opposite vectorial sense. The material flow is easier on this side of the tool pin as the pin surface helps the material flow backward.

Leading edge – the front side of the tool. The tool shoulder meets the cold workpiece material in this region. The tool shoulder sweeps the top layer sideways toward the retreating side and this can have implication of the overall material flow and weld nugget appearance.

Trailing edge – the back side of the tool. The trailing part keeps pumping heat in the workpiece after pin has crossed the region. This influences the microstructural evolution after the pin induced deformation.

Tool rotational rate or speed – the rate at which the tool rotates. This has major contribution to the heat input and material flow.

Weld speed – the travel speed of the tool. This impacts the overall thermal cycle.

Tilt angle – the angle between the plane normal of workpiece and the spindle shaft. Typically, an angle between 0 and 3 is selected.

Plunge rate – the rate at which the tool is inserted in the workpiece. It controls the rate of heat build-up and force during the start of the process.

Plunge depth – the programmed depth of the pin bottom from the top surface of workpiece.

Plunge force – the vertical force on the tool when shoulder meets the top surface of workpiece. For force-controlled runs, this is the target force.

Z-axis stroke – the workpiece normal is referred to as the z-axis and this is also the direction of plunge force. A convenient way to look at the forces is from tool's perspective. Vertical up direction is compressive force on the tool.

X-**axis stroke –** the travel direction is referred to as the x-axis. The tool pin experiences compressive force from front to back.

Y-**axis stroke –** the direction normal to the travel direction is the plane parallel to the top surface. The tool pin experiences compressive force from retreating side to advancing side because of the imbalance of material flow around the pin.

Severe plastic deformation – is a generic term which describes a group of metalworking processes, in which a large plastic strain is introduced into a bulk metal in order to create ultra-fine grained (d < 500 nm) or nano-crystalline structure (d < 100 nm) metals.

Recrystallization – a process by which deformed grains are replaced by a new set of undeformed grains that nucleate and grow until the original grains have been entirely consumed. It is usually accompanied by a reduction in the strength and hardness of a material and a simultaneous increase in the ductility.

Grain growth – the increase in the grain size of a material at high temperature. This occurs after recovery and recrystallization and further reduction in the internal energy can only be achieved by reducing the total area of grain boundary.

Recovery – a process by which deformed grains can reduce their stored energy by the removal or rearrangement of defects (dislocations) in their crystal structure. These defects are introduced by plastic deformation of the material and act to increase the yield strength of a material. Since recovery reduces the dislocation density the process is normally accompanied by a reduction in strength of the material and a simultaneous increase in the ductility.

INTRODUCTION

1.1 History and development of welding

Around 3000 years earlier, Egyptians started the concept of joining and they joined piece of iron and together with the help of forging. Several war weapons, tool and house holding devices of Egyptians stands for finest examples of forge welded paraphernalia's. At the age of bronze nearby 2000 years before, where circular gold boxes are made by using pressure welding. Numerous items were produced with iron and other metals during the Middle Ages. Iron Pillar of Delhi in India was one of the best examples of the largest welds during the 17^{th} century. Commercially welding techniques were invented in the 19^{th} century at various parts of the world.

During the mid-1800s period, Sir Humphrey Davies generated an arc between two carbon electrodes using a battery and invented an electric generator. However, this process (arc lighting) became popular in mid -18^{th} century. Arc welding, gas welding and cutting were investigated during the early 19^{th} century. The first US patent was made by C.L. Coffin for arc welding process by the use of a metal electrode in 1892. An arc is used to transfer the metal across the line of joint with the help of electrode. During the same period, gas welding and cutting were promoted by the addition of external blow pipe for supplying oxygen and later the liquefying of air.

The demand for metal materials production by welding was drastically increased as a servicing process at the time of World War – I, that lead to invent a new welding and joining techniques to meet the demand in the US and Europe. After War in the year 1919, The American Welding Society (AWS) was founded with the aim of advancing the welding and allied processes. In 1920, automatic welding and several grades of electrodes with and without coated were developed. In 1941, Heliarc welding (helium for shielding) was invented and patented by Meredith. The gas shielded metal arc welding was developed by Battelle Memorial Institute in 1948. The same principle was used in gas tungsten arc welding (GTAW) by replacing tungsten electrode. Later many welding techniques were developed to improve its applications. Electron beam welding was developed by French Atomic Energy Commission in 1940. In this welding technique, focused beam of electrons were used as a heat source under vacuumed chamber.

Friction welding was developed in the Soviet Union and later it gained approval in the USA and Great Britain. Laser beam welding was first developed as a communicator at the Bell Telephone Laboratories and later it is improved towards welding. The Welding Institute (TWI), Cambridge developed a novel solid-state welding technique called friction stir welding (FSW) in 1991 for joining of similar and dissimilar metals.

1.2 Fusion and solid- state welding methods

Currently there are several welding/joining techniques available and further, many more welding/joining techniques will be established as their need increases from industrialization. As of now the welding/joining techniques are categorized into two groups those are: solid-state welding and fusion welding processes. In fusion welding technique, melting of parent material takes place and some welding processes need consumable electrodes/filler wire rolls and some welding techniques (tungsten inert gas (TIG), metal inert gas (MIG), laser beam welding (LBW) and electron beam welding (EBW), etc.) don't need consumables for joining/welding of metals. These welding techniques operate at high-temperatures leading to the formation of non-favorable phase at the joint/weld. The formation of non-favorable phase decreases mechanical properties (tensile strength, fatigue strength, etc.,) of the weld. In fusion welding process, a high amount of heat is required to weld which creates a wide range of heat affected zone (HAZ) which decreases mechanical properties of the weld. To overcome these drawbacks in fusion welding process, solid - state processes were introduced (Ruifeng, L. et.al, 2011; Yi, L. et.al, 2011).

Solid-state welding techniques have several benefits compared with fusion welding processes. In solid – state welding, the joining is done below the melting temperature of the metal. It means there is no chance of formation of unfavorable phases at the line of joint and no need of filler materials/electrodes for joining metals. The inert ambiance is not required for joining of metal because it operates below melting temperature of the base metal. Explosive welding, hot pressure welding, forge welding, friction welding, friction surfacing and friction stir welding, etc., comes under solid-state welding. Dissimilar metal joining is possible in this solid-state welding techniques.

1.3 Friction stir welding

Friction stir welding (FSW) is one of the most pioneering techniques in solid-state welding techniques for welding of Al alloys. FSW is invented in the year 1991 and patented by The Welding Institute (TWI) Cambridge, United Kingdom (W.M. Thomas et al. 1991; W.M. Thomas et al. 1997). It was the most promising welding technique for aluminum alloys and is extended to joining of various materials like Mg, Cu, Steel, Ti, polymers and etc. In FSW, a rotating tool (having a shoulder with pin) is plunged into the joining line between two metal plates and traversed along the line of joint. The frictional heat produced by the rotating tool plasticizes the material around the tool and forms a joint. During the joining process, the material around the pin undergoes severe plastic deformation (SPD) and traverses towards retreating side (RS) from beneath the pin on the advancing side(AS) where it is forged to form the joint (Mishra R S et.al. 2003; Ma Z Y, 2008). Consequently, this results in a solid-state bond between two plates. The schematic diagram of the FSW is shown in Fig. 1.1.

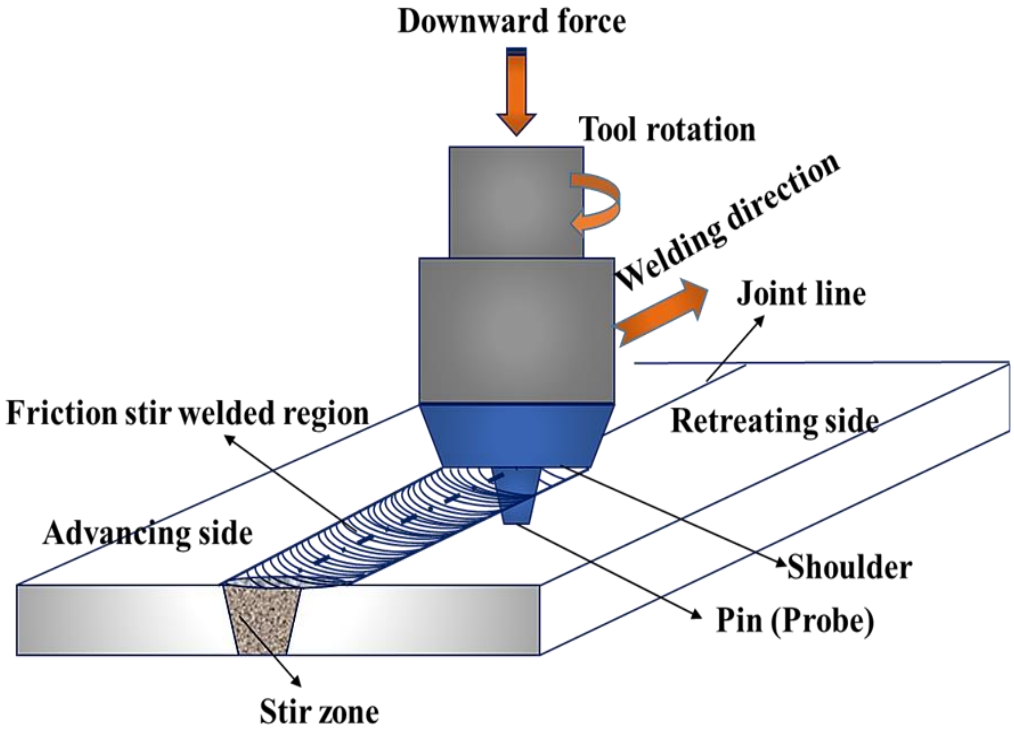

Fig. 1.1 Schematic diagram of FSW.

1.3.1 Process parameters

FSW is considered as a combination of extrusion, forging, and stirring of the material where a high strain rate and temperature are generated. Further, the process involves a complex movement of material and intense plastic deformation. To identify the effective process parameters of FSW on the quality of joining process, Ishikawa cause–effect diagram was created and presented in Fig. 12.

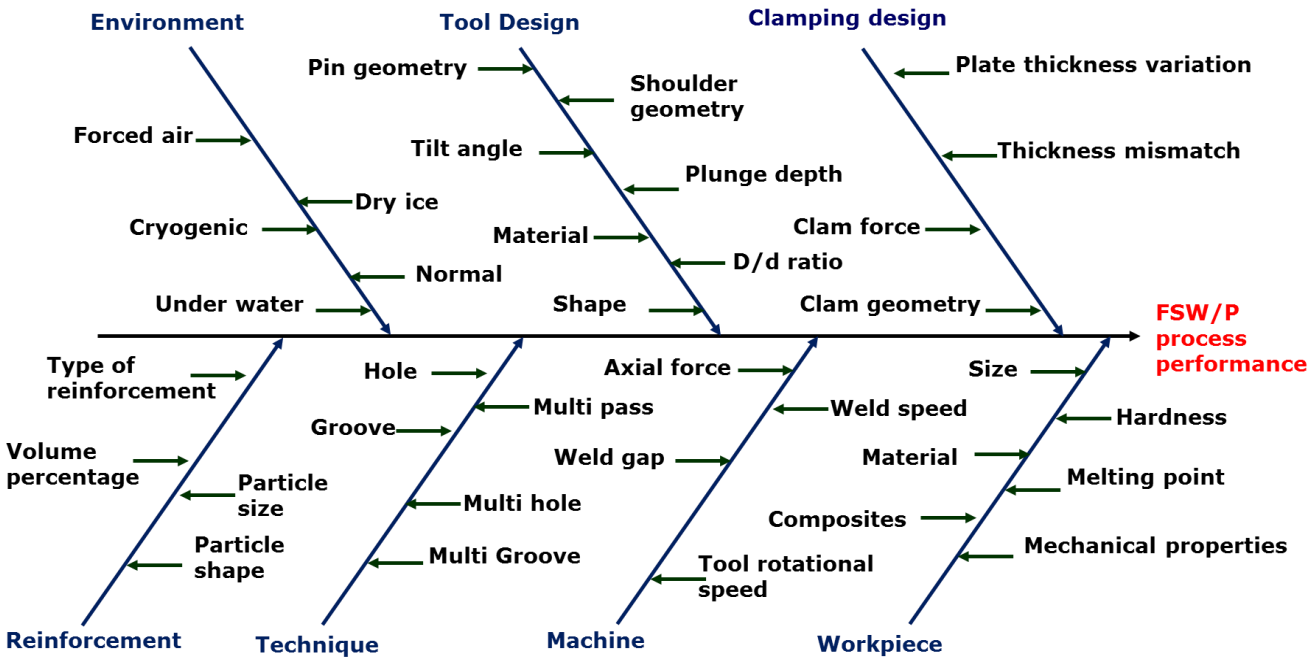

Fig. 1.2 Cause - effect diagram [A. K. Lakshminarayanan, V. Balasubramanian. 2007].

The main effective primary process parameters are tool geometry, tool rotational speed, traverse speed, axial force and tilt angle. In FSW, the frictional heat is generated between the tool and base material plate. Tool geometry plays a vital role for the generation of frictional heat. Improper selection of tool geometry leads to defective formation along the joint. The defects occur due to lack of heat generation in FSW. Tool rotational speed and traverse speed are the key parameters to generate enough heat. The unsuitable axial force also causes improper joint as well as defect formation. The tilt angle of the tool offers sufficient place to the plasticized material to travel around the processed region and leads to sound welds.

1.3.2 Tool geometry

In FSW, tool geometry plays a key role for the generation of frictional heat. For plasticization of material, grain recrystallization and formation of weld this frictional heat is essential. FSW tool mainly contains shoulder and pin as shown in Fig. 1.3.

The basic functions of the tools are as follows:

1. Heat generation
2. Plasticization of material to fabricate the joint.
3. Control the material flow within the processed region.

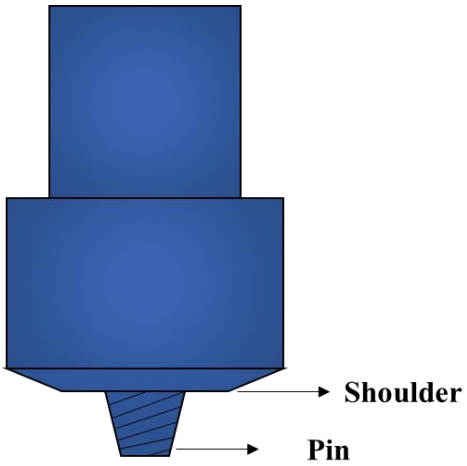

Fig. 1.3 Schematic diagram of FSW tool with pin

Initially, at tool plunging stage, the contact between the tool and workpiece produces heat. During plunging, a high amount of heat is generated which causes plasticization of material and it continues until the tool shoulder touches the surface of the workpiece. The second function of the tool is to ‘stir’ and ‘move’ the material. The plastic deformation and the frictional heating of the workpiece necessary for stirring of the material and is influenced by the FSW tool design (Mishra. R.S and Ma, Z.Y, 2005). Most of the heat during the process is generated with the help of shoulder by applying a downward force on the workpiece surface, constraining the plasticized material around the tool pin and preventing the escape of the plasticized material from the workpiece joint line (Mishra RS and Mahoney MW, 207).

The shoulder and pin diameter; tool pin profile and pin length; and shoulder profile are important parameters in determining the quality of welds. Another key parameter is the tool material which determines the suitability of a tool for a specific application (Givi and Asadi, 2014).

The tool shoulder performs the frictional heating and deformation in the welding of thin metal plates (Mishra and Mahoney, 2007). The tool shoulder may contain some geometric features for increasing the material friction. The most typical shoulder outer surfaces are shown in Fig. 1.4 (Thomas, 1996). Different shoulder features such as concave shoulder (serves as a reservoir for the forging action of the shoulder), scrolls, ridges or knurling, grooves, and concentric circles, convex shoulders were developed. The concave shoulder shape is capable of performing easy and sound welds. Also, restricts plasticized material from the sides of the shoulder (Mohanty HK et al, 2012).

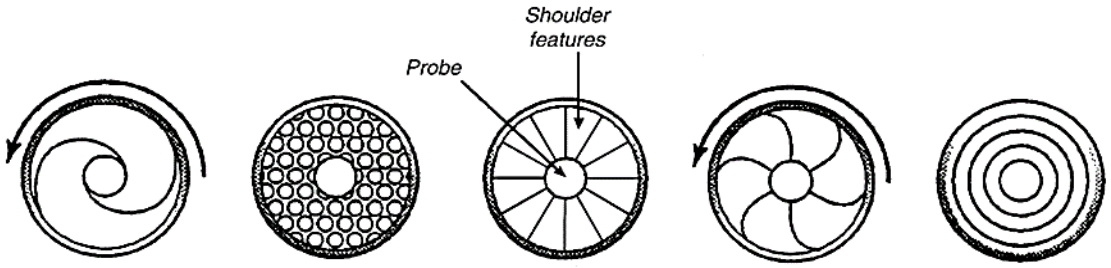

Fig. 1.4 Different tool shoulder geometries, viewed from underneath the shoulder (Mishra & Mahoney, 2007)[9].

The tool pin disrupts the contact surfaces of the workpieces to be welded, to shearing of the material in its front and movement of the material behind the tool. The tool pin is mainly responsible for controlling the weld speed and deformation depth (Thomas, 1991). Also, its geometry influences the plasticized flow of material and joint performance (Johannes and Mishra, 2007; Rai R.et al, 2011; Lorrain et al. 2010; Choi et al. 2010).

1.3.3 Advantages, limitation and applications of friction stir welding

Friction stir welding has many advantages over fusion welding processes such as

- Eco-friendly technique.
- Energy efficient process.
- Good mechanical properties can be obtained in the as- welded condition.
- No consumables are required like electrodes and gas shield.
- Similar and dissimilar joints can be easily done.
- Welding preparation is minimal.
- Reduces the distortion in parent components.
- Easily operated in all directions.
- No toxic fumes are released.
- Improved fatigue performance through elimination of stress concentrators.
- Maintenance cost is very low.

Limitations:

- Exit hole occurs when the tool is withdrawn after the process.
- Heavy down forces are required for large welds.
- Less flexible than fusion welding techniques.

Applications:

- Next generation monolithic metallic wing.
- Shipbuilding and Offshore
    - Hulls
    - Freezer panels
    - Honeycomb panels
    - Helicopter landing platforms
- Automobile industries
    - Aluminum Engine Cradles
    - Suspension struts

- Aerospace and aeronautical industries
    - Wings
    - Panels
    - Empennages
    - Cryogenic fuel tanks
    - Monolithic metal wings
    - Metallic fuselages
- Sports industries
- Fabrication industries
- Rail industries
    - Railway goods wagons
    - Rolling stocks
    - Railway tankers
    - Trams
    - Underground carriages

1.4 Friction stir processing

Based on the concept of FSW, a new grain refining technique, Friction stir processing (FSP) has been developed and increasingly investigated over recent years. The concept behind FSP is to use the severe deformation in the FSW process to refine the grain structure and second phase particles within a material. This is desirable because ultra-fine grained (UFG) structures are expected to exhibit superior mechanical properties [Markushev et al., 1997; Valiev et al., 2000; Zhao et al., 2004]. Therefore, the generation of the dynamic recrystallization zone (DXZ) is a key aspect of this method. During FSP, the material within the processed region is locally raised to elevated temperatures, and this allows severe plastic deformation to readily take place. Many investigations have also looked into the possibility of using FSP to produce large volumes of UFG structure in a material by carrying out multi-pass processing [Ma et al., 2006ii; Johannes & Mishra, 2007ii].

However, a better application of the FSP technique is to exploit its ability to modify surface of the components, where enhanced properties are required. There are many different variables and parameters that need to be considered for FSP, but ideally, with carefully selected processing parameters, the microstructure of the material can be controlled.

1.4.1 Advantages of FSP

- Microstructural refinements, homogeneity of grains and densification can be easily achieved by FSP.
- Properties of processed material can be optimized and controlled accurately by FSP.
- The depth of the microstructural refinement of the material can be refined as per requirements by adjusting the tool dimensions (pin length).
- No external heat supply is required during the operation and the frictional heat generated by FSP is eco-friendly.
- The change of size and shape of the processed region during the FSP is negligible than compared with other conventional processes.

1.5 Composites

Composite material is defined as a combination of two or more materials or different phases of single material, indestructible in one another properties and illustrates superior properties than any of the added component material. For fabrication of composite materials, the reinforcement particle size, amount and distribution in the matrix material takes an important role to get superior or limiting the overall properties of the composite material.

In nanocomposites one of the phases/materials contains the size in the range of nanometer (1nm -100nm) (Tachai Luangvaranunt, et.al, 2007; L.A. DobrzaĔski, et.al, 2008). There are several types of nanocomposites and are distinguished as ceramic matrix nanocomposites(CMNC), metal matrix nanocomposites (MMNC) and polymer matrix nanocomposites (PMNC).

1.5.1 Metal matrix nanocomposites (MMNC)

From the past two decades, use of metal matrix nanocomposites in manufacturing industries has increased massively due to their superior properties and durability. Several fabrication techniques have been designed to produce MMNCs. While manufacturing MMNCs it is not only important to get superior properties but also distribution of nano-reinforcement particles into the matrix and avoiding of un-interface bonding. Otherwise poor interface bonding and non-uniform distribution of reinforcement particles lead to deterioration of its properties and life of the component. A good combination of reinforcements and the metal matrix will improve the two distinct properties like ductility and high strength. This combination of strength to weight ratio MMCs application will increase massively in manufacturing industries. Aluminum metal matrix composites (AMMCs) are the best example for these kinds of MMCs. Around 40 years, AMMCs were exhibiting their usage in aerospace and defense sectors, especially for fabrication of space shuttle orbiter frame and rib truss members are made of continuous boron fiber reinforced aluminum matrix material. Some other applications like landing gear drag link for weight reduction and high-gain antenna boom for Hubble Space Telescope. An optimum combination of nano ceramic reinforcement and aluminum matrix composite material increases a wide range of applications in manufacturing industries.

1.5.2 Importance of metal matrix composites

Recently, aluminum alloys have been found to be very promising materials and have attracted considerable attention in aerospace, automobile, military, ship and transportation industries because of their outstanding properties (low density, good resistance to corrosion, excellent thermal conductivity and high specific strength, etc.). 6XXX series aluminum alloys are extensively used alloys in industries. It is a versatile extruded alloy with medium to high strength, inexpensive and easy to machine capabilities and this made these 6061 alloys an eye-catching material for industries (Moreira, P. M, et.al. 2008). In the last two decades, the use of metal matrix composites (MMC's) in manufacturing industries has become essential for producing high strength and light weight components. The combination of ductility and toughness of MMCs are showing a wide range of applications towards smart industries (M.K Surappa, 2003).

Most of the aerospace, automobile and defense industries are developing massive quantity of components by using Aluminum metal matrix composites (AMMCs). In addition to improving the properties of AMMCs, nano reinforcement particles are incorporated into the matrix. Nano-reinforced AMMCs show extraordinary potential in all manufacturing industries (J.U. Ejiofor and R.G. Reddy, 1997). Al_2O_3 and SiC particles are mostly used as reinforcement for Al alloys and a wide range of products. To achieve superior properties is not only a major factor, the distribution of reinforcement particle in an even manner is a difficult task obtained from conventional methods (Mazahery A, et.al, 2009). Fabrication of MMCs can be produced by applying various techniques. Producing the MMCs by Casting or liquid infiltration method provides good reaction between the reinforcement and the matrix material but simultaneously can lead to deterioration of properties of the MMCs because of its poor wettability. Squeeze casting or pressure methods take a short time to fabricate the composites and due to less reaction time between the molten metal and reinforcement, it leads to formation of conventional defects like shrinkage cavities and porosity (S.A. Sajjadi el.al. 2012).

Diffusion bonding is a solid-state technique for merging dissimilar or similar metals. In this process, the bonds form at a high temperature between the in-contact metallic surfaces due to inter-diffusion of atoms. By this technique, the orientation and volume fraction of the fiber reinforcement can be controlled easily but high processing temperature, pressure, and time make this technique expensive. This can be overcome by applying sinter-forging techniques to produce MMC's. The drawback of this technique is limited to producing smaller MMCs only. Since wear property is a surface deprivation property, the dispersion of reinforcement particles into the matrix and grain refinement are most important to get good surface properties of metal. It is very difficult to disperse the reinforcement particles into the matrix with improper technique (conventional surface modification methods) (Mazen A.A et. al, 1998). Considering the above complications, Friction stir process (FSP) is best suited for preparation of surface composites and surface modifications. Friction stir processing (FSP), a recently developed surface modification technique is found to provide a solution to the conventional surface processing issues and is related to differential fusion weld structures. Previously, few researchers have studied the effect of SiC on different grades of aluminum by using multiple passes of FSP (Mishra R S, et.al, 2003; Y. Morisada et.al, 2006). Many researchers worked on different reinforcements and combination with multi-pass FSP.

6061-T6 Aluminum alloy is chosen as base/matrix material for fabrication of surface hybrid composites in the present investigation. Hence in the research work, an effort has been made to study the effect of process parameters, the volume percentage of Al_2O_3 and SiC reinforcement, multi-hole and multi-groove techniques on microstructure, mechanical and wear properties of Aluminum alloy surface nanocomposites fabricated by FSP.

However, no investigation has been reported on the influence of volume percentage of reinforcements on MMCs by FSP. In this research, the effect of tool shoulder diameter and process parameters (tool rotational speed and traverse speed) on the fabrication of aluminum surface nanocomposite was investigated.

1.6 Definition of the problem

In manufacturing industries, the use of high strength light weight material has increased because of their productivity efficiency in several applications. Aluminum alloys have suitable properties like strength to weight ratio but its low wear resistance restricts their applications in manufacturing industries. Aluminum metal matrix composites (AMMC's) are the best replacement of monolithic materials (MK Surappa, 2003; J.U. Ejiofor and R.G. Reddy, 1997). For fabrication of AMMCs, friction stir processing is a suitable technique because it avoids the fabrication problems that occur with conventional techniques while producing AMMCs.

As on today, many researchers have worked on the fabrication of surface metal matrix composites using FSP. But unfortunately, there are only rare methods to improve the distribution of the reinforcement particles into the matrix like multi-pass FSP, etc. Little literature is available on the incorporation of reinforcement techniques in FSP. To improve the volume percentage of the reinforcement into the matrix as well as the dispersion of reinforcement throughout the processed region some new methods (multi-hole and multi-groove) has been implemented in this research work.

1.6.1 Objectives and scope of research work

The objective of the present work is to improve the wear and mechanical properties of a surface nanocomposite by adding higher volume percentage of nano-reinforcement particles into the base material along with the increase in the area of the composite region throughout the processed region.

Characterization includes:

(i) Microstructural observation

(ii) Mechanical properties

(iii) Tensile and fractography features

(iv) Wear properties

The scope of the present work is to:

1. Identify the friction stir process parameters to fabricate defect-free surface nano-composite by incorporating nano-reinforcement particles.

2. Identify the best tool shoulder diameter for improving the mechanical properties of surface nanocomposites of Aluminum alloy.

3. To study the effect of volume percentage of reinforcements (Al_2O_3 & SiC particles) on the mechanical properties of the Aluminum surface nanocomposites made by FSP.

4. To study the implementation of the novel technique to improve the strength and composite area throughout the processed region.

5. To study the microstructure analysis (i.e. material flow, defect characterization and bonding between the reinforcement matrix material), and worn morphology of Aluminum surface nanocomposites and correlate that with wear and mechanical properties.

6. To study the microstructure and worn morphology of Aluminum surface hybrid composites and correlate that with the wear and mechanical properties.

1.6.2 Methodology

To improve the surface properties of the composite by FSP, the investigation was done in the following sequence:

- Conducting trial test for getting defect-free condition (combination of tool rotational speed and traverse speed) by using suitable tool geometry.
- Conducting the experiments with varying reinforcements (Al_2O_3 & SiC) and its volume percentages (2, 4 & 6 vol.%).
- Determining the new reinforcement techniques to increase the volume percentage and composite region.
- Implementing and experimenting with new techniques (multi-hole and multi-groove technique).
- Determining the maximum volume percentage of reinforcement to be added.
- Conducting the experiments to get superior properties (wear, microhardness & mechanical properties) by adding hybrid nano reinforcements (Al_2O_3 and SiC).

1.6.3 Organization of thesis

- The thesis consists of the following chapters. A brief introduction to the contents of all chapters is given below:
- **Chapter 1** - It includes the importance, introduction to FSW/P process and its classification, process parameters which include FSW tools geometry, FSW/P applications, composites, Metal matrix composites and its application. Also, it has review of research and development in FSW/P process, problem definition, objectives and scope of the research work and methodology.
- **Chapter 2** - It presents the review of published literature related to FSW/P process, ultra-fine-grained structures, material flow, tool geometry, surface composites and hybrid surface nanocomposites.
- **Chapter 3** - It gives the details of the experimental procedure of the research work covering various aspects like selection of workpiece materials, FSW machine used, conducting of experiments by using optimum process parameters, tool geometry, implementation of multi-hole and multi-groove techniques.

- **Chapter 4** - It consists of characterization and analysis of fabricated surface nanocomposites.
- **Chapter 5** - It involves conclusions of the work and scope for the future work.
- **Appendixes**: List of publications.

LITERATURE REVIEW

2.1 Introduction

Heat treatable 6061-T6 Aluminum alloys are considered to have processing excellent welding characteristics and good strength over high strength Aluminum alloys. These qualities lead to the use of Al-Mg-Si alloys in ship building, automobile, and aircraft applications.

Metal matrix composites (MMCs) have excellent mechanical properties as compared to unreinforced metals. Poor wear resistance of MMCs limit its application in manufacturing industries. To improve wear resistance properties of MMCs ceramic reinforcements are incorporated into the matrix material. Addition of non-deformable ceramic particles into the matrix material causes a decrease in its ductility and toughness. Based on the use in manufacturing industries MMCs are to be produced. Many components life often depends on their properties of surface (hardness, corrosion, and wear). In these circumstances, surface metal matrix composites (SMMCs) are mostly suitable. By producing MMCs through conventional techniques (eg. casting) leads to defect formation like (porosity, blow holes etc.).

2.2 Friction stir welding (FSW)

Thomas. et.al invented and patented friction stir welding (FSW) in 1991 and conducted initial experiments on aluminum and its alloys at The Welding Institute (TWI) of UK (Thomas WM, et. al. 1991). FSW is an incessant hot shear process, in which a rotating tool (harder tool material) is plunged among the abutting faces of the joint (soft base material). The relative motion between the substrate and the rotating tool generates heat (frictional heat) that plasticizes the material around the tool. The plasticized material moves forward with respect to the tool traverse direction and joins the base materials. FSW can be applied to join similar, dissimilar, ferrous and non-ferrous materials and is suitable for aerospace, automobile, marine, rail and transportation industries (W. M. Thomas, et. al. 1997). FSW is a novel process to join aluminum alloy extrusions in solid state with efficient welding quality. Early periods PJ. Haagensen et.al. performed fatigue test on butt welded AA 6082 aluminum alloy by FSW and compared the results with MIG. The results showed that the welds formed with FSW were having 50% higher fatigue strength than welds fabricated with MIG (P J. Haagensen, et.al. 1995). G. Liu et.al. studied the microstructural and hardness properties of 6061-T6 aluminum alloy welds produced

with FSW using light metallography and transition electron microscopy. From the microstructural and hardness analysis, it was revealed that the grain size at the stir zone (SZ) was reduced to 10 µm and hardness was reduced to 65 Hv (G. Liu, et.al. 1997). C. G. Rhodes et.al., studied the effect of FSW on microstructural properties of 7075 aluminum alloy. The size of the nugget zone (NZ) was decreased to 2 – 4 µm due to the recrystallization of NZ and the dislocation density was decreased than parent metal (C.G. Rhodes, et.al. 1997).

Correlation of process parameters of FSW with modelling and experimentation was done first by K.V. Jata et. al. At dynamically recrystallized region (DXR), the grain size reduced to 9 µm and misorientation of grains (15 to 350) was observed by using orientation image microscopy. From the results, it was observed that the basic reason for recrystallization in the DRX was due to continuous dynamic recrystallization mechanism (K.V. Jata, et.al. 2000). The effect of tool wear during FSW was investigated by R.A.Prado et.al (R.A.Prado et.al. 2001). From the results, it was concluded that, tool rotational speed had significant effect on tool wear (with increase in tool rotational speed increases the tool wear). P.S.Pao et.al studied the fatigue behavior of friction stir welded aluminum alloy under air and NaCl solution. The fatigue crack growth of FSWed samples was higher in 3.5% NaCl than compared with air medium (Yutaka S. Soto, et. al. 2001).

2.3 Friction stir processing (FSP)

As FSP is a relatively new process, researchers are not only investigating the possible aluminum alloys that can be processed but are also looking into the effects of process parameters on various mechanical and microstructural properties. This process can be easily adopted as a processing technique to obtain finer grains. Extensive studies are carried out in FSP in order to make it cost effective in the aerospace and automotive industries. Many researchers (R.A. Prado, et.al. 2001, Yutaka S. Soto, et.al. 2001, P.S. Pao, et.al. 2001, Patrick B, et.al. 2001, Z.Y. Ma, et.al. 2002, Z.Y. Ma, et.al. 2003, R.S. Mishra, et.al. 2003, I. Charit, et.al. 2003, Z.Y. Ma, et. al. 2003, C.G. Rhodes, et.al.2003, Y.J. Kwon, et.al. 2003, Douglas C. Hofmann, et.al. 2005, and C.H. Chuang, et.al. 2005) have taken up the microstructural investigation of various friction stir welded and processed aluminum alloys like 1100, 2024, 5083, 6061, 7075 and 7475 results in significant enhancement of superplastic properties due to the grain refinement. Different material properties like tensile strength, micro-texture, fatigue and hardness are also being examined for

different alloys of aluminum (Jian-Qing Su, et.al. 2005, M.L. Santella, et.al. 2005, I. Charit, et.al. 2005, P. Cavalierea, et.al. 2005, Z.Y. Ma, et.al. 2005, Y. Morisada, et.al. 2006 and K. Nakata, et.al. 2006). There have also been efforts made to investigate the effect of various process parameters like rotational speed on the properties and microstructure evolved during FSP. The heat generated and residual stress during the process are being investigated experimentally as well as by modeling the process both numerically as well as using by finite element analysis. An attempt is made in the year 2001 to get ultra-fine grained (UFG) microstructure through FSW. 4 pass equal-channel angular (ECA) pressed material was taken as base material and again processed with FSW to get UFG microstructure. From the results, it was observed that, FSW method is one of the effective technique to get UFG microstructure with high strength and toughness (Douglas C. Hofmann, et.al. 2005).

Douglas C. Hofmann et. al. worked on Submerged friction stir processing (SFSP) to get bulk ultra-fined grain structure. The experiments were conducted under water by applying multi pass FSP and it was observed from the results that, the grain size was reduced to 200 nm significantly (C.H. Chuang, et.al. 2005). C.H. Chuang et. al. used FSP technique to fabricate bulk multi-element Mg base alloys by varying parts of AZ31 sheets, Al and Zn foils under liquid nitrogen cooling conditions. Multi pass technique was implemented to get finer microstructure with superior hardness. The fabricated multi-element MG based alloy exhibits superior hardness of 400 Hv at the processed region due to grain refinement and intermetallic phase formation that occurred under liquid nitrogen cooling condition (Jian-Qing Su, et.al. 2005). Jian-Qing Su et.al. investigated the effect of coolant (water, methanol & dry ice) and multiple overlapping passes for getting bulk UFG structure on aluminum alloys by FSP. The resulting microstructure reveals that the grain size was reduced to an avg. of ~250 nm successfully by applying multiple overlapping technique with rapid cooling effect.

This process gives non-uniform UFG in the processed region (M.L. Santella, et.al.2005). I. Charit and R.S. Mishra were studied the low temperature superplasticity nature of casted alloy for producing UFG microstructure through FSP. At low temperatures and high strain rates, the material shows superplasticity nature and produces UFG at stir zone. From the results it is observed that, FSP is not only solid-state process, it reduces the porosity as well as grin structure (from dendritic to fine grains). During the FSP, When the processed region reaches a temperature

above 3900C, the material undergoes severe superplasticity and causes microstructural heterogeneity in stir zone (I. Charit, et.al. 2005). Z.Y. Ma and R.S. Mishra studied the development of UFG microstructure at low temperature (0.48 Tm) superplasticity by FSP. At 1750C, maximum superplasticity of 240% was achieved with UFG structure (avg. grain size of 0.7 µm) (P. Cavalierea, et.al. 2005).

2.3.1 Microstructure

The typical cross section of a FSW joint has three different zones: 1) heat affected zone (HAZ), 2) nugget or stir zone and 3) thermo-mechanically affected zone (TMAZ) which is the region between HAZ and nugget, Figure 2.1. The stir zone is the central region of the weld where dynamic recrystallization occurs as a result of high temperature and severe plastic deformation, leading to the formation of fine equiaxed grains, Figure 2.1 (d). In FSW/FSP, tool geometry, composition and temperature of the work piece material, vertical pressure, cooling rate and process parameters significantly influence grain size in the nugget zone (Nandan R, et.al. 2008).

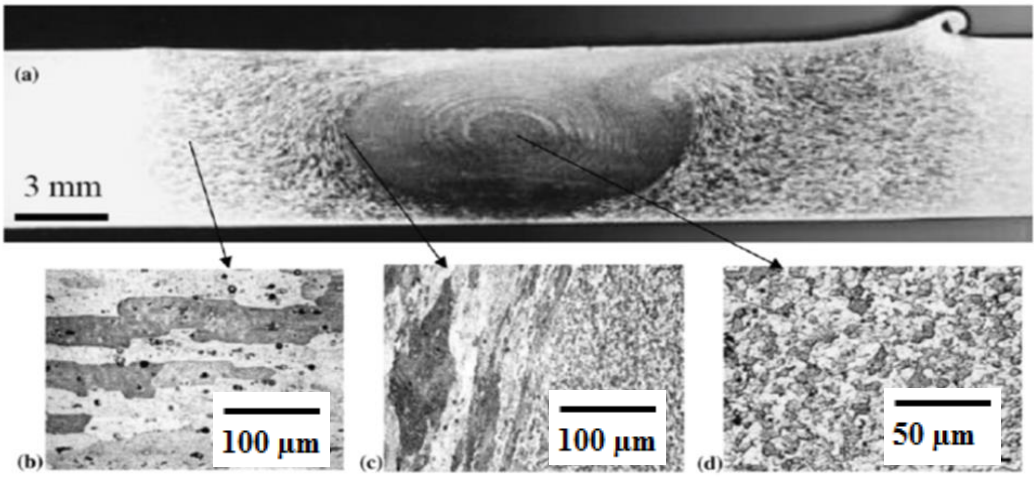

Fig. 2.1: Optical micrographs of microstructure of an Al 2014 friction stir weld showing different regions: a) weld overview, b) heat affected zone, c) TMAZ/stir zone boundary, and d) stir zone (Gerlich A, 2007).

Microstructures of the material in this region usually contain a banded structure consisting of the so called “onion rings”, Figure 2.1. The spacing between these bands equals the

distance the tool moves forward during each single rotation (Sutton MA, et.al.2002 and Krishnan K.N, et. al. 2002). Such microstructure is attributed to variations in: 1) grain size, 2) particles or precipitates distribution (Sutton MA, et.al.2002 and Mahoney MW, et.al. 1998), 3) crystallographic texture (Schneider JA, et.al.2004), 4) dislocation density (Threadgilll PL, et.al. 2009), and 5) chemistry due to intermixing of dissimilar alloys (Yin YH, et.al. 2010). Krishnan (Krishnan K.N, et. al. 2002) has shown that these variations are caused when frictional heating heats the material and the forward movement of the tool extrudes the material around to the retreating side which leads to the formation of the bands during tool rotation. In the TMAZ, grains are heated and plastically deformed but not completely recrystallized; therefore, they are not as fine and equiaxed as stir zone grains. Finally, HAZ is only affected by temperature and not by mechanical work so the main change in HAZ microstructure is the coarsening of the grains or precipitates (Gerlich A. 2007).

2.3.2 Material flow in FSW/FSP

Formation of a defect free weld directly depends on the material flow during FSW. On the other hand, in FSP, material flow determines the development of microstructural features and in the special case of composite fabrication by FSP, material flow in the stir zone governs the particle distribution. Thus, studying the material flow has been approached by many different methods in recent years, using various techniques such as tracking of tracer particles post welding by microscopy (Seidel TU, et. al. 2001 and Fratini, et. al. 2006), microstructural analysis of dissimilar alloy joints, in-situ observation using x-ray transmission systems (Morisada Y, et.al. 2011), simulation by numerical modeling (Colegrove PA, et.al. 2003, Bastier A, et.al. 2006, Nandan R, et.al. 2006 and Xu S, et.al. 2001), and using analog materials like coloured plasticine (Liechty BC, et. al 2007). This aspect is not completely understood yet and remains the subject of many papers (Yang Q, et.al. 2010 and Mukherjee S, et.al.2010). Three types of flow transport the deformed material during FSW/FSP (Nandan R, et.al. 2008): 1) tool rotation and the friction between the tool and the work piece material, heat and stir the softened material near the tool; 2) downward material flow in the region close to the tool created when using a threaded pin which in turn causes an upward motion at the outer periphery of the mixing region of the stir zone; and 3) material flow along the welding direction as a result of travelling movement of the rotating

tool. It is shown that majority of the material flow, caused by these three types, happens through the retreating side (Nandan R, et.al. 2008).

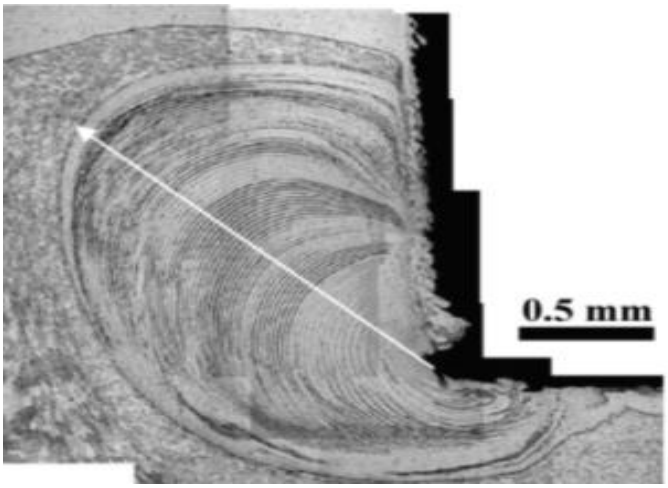

Fig. 2.2 Intermixed region of processed region (Su P, et.al.2007).

When considering FSP for fabrication of composites this mixing must be considered in order to control the distribution of material. First, stirring around the pin of the tool creates a rotating and mixing zone, the thickness of which depends on the materials is properties, welding parameters and rate of heat transfer to the tool (Nandan R, et.al. 2008). Second, as mentioned before, use of a threaded pin induces mixing which helps particle distribution in both vertical and longitudinal directions during composite fabrication by FSP. Generally, the amount of mixing increases when applying at higher rotation speeds or lower travel speeds (Threadgilll PL, et.al. 2009). Su et al. (Su P, et.al.2007) have shown that by using a threaded tool, intermixing happens during friction stir welding of dissimilar Al alloys, when the material from the locations beneath the shoulder and at the end of the pin is transferred to the top of the thread on the pin and is moved downward by the pin thread. This process happens during each single rotation of the tool and forms intermingled lamella which is then discharged from the bottom of the thread and moves outwards and upwards following a helical vertical rotational flow path, Fig. 2.2. Gerlich et al. (Gerlich A, et.al. 2008) have indicated that the width of this intermixed region increases with the dwell time in friction stir spot welding which implies larger intermixed regions may be achieved in friction stir seam welding by decreasing the travel speed.

2.4 FSP of different classes of materials

FSP was first investigated and used as a near surface modification and enhancement technique. An example of application is the fabrication of surface metal-matrix composites (Mishra et al., 2003; Morisada et al., 2006). The aim of the process in this case was to reinforce metal alloys with ceramic phases, usually carbide powder (SiC, TiC or WC) to increase strength, hardness, and resistance to wear, creep and fatigue at the surface of the material, while maintaining ductility and toughness at bulk. Commercially, the generation of a near surface metal matrix composite can also be achieved by using high energy laser melt treatments (Hu & Baker, 1995; Hu et al., 1995). In these techniques, the ceramic phases are coated onto the surface of the material, either pre-deposited or injected simultaneously with the laser beam. During processing, the powder coating is melted along with the surface layer of the substrate, allowing the ceramic particles to mix into the melted material. Unfortunately, the resulting resolidification of the localized melt pool is difficult to control, hence the microstructure that develops often results in poor mechanical properties. In comparison, it has been found that FSP can be used to generate surface metal-matrix composite with uniformly distributed SiC particles, and the microstructure is porosity and defect free (Mishra et al., 2003). The process also assists in particle break up, and produces a fine dispersion of particles within the microstructure, which can double the microhardness of the base material; e.g. from 85 HV to 173 HV, when a 27 vol.% of SiC particles was processed into the surface layer (Mishra et al., 2003).

In general, the composite layer ranges from 50 μm to 200 μm in depth, and by simply increasing the amount of pre-placed SiC particles on the surface of the alloy, a higher particle concentration can be introduced into the composite layer. However, there are several limitations to the processing parameters. Firstly, the transverse speed was found to be influential to the bonding between the surface composite layer and the material substrate. As the transverse speed increases, the bonding strength of the surface composite layer is poor and is observed to separate from the alloy substrate. Secondly, the plunge depth must be controlled, as with too large a plunge depth, the pre-placed SiC particles on the surface were pushed away from the tool, and no particles were incorporated into the alloy. However, too low plunge depths were found to be ineffective in mixing the SiC particles into the alloy.

Shafiei-Zarghani et al. have recently attempted to incorporate nano-sized Al_2O_3 into the surface layer of 6082 Al alloy (Shafiei-Zarghani et al., 2009). After a single pass FSP, the Al grains were refined down to ~4.8 μm. However, although the nano-particles were integrated into the Al matrix, they tended to be agglomerated, and distributed in clusters. The dispersion of the nano-sized Al_2O_3 particles was improved by multi-pass processing. The grain size was also further reduced to ~0.7 μm after 4 FSP passes because the homogeneously distributed Al_2O_3 particles were effective in pinning and suppressing grain boundary migration. As a result, the hardness and wear resistance of the surface composite layer increased by three times, compared to the base material (Shafiei-Zarghani et al., 2009). Research has also suggested the potential of using FSP as a bulk processing technique for thicker alloy plates. Microstructure refinement of a greater material volume and further depth can be achieved by using friction stir tools with a larger pin size (Su et al., 2005). This is particularly attractive for the production of superplastic materials.

Generally, superplasticity is defined as the ability of a solid crystalline material to deform and elongate beyond 200 % of its original length during tensile deformation (Ma et al., 2002; 2003; Charit & Mishra, 2005; Johannes et al., 2007). Materials that exhibit such behavior can be shaped into complex objects with ease. Many aerospace components made from aluminum and titanium alloys are commonly super plastically formed. There are two basic but important requirements for a crystalline material to exhibit superplasticity. Firstly, the microstructure must consist of a fine grain structure, typically < 20 μm in grain size. Secondly, finely dispersed thermally stable particles must be present within the material in order to pin the grain boundaries and stabilize the fine grain size microstructure during forming (Ma et al., 2003). Due to these necessities, FSP appears to be a promising processing method.

The potential of generating superplasticity by FSP has been investigated on a variety of Al alloys (Ma et al., 2002; Charit & Mishra, 2005; Johannes et al., 2007i, 2007ii; Liu & Ma, 2008). Results from single pass processing have shown an increase in uniform elongation from alloys that initially showed no superplasticity at low temperatures (< 0.5 Tm). However, since superplasticity is dependent on the size of the grains and the stability of the refined microstructure, the temperature and strain rate for which maximum elongation could be achieved differ with different processing parameters and different alloys. Liu & Ma have shown that by

water cooling a 7075 Al alloy from FSP, an UFG microstructure with average grain size of 0.8 μm can be obtained (Liu & Ma, 2008), and a maximum ductility of 540 % at 350 °C was achieved. When combined with the optimized conditions, some of the processed alloys were capable of straining beyond 1000 % (Charit & Mishra, 2003). Many experiments have also looked into the possibility of using multi-pass processing to refine a larger volume of the microstructure. Promisingly, these reports have commented on successfully producing homogeneous microstructures with a fine grain size (Johannes & Mishra, 2007ii).

However, even though superplasticity was achieved after multi-pass processing, the ductility of the alloy was found to be reduced from that of a single pass process. The use of FSP as a property optimizing technique has also shown its potential in several other metallic alloys (Park et al., 2003; 2004; Zhang et al., 2005; Reynolds et al., 2005; Morisada et al., 2006; Sato et al., 2007), and in particularly FSP of magnesium alloys is increasingly being investigated. The formability of Mg is generally poor, due to a lack of active slip systems within its hexagonal close pack (HCP) crystallographic structure. However, recent research has suggested that the formability of Mg can be enhanced by refining the grains of the alloy to less than 20 μm (Sato et al., 2007). Similar to superplasticity, this improvement in ductility is believed to be the result of an increased non-basal slip systems activity and grain boundary sliding that appears to occur within the material when it has a refined microstructure. Fracture limits similar to pure Al have been observed in Mg alloys with grain refined down to ~3 μm. Results have shown that the microstructure produced from processing parameters which induced a lower peak temperature to the material, during processing, were finer than the microstructure that was developed from a higher temperature process, or from the base material (Sato et al., 2007). This suggested that the refined microstructure of Mg alloys after FSP is unstable and sensitive to temperature.

However, the effect of multi-pass processing on the grain size was noted as negligible. Therefore, it is believed that the refined microstructure after processing is capable of being sustained to the maximum temperature that was reached during processing, because the peak temperature of 77^0 C with increasing distance from the processed zone, so the temperature exposed to the original processed region during multi-pass processing will never be higher than that of the previous pass. This phenomenon can also be seen in Al alloys which do not have thermally stable particles in the alloy to stabilize the refined microstructure (Sato et al., 2007).

FSP can also be used to refine the microstructure of cast Mg alloys. Ma et al. have shown that the coarse network-like eutectic β-Mg17Al12 phase within AZ91 Mg alloy, which is otherwise detrimental to the mechanical properties, can be broken up and solutionised during FSP [Ma et al., 2008]. By refining the microstructure of the cast material, followed by post ageing to allow the dissolutionised β-Mg17Al12 phase to precipitate finely and homogeneously, the yield and ultimate tensile strengths of the alloy was increased from 73 MPa and 111 MPa, to 177 MPa and 337 MPa respectively (Feng & Ma, 2007). The potential of using FSP to enhance the mechanical properties of Ni-Al bronze alloys have also been investigated (Oh-ishi & McNelly, 2004; 2005). This material is widely used in marine applications due to its good combination of corrosion resistance, strength, fracture toughness, and non-sparking behavior (Duma, 1975). However, NiAl bronze components with thick cross sections are usually cast, and the slow cooling rates often lead to development of a coarse microstructure, which reduces the physical and mechanical properties (Ferrara & Caton, 1982). But, with FSP it is believed that localized surface strengthening can be achieved. Oh-ishi and McNelly have extensively investigated FSP of an Ni-Al bronze alloy, with composition Cu-9Al-5Ni-4Fe (wt %).

2.5 Ultra-fine-grained structure by FSP

An attempt was made in 2001 to get ultra-fine grained (UFG) microstructure through FSW. 4 pass equal-channel angular (ECA) pressed material was taken as base material and again processed with FSW to get UFG microstructure. From the results, it was observed that, FSW method is one of the effective techniques to get UFG microstructure with high strength and toughness (Y.J. Kwon, et.al. 2003). Douglas C. Hofmann et. al. worked on submerged friction stir processing (SFSP) to get bulk ultra-fined grain structure. The experiments were conducted under water by applying multi pass FSP and it was observed from the results that the grain size was reduced to 200 nm significantly (Douglas C, et.al. 2005). C.H. Chuang et. al. used FSP technique to fabricate bulk multi-element Mg base alloys by varying parts of AZ31 sheets, Al and Zn foils under liquid nitrogen cooling conditions. Multi pass technique was implemented to get finer microstructure with superior hardness. The fabricated multi-element Mg based alloy exhibits superior hardness of 400 Hv at the processed region due to grain refinement and intermetallic phase formation occurred under liquid nitrogen cooling condition (C.H. Chuang, et.al. 2005).

Jian-Qing Su et.al. investigated the effect of coolant (water, methanol & dry ice) and multiple overlapping passes for getting bulk UFG structure on aluminum alloys by FSP. The resulting microstructure revels that the grain size was reduced to an avg. of ~250 nm successfully by applying multiple overlapping technique with rapid cooling effect. This process gives non-uniform UFG in processed region (Jian-Qing Su, et.al. 2005). I. Charit and R.S. Mishra studied the low temperature superplasticity nature of cast alloy for producing UFG microstructure through FSP. At low temperatures and high strain rates, the material shows superplasticity nature and produces UFG at stir zone. From the results it is observed that, FSP is not only solid-state process, it reduces the porosity as well as grain structure (from dendritic to fine grains). During the FSP, when the processed region reaches temperatures of above 390^0C, the material undergoes severe superplasticity and causes microstructural heterogeneity in stir zone (I. Charit, et.al. 2005). Z.Y. Ma and R.S. Mishra studied the development of UFG microstructure at low temperature (0.48 Tm) superplasticity by FSP. At 175^0C a maximum superplasticity of 240% was achieved with UFG structure (avg. grain size of 0.7 μm) (Z.Y. Ma, et.al. 2004).

2.6 Surface composites by FSP

Initially FSP was applied to modify the surface properties of the material by changing grain recrystallization. In 20^{th} century, reinforced metal matrix composites were fabricated by FSP. Many researchers were worked on improvement of hardness and wear properties of soft matrix materials by incorporating hard reinforcement particles into the matrix. A. Shafiei-Zarghani, et al studied the effect of Al_2O_3 nano reinforcement particles into the Al matrix material by applying multi-pass FSP. From the results it was observed that, the grain size was reduced to ultra-fine-grained structure with decrease in the agglomeration of added reinforcement particles. With more uniform dispersion, the reinforcement particles exhibited uniform increase in hardness and wear throughout the processed region (A. Shafiei-Zarghani, et. al. 2009 & 2011). Similarly, Al_2O_3 nano reinforcements was used to improve the wear and microstructural properties of aluminum alloy by FSP (M. Sharifitabar et al. 2011 and Y. Mazaheri et al. 2011).

Some researchers maintain that SiC reinforcement particles may be used to increase the mechanical, wear resistance and microstructural properties of aluminum alloy through FSP. Higher hardness and wear properties were achieved with the addition of SiC reinforcement particles (A. Dolatkhah et al. 2012).

Essam R.I. Mahmouda et al., studied the effect of Al_2O_3 and SiC micro reinforcement particles into the Al alloy by FSP. By varying the combination (20/80, 50/50 & 80/20) of Al_2O_3 and SiC volume percentages into the aluminum alloy, good wear resistance and hardness properties were achieved. But superior wear resistance properties were achieved at 20% Al_2O_3 + 80% SiC combination than other combination of SiC and Al_2O_3 (Essam R.I. Mahmouda et al. 2010). Some of the researchers investigated the effect of multi walled carbon nano tubes (MWCNT) introduced into aluminum. For uniform distribution of MWCNT into the matrix material, multi-pass FSP was applied. From the results it was observed that, good dispersion of MWCNT were taken place into the matrix with increasing microhardness as twice of in it alloy form (Hossein Izadi et al. 2012 and Qiang Liu et al. 2013).

Very few researchers have investigated the effect of different reinforcement particles on microstructural, mechanical and wear properties of metal matrix composites. For example, Cr_2O_3 reinforcement powder is added into the Al alloy, SiC particles into the Copper matrix, Gr/Cu and Al/TiC etc.

EXPERIMENTAL PROCEDURE AND TESTING

3.1 Introduction

In the present work, FSP was tried to incorporate nano-sized Al_2O_3 and SiC reinforcement particles into 6061-T6 Al alloy to form particulate hybrid surface composites. The effect of nano Al_2O_3 and SiC reinforcement particles on microstructural, mechanical and wear and properties of Al/Al_2O_3, Al/SiC and Al/Al_2O_3+SiC surface composites produced by FSP were studied. Details of the base material, reinforcement particles, FSP process parameters, Multi hole, Multi groove, metallographic studies, wear test and mechanical testing are presented in this chapter.

This section outlines the experimental techniques used to fabricate and characterize the microstructure, mechanical, microhardness and wear properties described in the results section in this study. Most of the techniques are well known so will be described briefly.

3.2 Experimental Layout

The overall experimental plan is shown in Fig. 3.1.

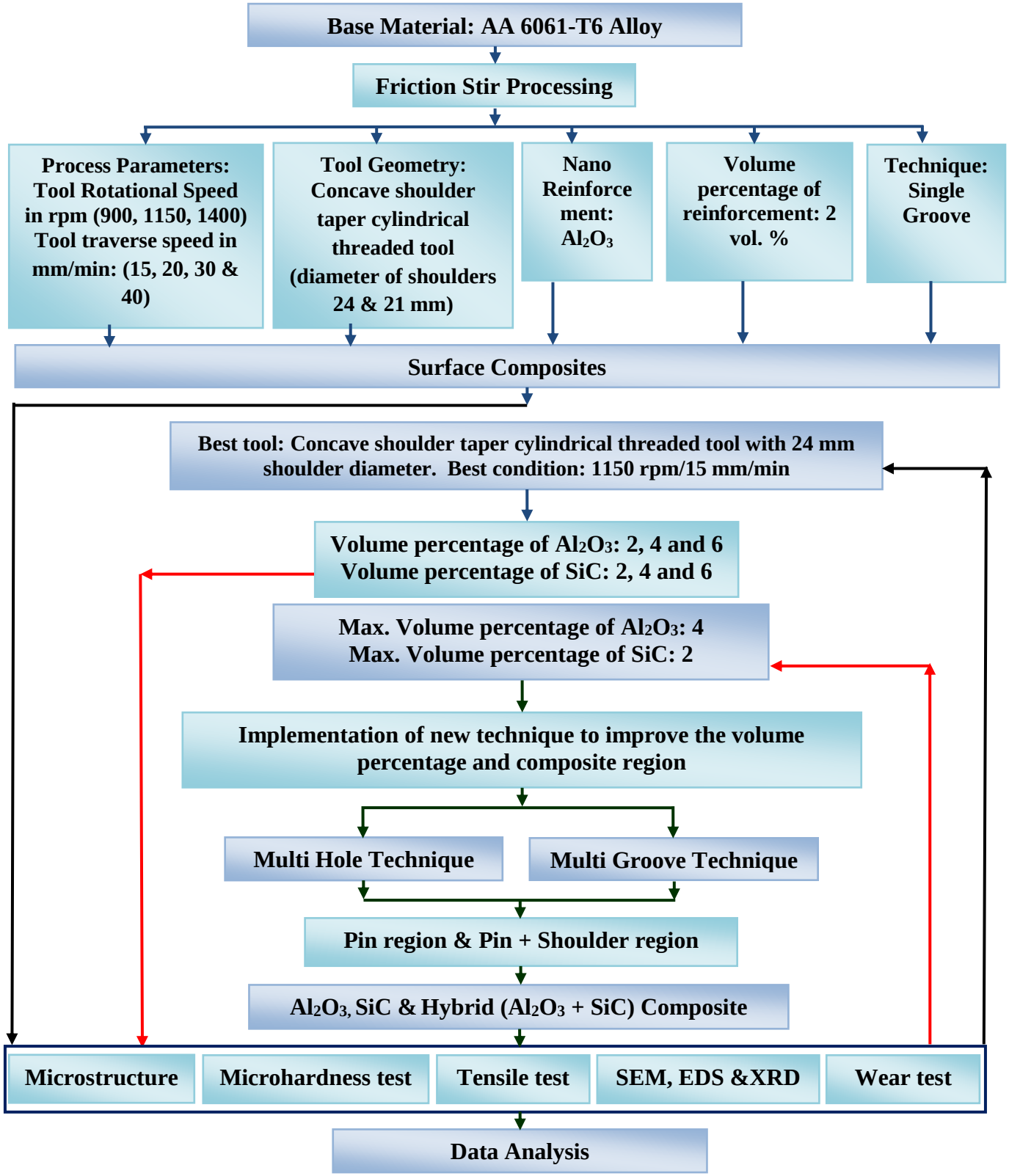

Fig. 3.1 Experimental layout.

3.3 Selection of workpiece and tool materials

In the current investigation, 4 mm thick 6061-T6 Aluminum alloy was taken as base material. For the fabrication of surface nanocomposites Al_2O_3 and SiC nano particles having size of ~50nm were used as reinforcement particles. Table 3.1 shows the chemical composition of Aluminum alloy (base material) and Table 3.2 shows the mechanical properties of the base material respectively.

Table 3.1 Chemical composition of 6061-T6 Aluminum alloy (Wt. %).

Element	Mg	Si	Cu	Zn	Ti	Mn	Cr	Al
Amount (Wt %)	0.85	0.68	0.22	0.07	0.05	0.32	0.06	Balance

Table 3.2 Mechanical properties of 6061-T6 Aluminum alloy.

Material	Microhardness (Hv)	Ultimate tensile strength (MPa)	Yield strength (MPa)	Elongation (%)
6061-T6 Aluminum alloy	104	294	271	12

Table 3.3 Chemical composition of AISI H13 Tool steel (Wt. %).

Element	C	Mn	P	S	Si	Cr	V	Mo
Amount (Wt %)	0.42	0.28	0.015	0.003	1.00	5.20	1.05	1.45

In this experiment, AISI H13 tool steel is selected as tool material. This is due to tool steel having higher elevated temperature and stability, resistance to wear, thermal fatigue strength, machinability, accessibility and low cost. The typical chemical composition of H13 tool steel is presented in Table 3.3.

3.4 Selection of tool profiles

Two different tools having concave shoulder with taper threaded cylindrical tools with varying shoulder diameters (Ds = 24mm and Ds = 21mm) and pin diameter (Dp = 8 and Dp = 7). The schematic diagrams of different tool geometries are shown in Fig. 3.2.

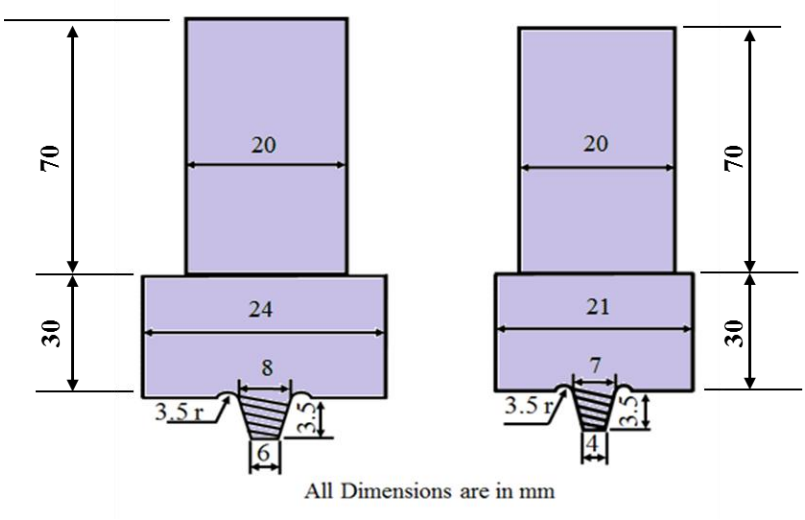

Fig. 3.2 Tool geometry of different tools.

3.5 FSW machine details

The experiments were conducted on FSW - 3T - NC machine (make: R.V. M/C Tools, 3 Ton, 10 HP, 3000 rpm computer controlled) shown in Fig. 3.3. The detailed specifications of the vertical milling machine are depicted in Table 3.4.

Fig. 3.3 Friction stir welding machine.

Table 3.4 specifications of the FSW -3T - NC machine.

Sr. No.	Details	Specifications
01	Manufacturer	R.V Machine Tools
02	Control System:	NC
03	Spindle Motor Power:	11kW/1400RPM/440V
04	Tool holder	ISO 40 Arbor
05	Spindle RPM:	3000(max)
06	Spindle torque:	75N-m @1400 rpm
07	Z-axis Stroke:	300 mm
08	Z-axis Thrust:	30 kN
09	Z-axis Rapid traverse:	0-1000 mm/min
10	X-axis Stroke:	400 mm
11	X-axis Thrust:	15 kN
12	X-axis Rapid traverse:	0-1000 mm/min
13	Y-axis Stroke:	200 mm
14	Y-axis Drive:	Manual
15	Table Size with threaded Holes:	400 x 300 mm
16	Control:	2 Mode- Force & Position
17	Data acquisition & analysis:	Spindle speed/Axis velocity against time

3.6 Preparation of aluminum plate for fabrication of surface composite with single groove technique by FSP

Fabrication of surface composites by single groove technique is very flexible and easy process. In this technique, a groove (square in shape) was made as per the volume percentage of reinforcement to be incorporated into the base material (matrix material). The groove must be tangent to the pin on the advancing (AS) of the tool rotation. Fig. 3.4 shows the operating principle of FSP.

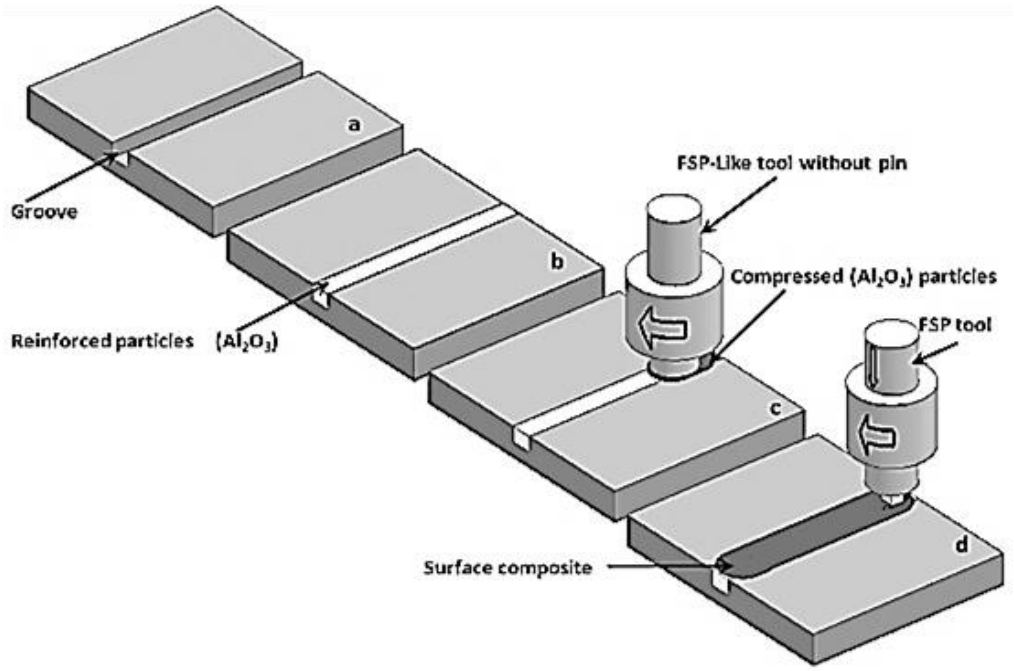

Fig. 3.4 Schematic view showing the operating principle of FSP.

3.7 Effect of groove position on aluminum plate for fabrication of surface composite by FSP

In friction stir processing, the material flow takes place from the retreating side (RS) of the tool rotation to advancing side (AS) of the tool. During the process, the combination of tool rotation and liner movement shears the material with the help of probe and material flow takes place from RS to the AS. A square groove was made on Al alloy plate and the groove position was changed in three locations. In the first case, groove was made at advancing side underneath the shoulder. In the second case, groove was made at advancing side tangent to the pin. In the third case, groove was made along the centerline. Defect-free surface composites were observed when the groove position is at the advancing side tangent to the pin due to sufficient material flows from advancing side to the retreating side during FSP. The schematic diagram of groove positions is highlighted in Fig. 3.5.

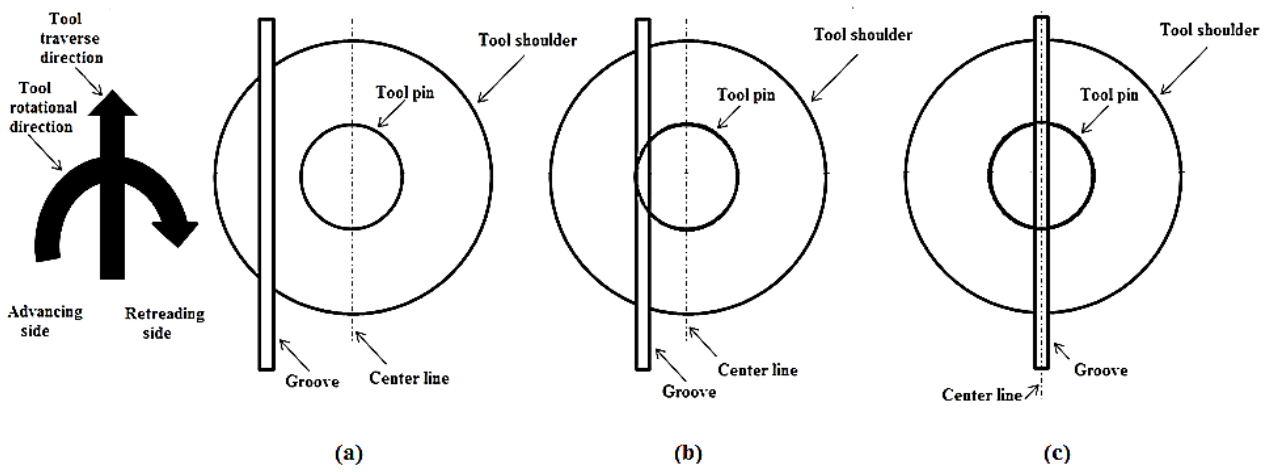

Fig. 3.5 Schematic diagram of groove positions a) Advancing side underneath the shoulder b) Advancing side tangent to the pin and c) Along the centerline.

3.8 Implementation of new fabrication techniques

To improve the composite region and volume percentage of reinforcements, novel techniques were implemented. These are:

- Multi hole technique.
- Multi groove technique.

3.8.1 Multi hole technique

In the present research, a new technique was implemented to improve the composite region up to the processed region called as multi hole technique. Initially double series of holes were made on the pin region and later the holes were made on the shoulder region on the advancing side of the tool. A schematic diagram of multi holes is represented in Fig. 3.6.

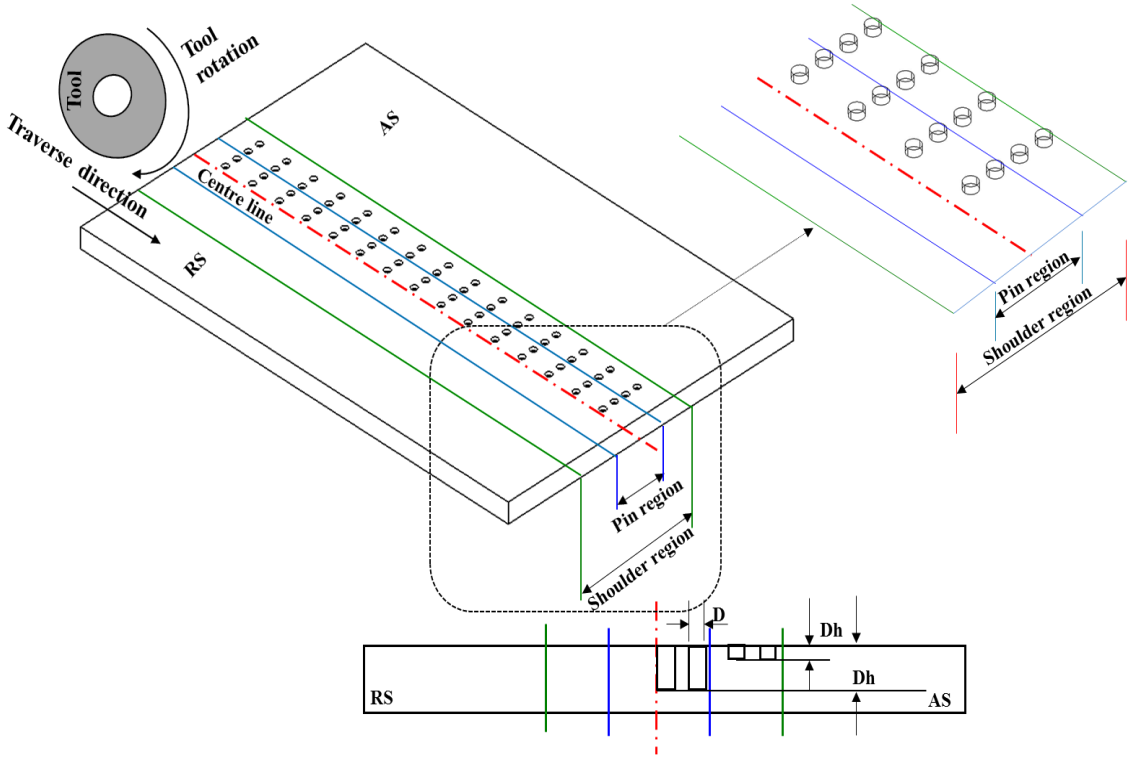

Fig. 3.6 Schematic diagram of multi hole technique.

Table. 3.5 Details of symbols used in multi hole technique.

Symbols	Representation
D	Diameter of the hole
Dh	Depth of hole
AS	Advancing side
RS	Retreating side

3.8.2 Multi groove technique

A novel technique was used to develop a surface nano composite with high vol.% of reinforcement into the matrix material. To increase the reinforcement vol.%, the groove dimensions had to be changed as per the vol. % of reinforcement. This leads to an increase in the defect formation during the fabrication of high volume percentage of composites. So, to avoid the defect formation and increase the volume percentage of reinforcement, a novel technique called multi groove technique was implemented to fabricate successful surface composites with single pass FSP. A schematic diagram of multi groove technique is represented in Fig. 3.7.

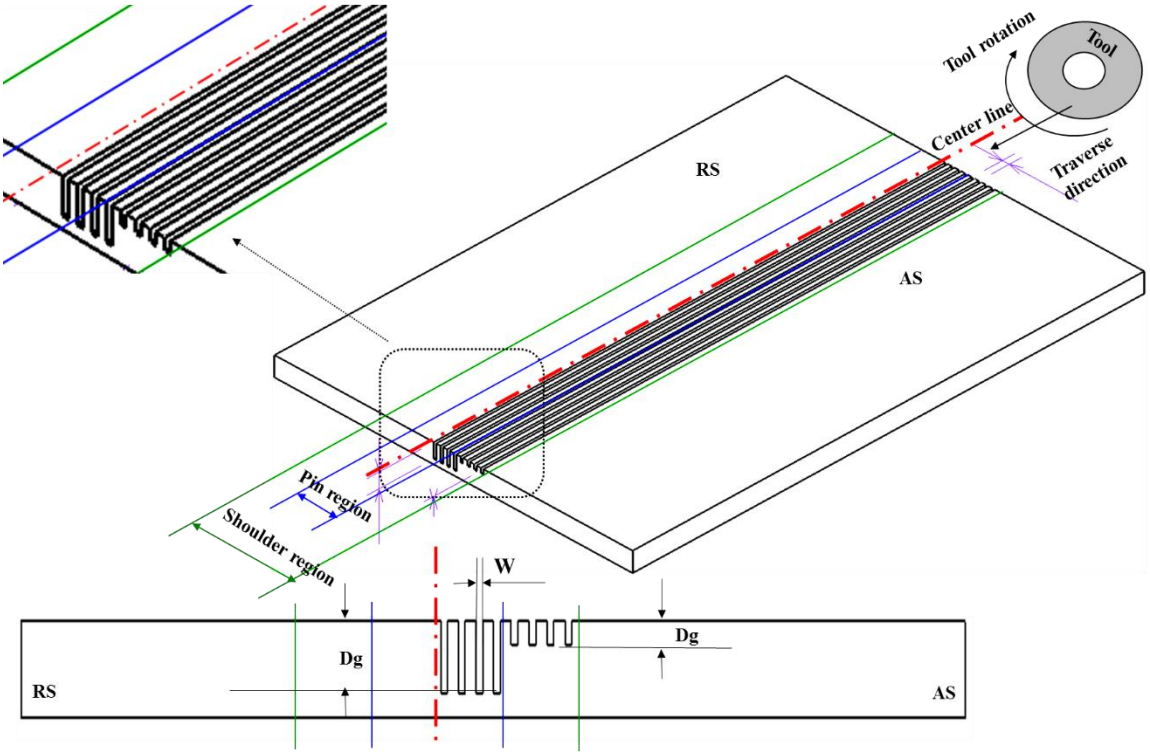

Fig. 3.7 Schematic diagram of multi groove technique.

Fig. 3.7 shows that the grooves were made on the pin region as well as on the shoulder region too. Here, the width of the groove is 0.5 mm as mentioned above for all the regions but the depth of the shoulder is restricted to 1 mm only. Further increase in depth in the shoulder region leads to defect formation.

Table 3.6 Details of symbols used in multi groove technique.

Symbols	Representation
W	Width of the groove
Dg	Depth of groove at pin region
AS	Advancing side
RS	Retreating side

3.9 Characterization of fabricated surface nanocomposites

3.9.1 Metallography study

All the fabricated surface composites were sectioned longitudinal, transverse as per ASTM standards with the help of Electrical discharge machine (EDM) to study the microstructural, microhardness, mechanical and wear behavior of the composites. To study the microstructural characterization, samples were polished with emery papers having different grades as shown in Table 3.7, later samples were electropolished using disk polishing machine. Here diamond paste is used as a lubricant. After completion of polishing, samples were cleaned using methanol and dried for 5 minutes. later samples were etched with Keller's reagent.

Table 3.7 Polishing procedure for microscopy.

Sr. No.	Abrasive (Grit SiC paper)	Time (sec)
1	200	90
2	400	90
3	600	90
4	800	90
5	1000	120
6	2000	120
7	3000	120
8	4000	120

3.9.2 Disk polishing machine

Samples of fabricated surface nanocomposite samples were mounted for easily handling during the polishing. After mechanically polished the samples were cleaned with methanol to remove the formation of surface impurities. To get mirror finished surface using double disc (8” Double Disc Polisher) polishing machine shown in Fig. 3.8 and the specifications are listed in Table 3.8.

Fig. 3.8 Disc polishing machine.

Table 3.8 Specifications of disc polishing machine.

Sr. No.	Details	Specification
1	Variable Speed	50-1000 rpm
2	High torque Motor	0.5 HP
3	Drive speed	Variable
4	Water jet with control value	Flexible
5	Aluminum Disc 8” Diameter	2 Nos
6	Spring	1 No
7	Stainless Steel Holding Ring (Press type)	1 No
8	Size	710 × 660 × 310 mm

3.9.3 Stereo zoom microscopy

All fabricated surface composite samples were examined with stereo zoom microscopy to observe the distribution of the reinforcement particles into the base material at low magnification. It helps to study the surface of the composites at lower magnifications with effective results. Prime-100 stereo zoom microscope (model: prime 100; make: Madimage technologies Pvt. Ltd.) is utilized to study the surface of the fabricated composites. The stereo zoom microscope is shown in Fig. 3.9 and specification are given in Table 3.9.

Table 3.9 Specifications of stereo zoom microscopy.

Sr. No	Details	Specification
1	Model	Prime – 100
2	Head	Binocular body
3	Eyepieces	Includes widefield 20x / 10 mm high
4	Objective Lenses	Zoom range of 0.7x - 4.5x.
5	Total Magnification	14x - 90x
6	Specimen Stage	95mm glass stage plate
7	Stand:	Post stand has built in top and bottom
8	Working Distance	100mm
9	Focusing	Rack & pinion focusing
10	Illumination	Transmitted and reflected LED illumination

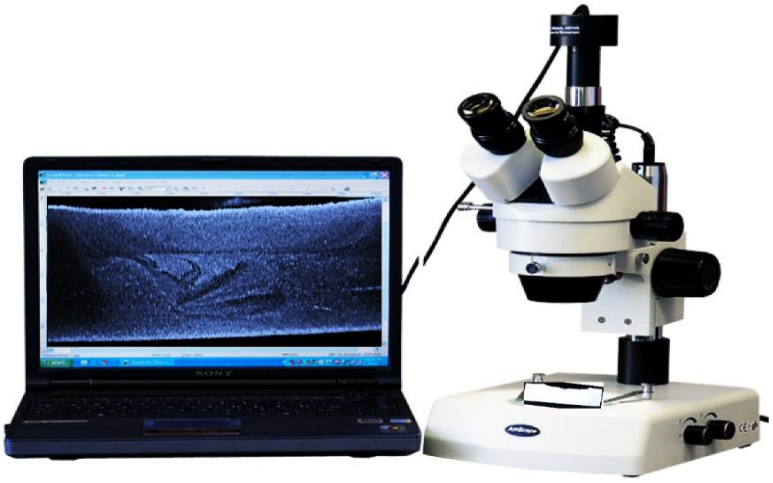

Fig. 3.9 Stereo zoom microscopy.

3.9.4 Optical microscopy (OM)

To view the microstructural characteristics of fabricated surface nanocomposite samples were done by using Optical microscopy (OM). An inverted optical microscope is used in this study as shown in Fig. 3.10 and the specifications are shown in Table 3.10.

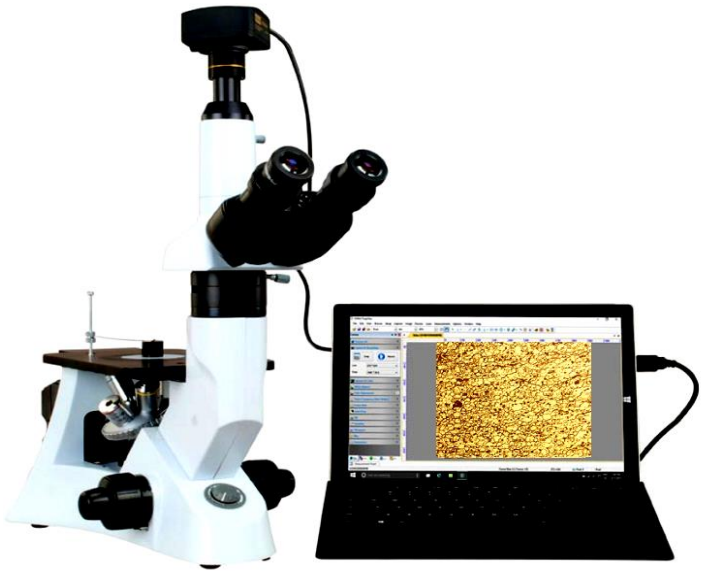

Fig. 3.10 Inverted optical microscopy.

Table 3.10 Specifications of inverted optical microscopy.

Sr. No.	Details	Specification
1	Model	Model MVDC-1300
2	Total Magnification	40X, 100X, 200X, 500X &1000X
3	Eyepiece	A pair of high eyepoint widefield EW10X/20
4	Objective	Plan 4X/0.10, ∞/- Plan 10X/0.25, ∞/- Plan 20X/0.40, ∞/- Plan 50X/0.65, ∞/- Plan 100X/0.80, ∞/0
5	Stage	Mechanical stage attachment: stroke 120mm x 78mm
6	Focusing	Coaxial fine and coarse knobs on both side with focus stop
7	Illumination	Reflected illumination
8	Digital camera:	True color 3584x2748 pixels (10M pixels)
9	Software	Metavis 4.1v

3.9.5 Scanning electron microscopy (SEM)

A Tescan; Model: Vega 3 LMU Scanning Electron Microscope (SEM) working with a tungsten filament at an accelerating voltage of 20kV was utilized for tensile and fractography. Microstructures at different locations of welds was carried out using SEM. The photograph of scanning electron microscope is shown in Fig. 3.11 and specifications are shown in Table 3.11.

Table 3.11 Specifications of SEM.

Sr. No.	Details	Specifications
1	Electron Gun	Tungsten heated cathode
2	Resolution	High Vaccum Mode :3 nm at 30 kv / 2 nm at 30 kb. Low Vaccum Mode: 3.5 nm at 30 kv / 2.5 nm at 30 kv
3	Magnification	2x – 1,000,000X
4	Maximum field of view	24 mm at WD 30 mm
5	Accelerating Voltage	200 V to 30 kV
6	Probe current	1 µA to 2 µA
7	Scanning Speed	From 20 ns to 10 ms per pixel
8	Number of ports	11
9	Chamber suspension	Pneumatic
10	Specimen Stage type	Motorized, Compucentric
11	Stage Movements	X= -40 mm to + 40 mm Y= -30 mm to + 30 mm Z= 47 mm Rotation: 360º continuous Tilt: -80º to + 80º

Fig. 3.11 Scanning Electronic Microscopy.

3.9.6 Energy dispersive spectroscopy (EDS)

The energy dispersive X-ray spectroscopy (EDS) was utilized to study the chemical composition of the material. The EDS analysis were conducted by applying SEM equipped with EDS system. Line intercept method was employed for analyzing grain size. For the measurement of grain size ASTM E 112 standard was used.

3.9.7 X-ray diffraction (XRD)

PANalytical's X-ray diffractometers is used to study the phase formation of fabricated sample. A detailed specification of PANalytical's X-ray diffraction are given in Table 3.12 and schematic diagram of machine is represented in Fig. 3.12.

Fig. 3.12 Schematic diagram of X-Ray diffraction set-up.

Table 3.12 Specifications of X-Ray diffraction.

S. No.	Details	Specifications
1	Make	PANalytical
2	Model	X'Pert pro
3	Diffraction type	DY 1850
4	Tube anode	Cu
5	Ration Alpha 1:2	0.5000
6	Divergence slit	Prog.Div.Slit
7	Receiving slit	Prog.Rec.Slit
8	Generator voltage (kV)	40
9	Tube current (mA)	45
10	Detector	X'celerator
11	Data angle range (^{0}2Θ)	2.000-40.000
12	Scan type	Continuous

3.10 Mechanical testing

3.10.1 Microhardness test

Hardness (Hv) is well-defined as the resistance of the material to the indentation. For conducting the microhardness test, the samples were prepared as shown in Fig. 3.13. In order to characterize the FSWed surface, hardness test was performed by using Vickers digital microhardness tester (Make: Chennai Metco Pvt. Ltd, Chennai, Model: ECONOMET VH-1 with Monitor attachment consist CCD Camera, Adapter and Monitor) as shown in Fig. 3.16 and mentioned below the specifications in Table 3.13. Figs. 3.14 and 3.15 show, the microhardness measurement direction (X-X and Y-Y) of samples fabricated with multi hole and multi groove techniques (pin region and pin + shoulder region).

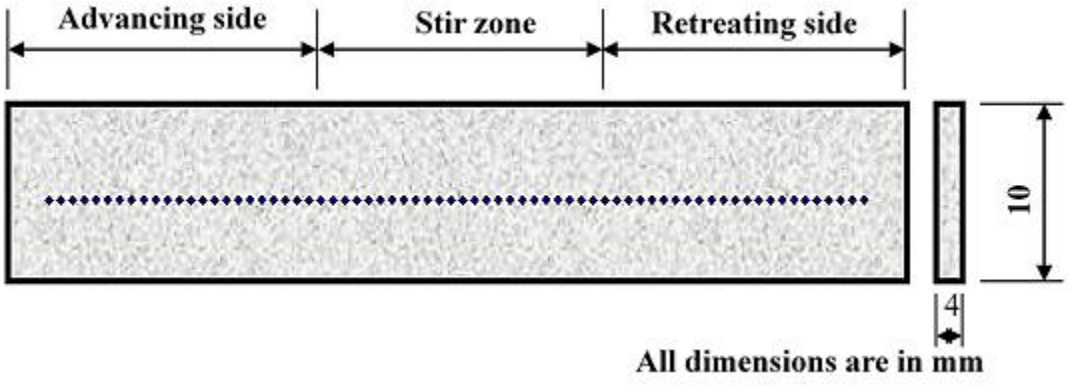

Fig. 3.13 Schematic sketch of microhardness sample.

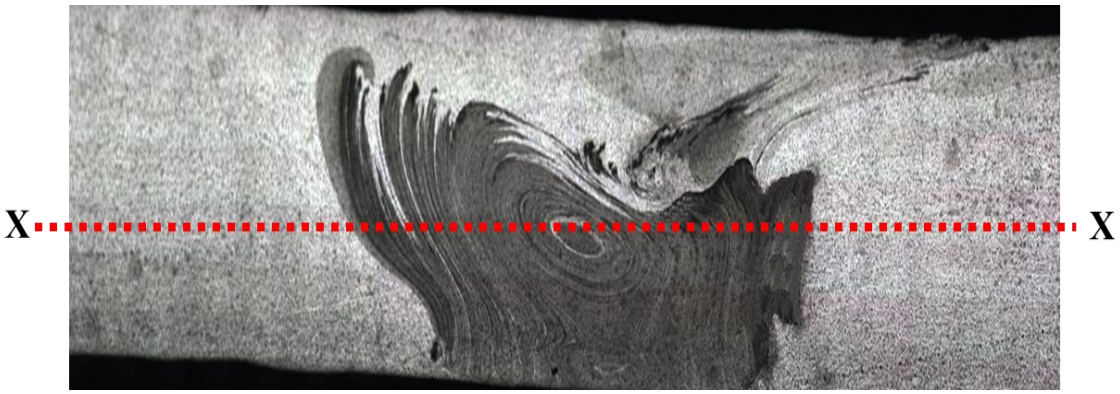

Fig. 3.14 Microhardness measurement at pin driven region in X-X direction (pin region).

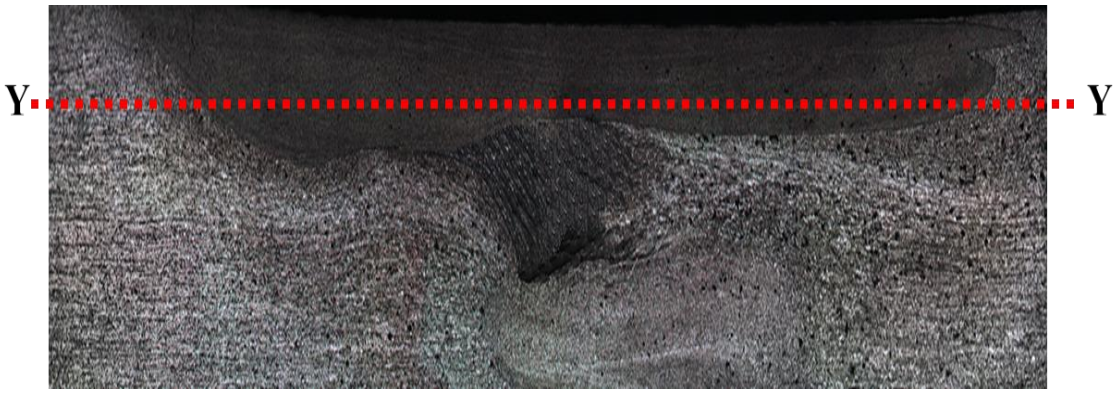

Fig. 3.15 Microhardness measurement at Shoulder driven region Y-Y direction (shoulder region).

Fig. 3.16 Vicker's microhardness tester.

With this instrument indentation can be measured clearly; use of 10X and 40X lens makes a wider measurement field. This instrument has a digital microscope to observe the microstructure of specimens and hardness value can be directly seen on the LCD screen. This is used for all type of metals like steels, super alloys, ceramic based and coatings etc. The testing force ranges from 10 to 1000 grams and magnification of microscope is 100X and 400X.

Table 3.13 Specifications of microhardness tester.

Sr. No.	Details	Specification
1	Objective Lens	10X and 40X
2	Testing Force	10 gf to 1000 gf
3	Loading Control	Automatic (Loading, Dwell, and Unloading)
4	Dwell time of the test force	0 to 60 secs
5	Resolution	0.0625 Microns
6	Range	8-2900 HV
7	Data Output	LCD Screen
8	Accuracy	EN-ISO6507, Instrument Throat: 95 mm
9	X-Y Testing table	100×100 mm
10	Indenter	Vickers
11	Power Supply	10V/230V, 60/50 Hz
12	Overall Dimension	405×290×480 mm

3.10.2 Tensile test

Tensile test samples were cut from the fabricated surface nanocomposites using Wire cut EDM machine. For tensile test, all the samples are sectioned as per ASTM: E8/E8M-11 standard along the processed direction. Fig. 3.17 shows the tensile test specimen schematic diagram. The tensile tests were carried out at 0.1 mm/min constant cross head speed until failure of the specimens on a computer controlled universal testing machine. Before starting the experiment, all the gauge lengths of the specimens were measured and recorded.

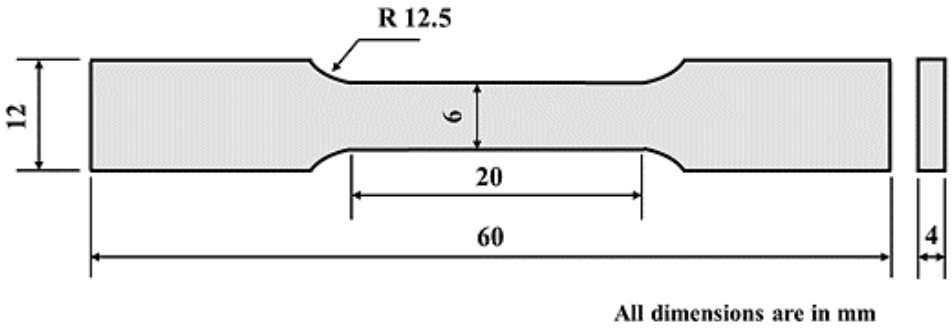

Fig. 3.17 Schematic sketch of tensile specimen.

The tensile machine used for tensile testing is a HEICO (HLC 693-30) Universal Testing Machine (UTM) shown in Fig. 3.16. The specifications of the UTM are given in Table 3.14.

Table 3.14 Specification of UTM (HEICO (Hydraulic and Engineering Instruments)).

Sr. No	**Details**	**Specifications**
1	Model	HLC 693-30
2	Capacity	20 kN
3	No of columns	2
4	Max Speed (mm/min)	500
5	Min Speed (mm/min)	0.01
6	Max Force at full speed (kN)	20
7	Max Return Speed (mm/min)	1000
8	Position Control (mm)	0.5
9	Total Crosshead travel (mm)	1130
10	Max Power Required (VA)	1000
11	Dimension (LxBxH) (mm)	760 x 600 x 2000

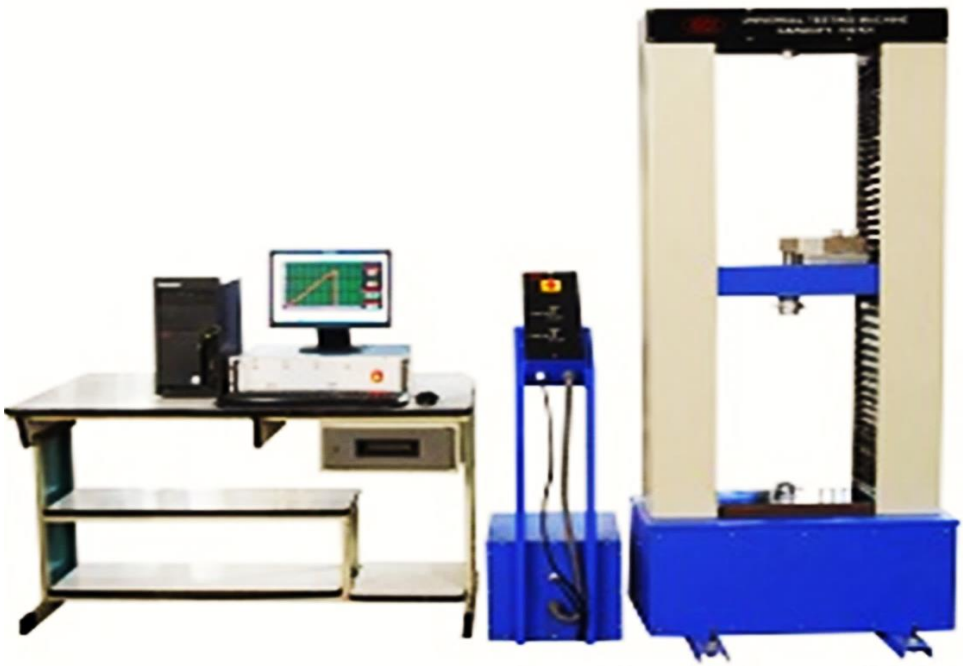

Fig. 3.18 HEICO (HLC 693-30) universal testing machine.

3.10.3 Wear test

To study the wear behavior of the fabricated composites, wear test is performed on a pin-on-disk tribometer and the samples were made as per ASTM: G99-05 standard. Fig. 3.19 shows a pin-on-disk tribometer and complete details of it are given in Table 3.15.

Fig. 3.19 Pin on disc friction and wear testing machine.

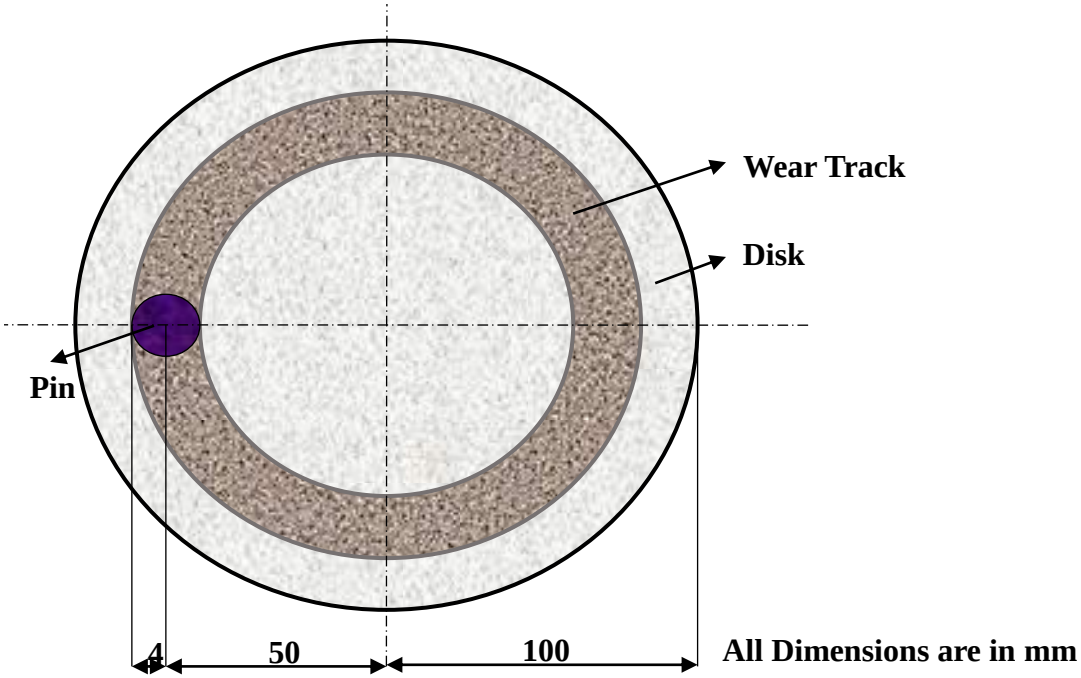

Fig. 3.20 Schematic configuration of pin-on-disk tribo meter.

Table. 3.15 Specifications of pin on disc friction and wear testing machine.

Sr. No.	Details	Specifications
1	Make	Magnum Engineers
2	Model	TE-165-LE
3	Pin Dimension	φ3- φ12 mm, 25-30mm
4	Ball Diameter	10mm
5	Disk Material	EN31 steel
6	Size	φ165mm, 8mm thickness
7	Wear track	50-100mm
8	Disk Rotation	200-2000 rpm
9	Normal load range	5-200 N
10	Wear measurement range	0-2000 μm
11	Frictional force range	0-200 N with a resolution of 1N with tare facility

Wear test samples were cut from the stir zone (SZ) with the diameter of 8 mm. Dry sliding wear tests were conducted at constant load of 20 N, rotational speed of 450 rpm and sliding speed of 3 m/s. Fig. 3.20 shows the schematic diagram of pin-on-desk tribo meter.

Wear rate is calculated by,

Wear rate (mm^3/m) = Volume loss/Sliding distance.

3.11 Conduct the experiments as per the plan given below

3.11.1 Determine the working range of the identified process parameters

Pilot experiments were performed at various working range of tool rotational speed, and weld speed was explored using taper threaded cylindrical tool. It was observed that at tool rotational speed of 900 rpm and weld speed of 40 mm/min, better mechanical properties were obtained. The experiments were conducted as per the plan shown in Table 3.16.

Table 3.16 FSP process parameters.

Process parameters	Values
Pin profile	Concave shoulder tapered threaded cylindrical
Rotation Speed (rpm)	900, 1150 & 1400
Welding Speed (mm/min)	15, 20, 30 & 40
Axial Force (KN)	5
Pin Length (mm)	3.7
Shoulder diameter, Ds (mm)	24 & 21
Pin diameter, Dp (mm)	7 & 5
Tilt angle (degree)	2.5
Tool material	AISI H13 tool steel

RESULTS AND DISCUSSIONS

This chapter deals with the characterization of Al/Al_2O_3, Al/SiC and $Al/(Al_2O_3 + SiC)$ surface nanocomposite produced by friction stir processing. The effect of process parameters (tool rotational speed & traverse speed), tool shoulder geometry and nano reinforcements particles (Al_2O_3 & SiC) on microstructural, mechanical and wear properties of Aluminum alloy based surface nanocomposites produced by FSP were studied.

In this chapter, several novel techniques (multi hole & multi groove) were implemented to improve the microstructural, mechanical and wear properties of surface nano composites fabricated by FSP. To understand the characterization of novel techniques, all the fabricated surface nanocomposites were tested, analyzed and results were drawn briefly. The observations on microhardness, ultimate tensile strength (UTS), yield strength (YS), Percentage of elongation (%EL) and wear rate of surface nanocomposites and as-received Al alloy are illustrated.

4.1 Effect of tool rotational speed, traverse speed and tool shoulder geometry on fabrication of Al/Al2O3 surface nanocomposite by FSP

Fabrication of the surface nanocomposites by FSP is mainly affected by the process parameters (tool rotational speed and traverse speed) and tool geometry. A great deal of efforts has been embraced towards understanding the effect of process parameters on the material flow behavior, defect formation, microstructure formation, mechanical and wear properties of friction stir processed surface nanocomposites. Finding the most effective process parameters, shoulder geometry for fabrication of surface nanocomposites as well as realizing their influence on the microstructure, mechanical and wear properties. The surface nanocomposite of AA 6061-T6 Aluminum alloy and Al_2O_3 nano reinforcement were fabricated at various combinations of process parameters and tool shoulder geometry are presented in Table 4.1. Two different tool shoulder geometries (diameters: Ds = 24 and 21 mm) are selected for fabrication process.

Table 4.1 Different tool rotational speed, traverse speed and tool shoulder geometry for fabrication of surface nanocomposites.

Process parameters	Concave shoulder taper cylindrical threaded tool (Ds = 24 mm)	Concave shoulder taper cylindrical threaded tool (Ds = 21 mm)
Tool rotational speed (rpm)	900, 1150 and 1400	900, 1150 and 1400
Tool traverse speed (mm/min)	15,20,30 and 40	15,20,30 and 40

Ds = Shoulder diameter

4.1.1 Surface appearance of fabricated surface nanocomposite

Fig. 4.1 shows the successfully fabricated defect-free Al/Al_2O_3 surface nanocomposites. From the visual examination, it is observed that the fabricated surface nanocomposites were formed with semicircular structure on the processed surface region with crowns (material flash) on the retreating side (RS) (K. Colligan, et.al. 1999) [1]. There are no such visible macro deformations and defects observed in all other obtained surface nanocomposites. Depending on tool rotational speed, and traverse speed of FSP produces various surface finished composites. All the surface nanocomposites were produced by applying single pass FSP. The appearance of the fabricated surface nanocomposites was excellent and reveals the characteristics of an existing hole at the end of the process.

Fig. 4.1 Fabricated Al/Al_2O_3 surface nanocomposite.

4.1.2 Microstructure

Microstructural investigations of fabricated surface nanocomposites were done by using different techniques such as stereo zoom microscopy, inverted optical microscopy (OM) and scanning electron microscopy (SEM). Microscopic examinations reveal that the process variables have a significant impact on the fabrication of surface nanocomposites. Fig. 4.2 shows flow partitioned deformation zone. From the Fig. 4.2 it is observed that, the friction stir processed region is mainly divided into two regions (advancing side (AS) & retreating side (RS)) with respect to the tool rotational and traverse directions. From the Fig. 4.2 it is shown that, the friction stir processed region or deformation zone or processed region is manly divided into three regions like mechanically mixed region (MMR), severe induced plastic region (SIPR) and unmixed region (UMR) ([2,3].

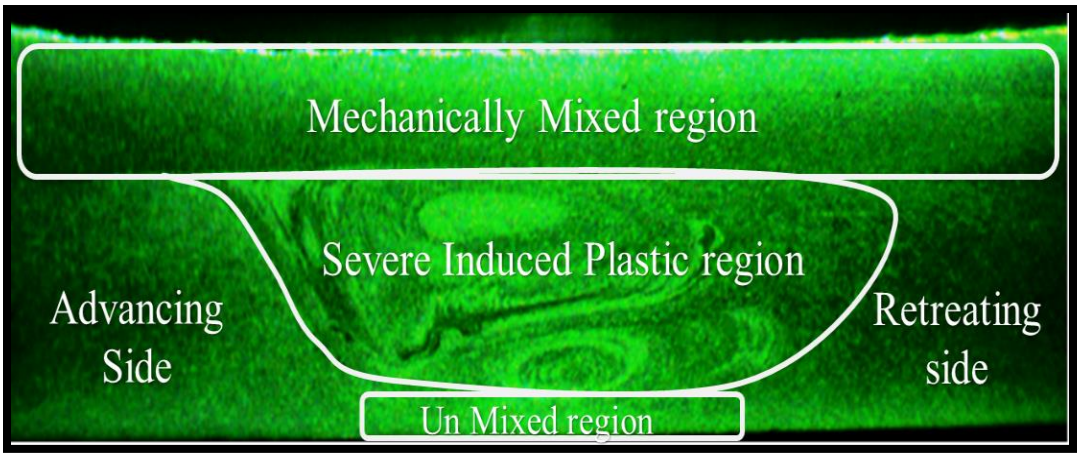

Fig. 4.2 Flow partitioned deformation zone in FSP.

Fig. 4.3 shows the material flow pattern occurred during the fabrication of Al/Al_2O_3 surface nanocomposite. Initially, as the tool rotates steadily the plasticized material presented on the bottom of the probe or pin is forged towards MMR on RS. The rotating motion of the tool drag the plasticized material presented on the RS towards MMR of AS. Later the material is converged by the tool shoulder towards SIPR on AS. At this period, the highly plasticized material travers extreme downwards to reach the bottom of the pin to complete the flow pattern. Like this, the plasticized material completes its flow pattern in the deformation zone during the fabrication process.

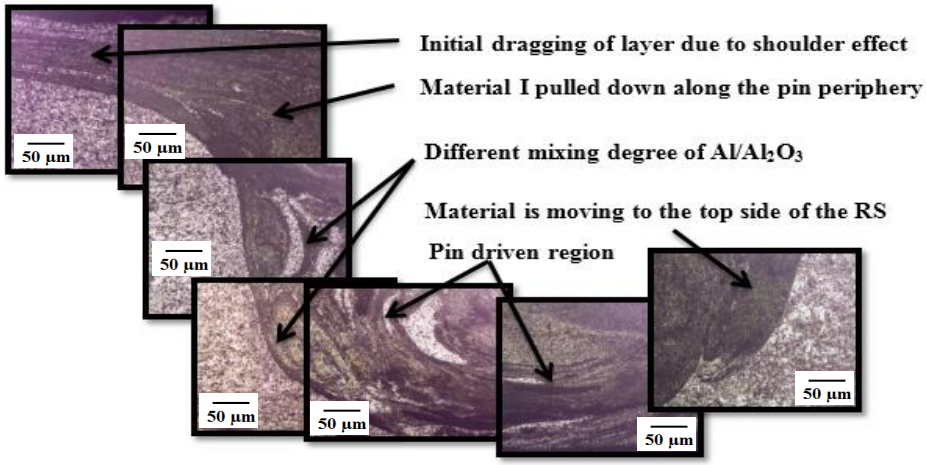

Fig. 4.3 Material flow pattern during the fabrication in FSP.

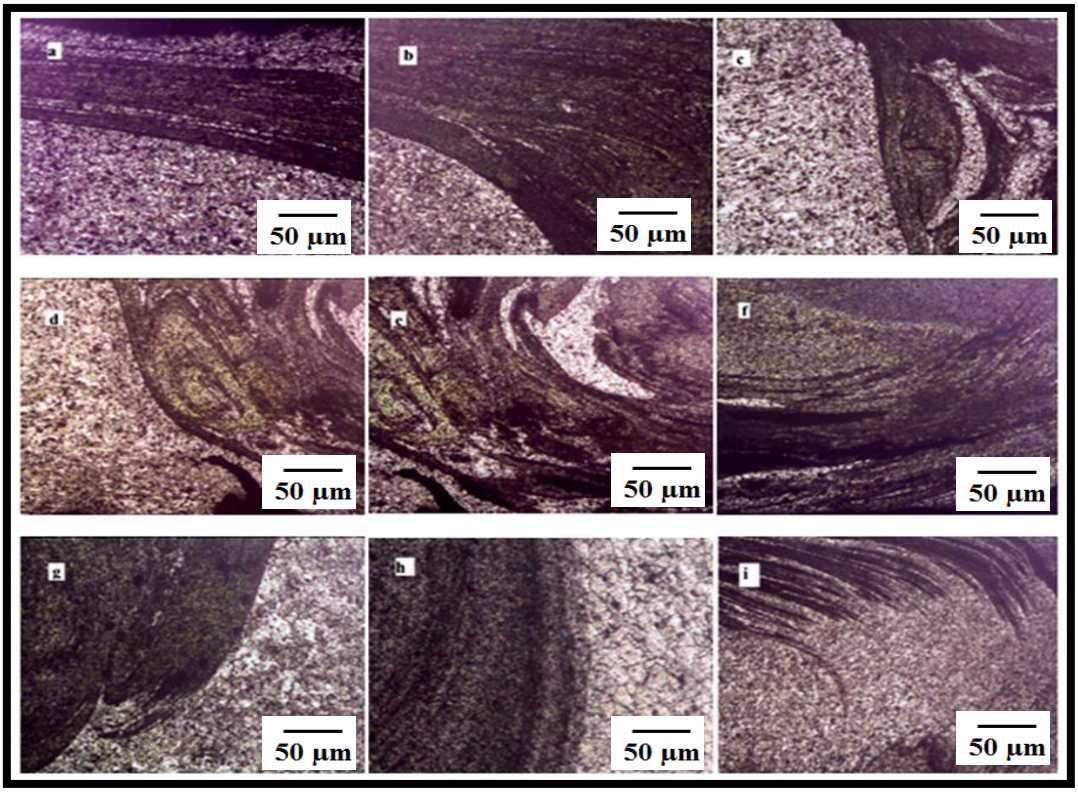

Fig. 4.4 Flow of material in processed zone in FSP: (a) material flow at upper surface of the RS; (b) shoulder and the pin interface region; (c) flow of the material at severe induced plastic region; (d) stir zone on AS; (e) stir zone on RS; (f) microstructure of the un-mixed region (UMR); (g) rising material flow towards RS at beneath the pin; (h) rising material flow towards RS at SZ; (i) the material is dragged and converges towards AS.

Fig. 4.4 shows the sequential order of flow pattern occurred during the fabrication process. Fig. 4.4(a) shows the dragged plasticize material from RS to AS is presented on MMR. Fig. 4.4 (b) shows the converging material flow by the shoulder of the tool towards SIPR. Figs. 4.4(C) and (d) show the severe plasticized material is travelling towards bottom of the pin on AS due to the large downward forces applied on the tool during the process. From the Figs. 4.4(e) and (f) it is observed that, the severe plasticized material travelled beneath the pin and occupied complete stir zone (SZ). At bottom of the pin the flow of material readily rises and merges with the material presented on RS. A rising material flow towards RS can be observed from the deformation zone shown in Fig. 4.4(g) and (h). At the top surface of the deformation zone, the material is dragged and converges towards AS of the material as shown in Fig.4.4(i). During the friction stir processing, the frictional heat generates between the tool contact region and the surface of the base material. This heat dissipated during the process makes several changes in terms of material flow and grain size and grain structure. From the Fig. 4.5, it is tried to explain the friction heat effect on the microstructural properties of surface nanocomposite.

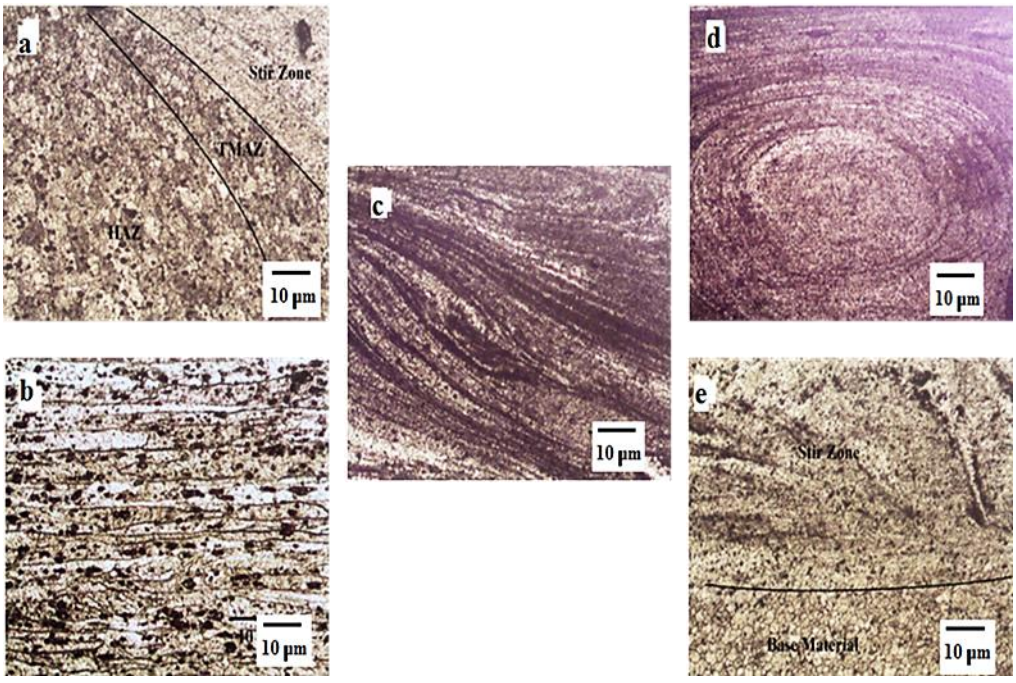

Fig. 4.5 Different regions and zones of fabricated Al/Al_2O_3 surface nanocomposite: (a) transitional regions of fabricated composite; (b) un-affected region; (c) mechanically mixed region (MMR); (d) severe induced plastic region (SIPR), (e) un - mixed region (UMR).

Fig. 4.5(a) shows that three different transitional zones (stir zone (SZ), thermo-mechanically affected zone (TMAZ), and heat affected zone (HAZ) [4]) occurred during the fabrication of surface nano composite. During the process, frictional heat is produced between the tool probe and workpiece and it dissipates along the retreating side and advancing side. The level of heat dissipation in the processed region causes various transitional zones. Fine grains were observed at SZ and it is evident from dynamic recrystallization which occurred during the process in the SZ because of pinning effect. Severely coarsened grains were observed at TMAZ and coarsened grains were formed at HAZ. Long elongated grains structure was observed at base material shown in Fig. 4.5(b). Fig. 4.5(c) shows the material from the MMR departing towards SIPR. On the top of the deformation zone, the material is highly affected by the heat input produced by the shoulder of the tool and it causes a high degree of plastic deformation in the material [7]. A larger contacting area of the shoulder of the tool and work piece generates a high amount of heat. This generated heat leads to mixing of the nano Al_2O_3 particles in the aluminum alloy at higher rate and creates lamellar flow. Fig. 4.5(d) shows a uniform mixed region of nano Al_2O_3 with Aluminum alloy in the SIPR. The region is mainly caused by the probe of the tool which is evident from the dynamic recrystallization. A rich amount of nano Al_2O_3 reinforcement particles with aluminum alloy material flow is formed like clockwise rotating cells (onion ring like structure).

Fig. 4.5(e) shows, unmixed region (UMR) beneath the tool probe at the bottom of the deformation zone. It is clearly observed that fine equiaxed grains are formed in the SZ but a larger stressed grain is produced in the unaffected region. A lamellar type of a material flow is observed in the MMR caused by the shoulder of the tool [8]. In this region, the force applied on the composite during the process and the traverse speed creates severe plastic deformation and forms a lamellar flow in the MMR. The banded like structure consisting of alternative lamellae of mixed material (Al/Al_2O_3) becomes narrower in the width of 6061– Al lamellae with increasing distance from the center of the weld. During the process, the material underneath the probe flows towards upper surface of the retreating side (RS) along the traverse speed and dragged towards advancing side of the deformation zone.

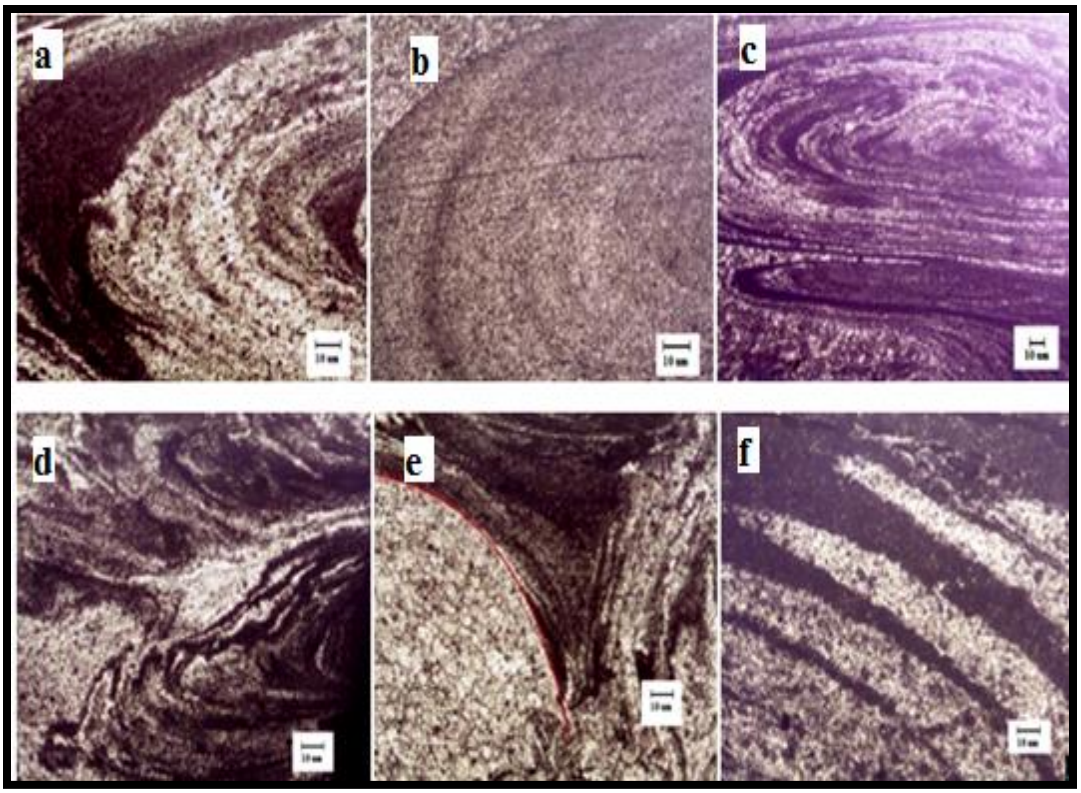

Fig. 4.6 Different types of material flow occurred during the fabrication process: (a) dark and white flow combination in the SZ, (b) uniform mixture of nano particle in the SZ, (c) onion rings formed at SZ, (d) un even mixture of nano particle at SZ, (e) material is forged by the tool shoulder into the SZ, (f) vortex-flow caused by the tool shoulder.

In the fabrication of surface nanocomposites, different kinds of material flows were observed. Fig. 4.6(a) shows the dark and light flow combination in the SZ. The rich amount of Al_2O_3 particles appeared as a dark region and less amount of reinforcement particles shown as a white region. Fig. 4.6(b) shows an abundant amount of nano Al_2O_3 particles were found in SZ. Uniformly distributed Al_2O_3 particles can be seen in the SZ because of high tool rotational speed and low traverse speed. High rotation speed and traverse of the tool creates onion rings like structure into the flow because of high traverse and rotational speeds require faster completion of material flow around the tool pin as shown in Fig. 4.6(c). But sometimes the material flow was unable to complete full rotations; at this period and the material takes back turn and forms multiple onion rings in the processing region [9]. From Fig. 4.6(d) it is observed that, uneven distribution of the nanoparticles into the base material takes place. Fig 4.6(e) shows that the material is forged by the shoulder and dragged towards the deformation zone due to large

downward forces acting on the tool. The vortex-like flow is caused by the tool shoulder featured at SPFR is shown in Fig. 4.6(f).

In friction stir processing, fabrication of defect-free surface nanocomposite mainly depends on the process parameters like tool rotational speed, traverse speed and tool geometry. The improper combination of the process parameters produces defective composites and also effects the surface finish of the composite. From the Figs. 4.7 and 4.8 it is tried to explain the effect of process parameters and tool shoulder geometry on fabrication of surface nanocomposite by FSP. In this research work, initially two tool shoulder diameters (Ds = 24 and 21 mm) are selected for fabrication of surface nanocomposites by FSP. By varying the combinations of process parameters, the surface nanocomposites were produced.

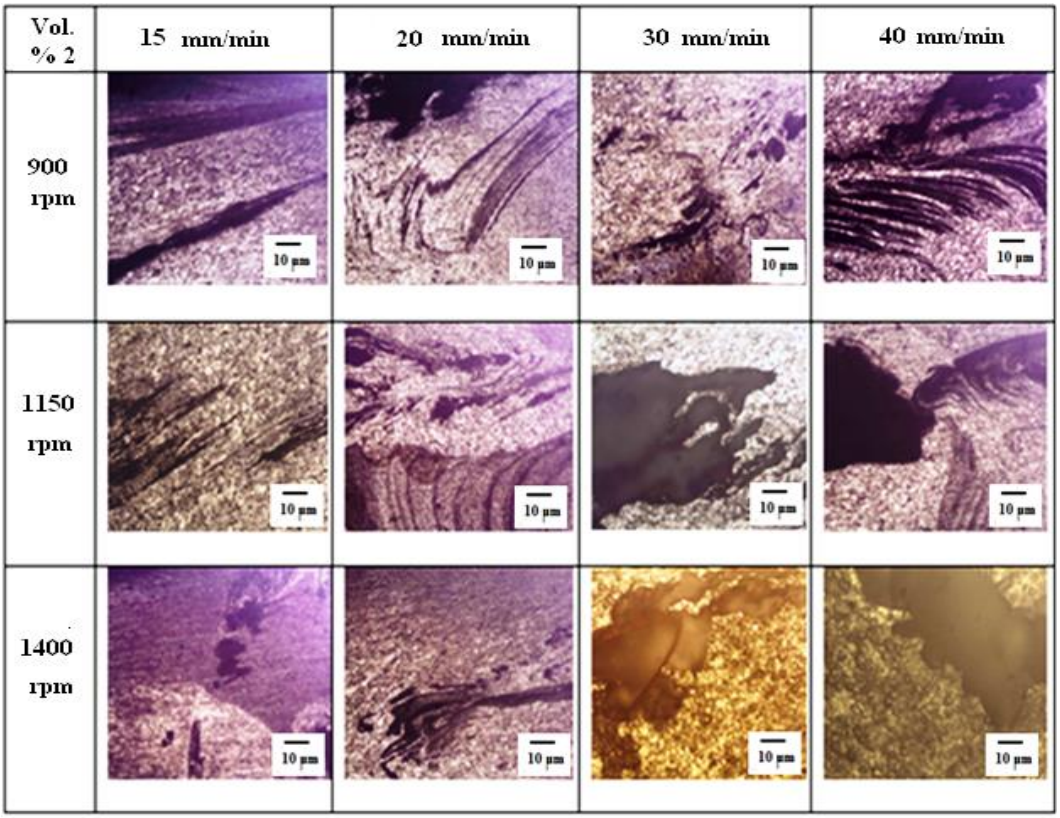

Fig. 4.7 Ds = 21 Microstructures of surface nanocomposites at various tool rotational speeds and traverse speeds.

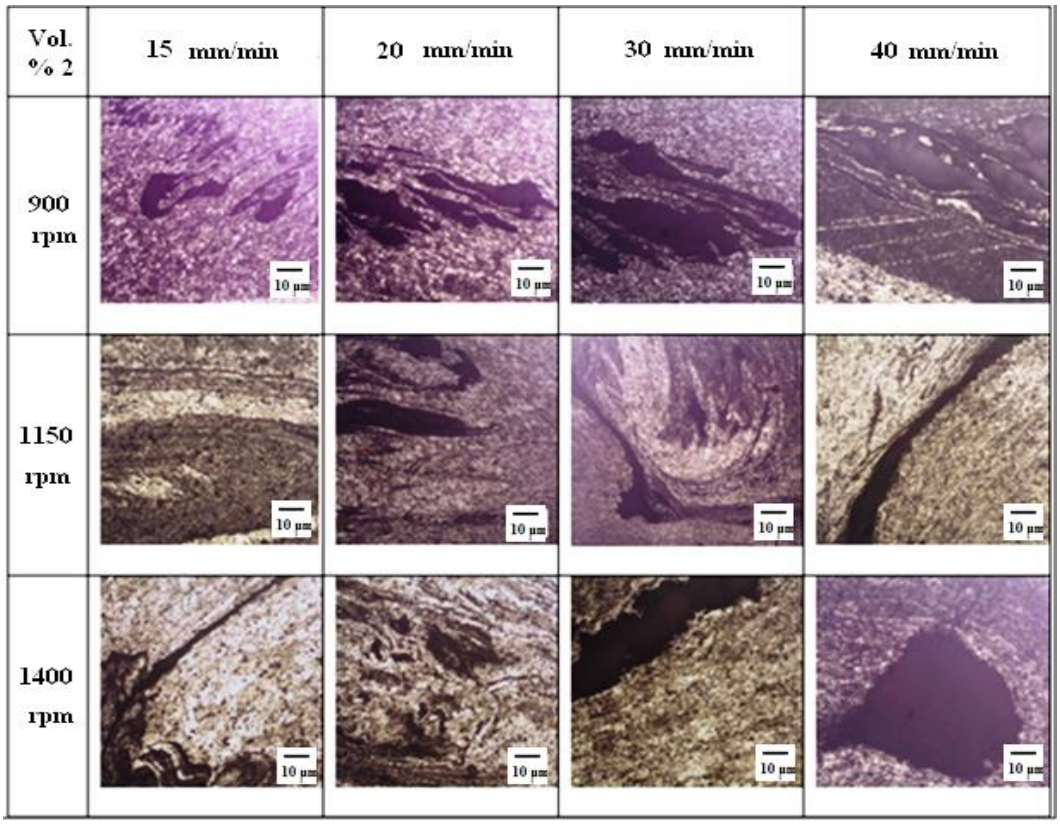

Fig. 4.8 Ds = 24 Microstructures of surface nanocomposites at different tool rotational speeds and traverse speeds.

Fig. 4.7 shows the microstructure of composites by using tool shoulder diameter of 21 mm and Fig. 4.8 shows the microstructures of produced composites using tool shoulder diameter of 24 mm. At constant tool rotational speed of 900 rpm with varying traverse speed like 15, 20, 30 and 40 mm/min, all the fabricated surface nanocomposites exhibited defects. From the micrographs it is revealed that, the distribution of the nano reinforcement particles was not uniform in the deformation zone and mixing with the matrix material (aluminum) was improper which causes agglomeration in the SZ. Insufficient heat generation during the process causes the agglomeration and inadequate material flow in the deformation zone. The defect formation in the composites increased with increase in traverse speed from 15 to 40 mm/min. Insufficient heat generation causes wormhole defects on the AS of processed region. A good dispersion of reinforcement particles into the deformation zone is observed at 1150 rpm tool rotational speed with traverse speed 15 mm/min. At a tool rotational speed of 1150 rpm and 15 mm/min traverse speed, a defect-free surface nanocomposite was obtained by using 24 mm shoulder diameter of

tool shown in Fig. 4.8. But under the same conditions, by using 21 mm shoulder diameter tool with concave shoulder, micro cracks were observed as shown in Fig. 4.7. It shows insufficient heat was supplied which resulted deficient material flow. At constant tool rotational speed of 1150 rpm with varying traverse speed of 20, 30 and 40 mm/min, the fabricated composite found to be defective as shown in Figs. 4.7 and 4.8. With the increase in traverse speed, the defect size is increased from micro cracks to voids due to insufficient heat generation.

At high tool rotation speed like 1400 rpm, the distribution of the reinforcement particle was uniform than other speeds. High frictional heat plasticizes the base material easily and creates a path to reinforcement particles to mix with the base material. Some onion rings may occur at high tool rotational speeds. The material flow in the deformation zone primarily depends on traverse speed of the tool. Improper material flow leads to defect formation during the fabrication. Distribution of a reinforcement particle into the metal matrix is a significant task during the fabrication of surface nanocomposites. At lower tool traverse speed of 15 mm/min, the distribution of the reinforcement particles was uniform and it increases the average spacing between reinforced particles and this helps to disperse the reinforcement particle freely into the matrix material. Higher residing time of the friction which results in higher plastic strain helps to plasticize more amount of the material leading to increase in large region of the surface composite. Figs. 4.7 and 4.8 show the defective microstructures even at higher tool rotational speed of 1400 rpm with 15, 20, 30 and 40 mm/min. All the combination of process parameters with changing tool shoulder diameter 21 and 24 mm, the fabricated surface nanocomposite shown defects due to excessive frictional heat generation. Micro voids, voids and tunnel defects were observed at these conditions. From these microstructural studies, it is observed that the fabrication of defect-free surface nanocomposite mainly depends on selection of suitable process parameters and tool geometry.

4.1.3 Microhardness

The hardness of the fabricated surface nanocomposites mostly depends on the grain structure, grain size, addition of reinforcement particles and type of reinforcement particles and etc. All the fabricated Al/Al_2O_3 surface nanocomposites were tested under the same condition (25 gm of load with 10 seconds dwell time) and the results were drawn in the form of graphs as shown in Figs. 4.9 and 4.10.

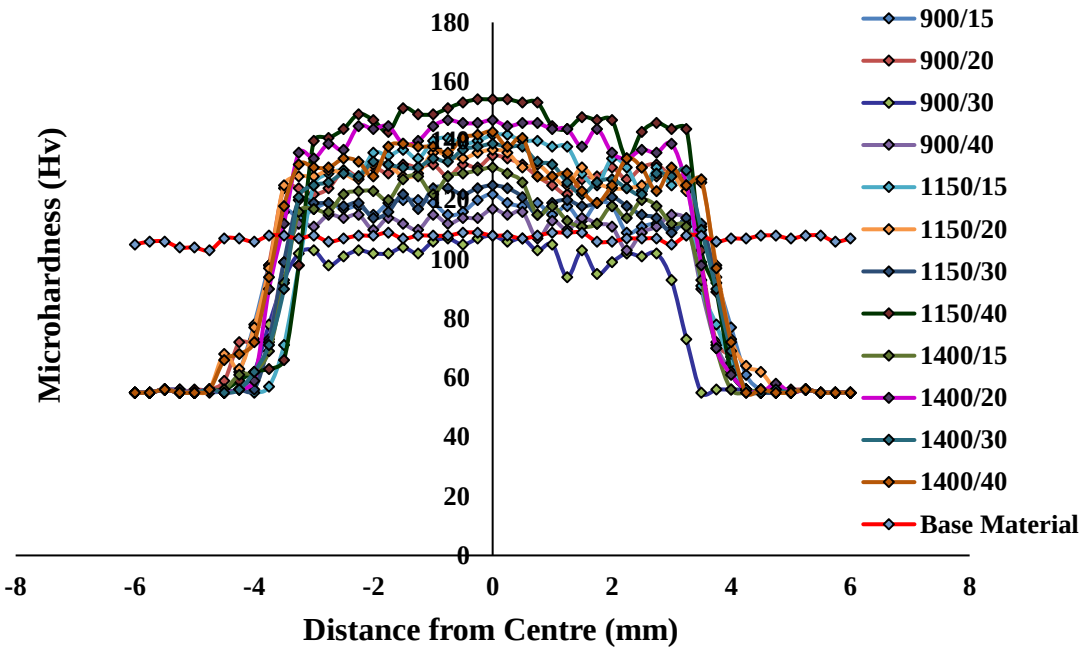

Fig. 4.9 Microhardness survey of fabricated surface nanocomposites and base material (Ds = 21).

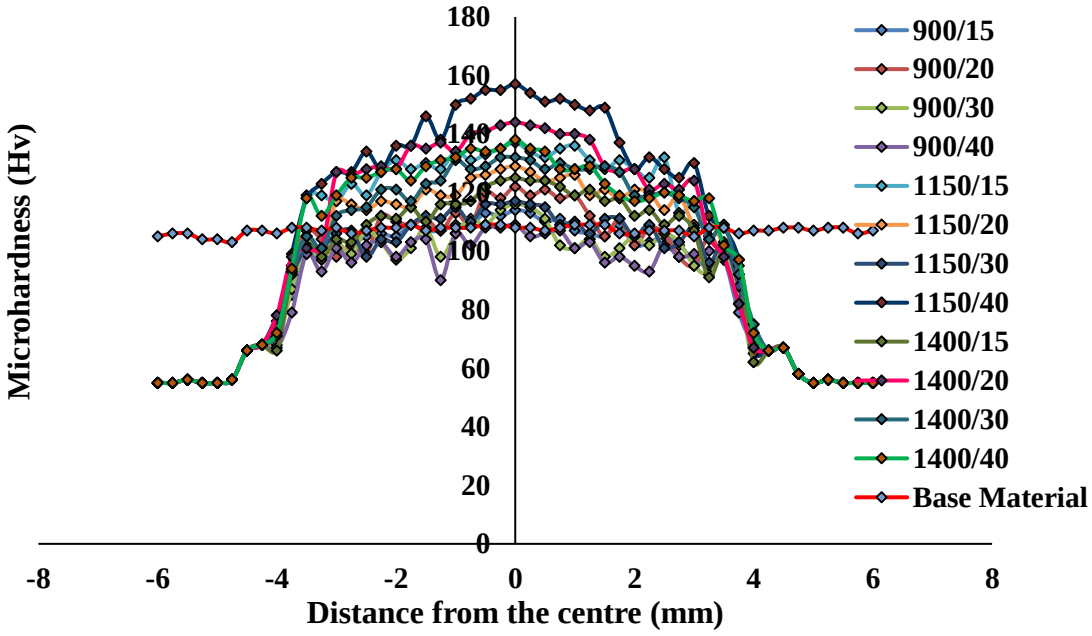

Fig. 4.10 Microhardness survey of fabricated surface nanocomposites and base material (Ds = 24).

From the Fig. 4.9 and 4.10 it is revealed that, the addition of Al_2O_3 reinforcement particles showed higher microhardness values than as received Al alloy. The occupancy of the

reinforcement particle is mainly at the grain boundaries of the base material which restricts the grain growth and leads to fine grain structure. Here the hardness of the surface composites was increased based on strengthening mechanisms (Hall-Petch relation and Orowan theory) [15]. Figs 4.9 and 4.10 show the microhardness values of the Al/Al_2O_3 surface nanocomposites at different process conditions. Higher microhardness values were obtained at 1150 rpm with 40 mm/min condition and lower hardness values were obtained at 900 rpm with 20 mm/min. At defect-free condition, an average of 132 Hv microhardness was obtained by using Ds = 24 shoulder diameter tool. From the results, it is observed that the addition of the Al_2O_3 nano reinforcement leads to increase in microhardness of the aluminum matrix material.

4.1.4 Tensile and fractography

The tensile test was performed at defect-free condition (1150 rpm/15mm/min) obtained by the tool having a shoulder diameter of 24 mm and this was compared with the result of 6061 T6 Al alloy properties. The obtained tensile properties (Yield strength (YS), Ultimate tensile strength (UTS) and Elongation (El)) of fabricated Al_2O_3 reinforced aluminum surface nanocomposites are shown in Table 4.2. Fig. 4.11 shows the SEM fractography of the fabricated surface composite obtained at best condition i.e., 1150 rpm tool rotational speed with 15 mm/min tool traverse speed by using 24 mm shoulder diameter.

Table 4.2 Mechanical properties of Al/Al_2O_3 surface nano composite at 2 Vol.% and 6061-T6 alloy.

Sample	**Ultimate Tensile Strength(UTS, MPa)***	**Yield Strength (YS, MPa)***	**Percentage of Elongation (%EL)***
BM	296	272	12
Al/Al_2O_3	176	102	9.4

*Average of three values, base material (BM)

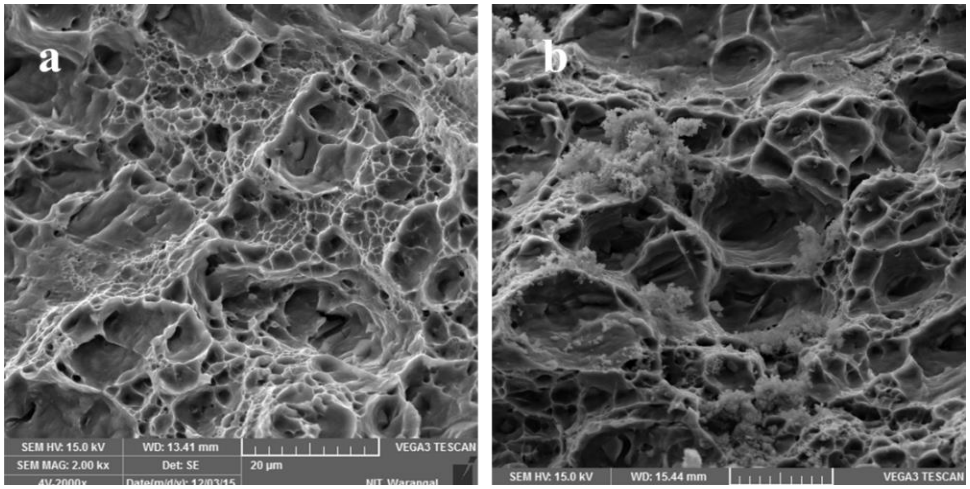

Fig. 4.11 SEM fractography of base material and Al/Al_2O_3 surface nanocomposite. (a) base material; (b) Al/Al_2O_3 surface nanocomposite.

The FSPed nano particles composite shows finer dimples, which are associated with finer reinforcement of nano particles in the base material. The increase in dislocation density causes the reduction of elongation. The nano reinforced composites and fracture morphologies shows larger dimple size with reduced ductility. With the combination of Al_2O_3 particles and aluminum matrix material, the composite is becoming brittle to some extent in nature. The failures were of ductile type failure since the characteristic fine dimples were observed. Cup and cone like failure can be observed.

4.1.5 Wear properties of Al/Al_2O_3 surface nanocomposite

For wear characterization, the samples were made as per standard dimensions. Fig. 4.12 shows the graph between the sliding distance versus rate of wear of fabricated surface nanocomposite and base material (as received). From the starting of the wear test it is observed that, the wear loss is more in base material than surface nano composite. The loss of material from the base material is increased with increase in sliding distance. The difference between the initial and final wear loss of the base material is more than compared with Al/Al_2O_3 surface nanocomposite shown in Fig. 4.12. The same results wear observed in Fig. 4.13.

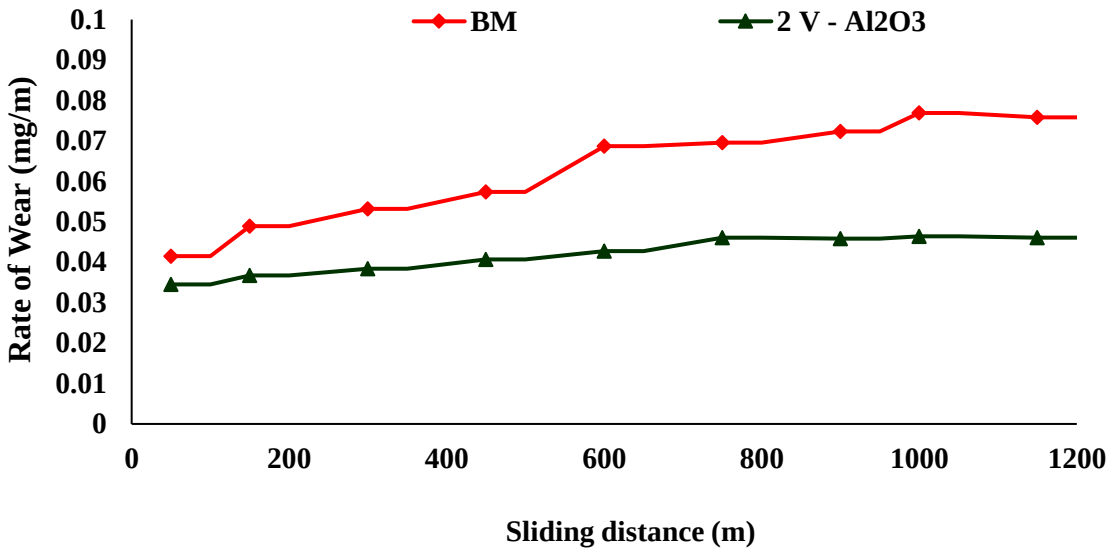

Fig. 4.12 The variation of rate of wear with sliding distance for base material and surface nanocomposite layer.

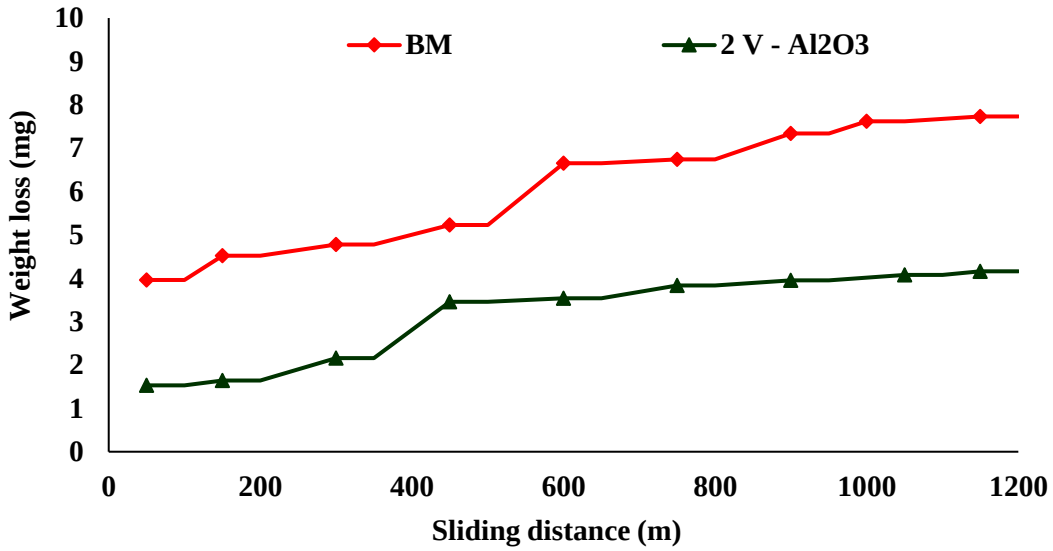

Fig. 4.13 Weight loss change in base material and surface nanocomposite.

From the Fig. 4.13 it is observed that, removal of material from the Al/Al_2O_3 composite and base materials are very less but later with increase in sliding distance, more amount of material is removed from the surface of the base material than Al/Al_2O_3 composite. The loss of material from the surface nanocomposite is very less than base material even at higher sliding distances. Fig. 4.14 shows the coefficient of friction versus sliding distance between the base

material and Al/Al_2O_3 surface nanocomposite. Coefficient of friction of base material is less at initial distances but later it is increased with increase in sliding distance. Uneven change in coefficient of friction is observed in base material than compared with Al/Al_2O_3 composite. The coefficient of friction of base material is an average of 0.53 and Al/Al_2O_3 surface nanocomposite is 0.45 due to the presence of nano reinforcement particles into the matrix acted as load acting barriers at the time of wear test.

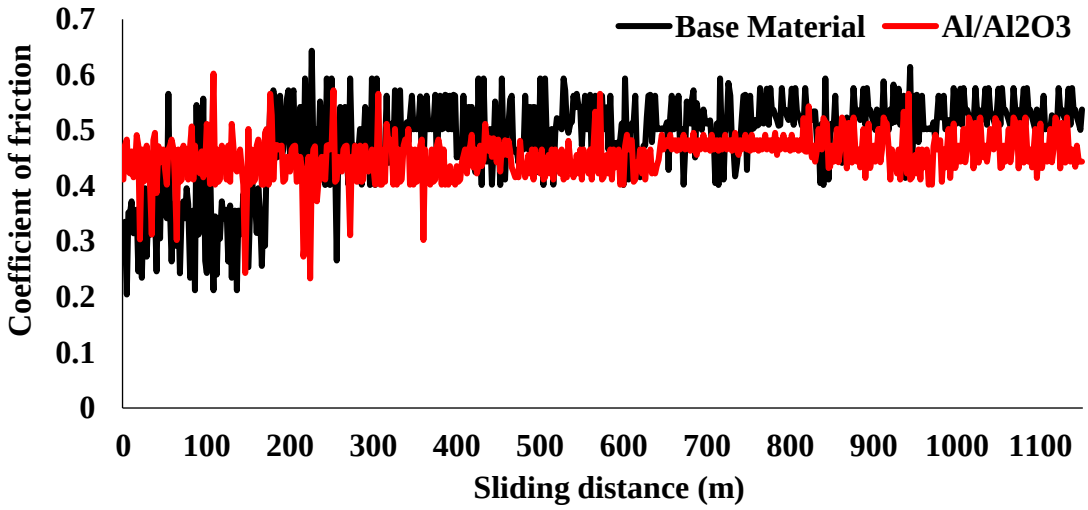

Fig. 4.14 Variation in the coefficient of friction with sliding distance for as-received Al alloy and surface nano composite of Al/Al_2O_3.

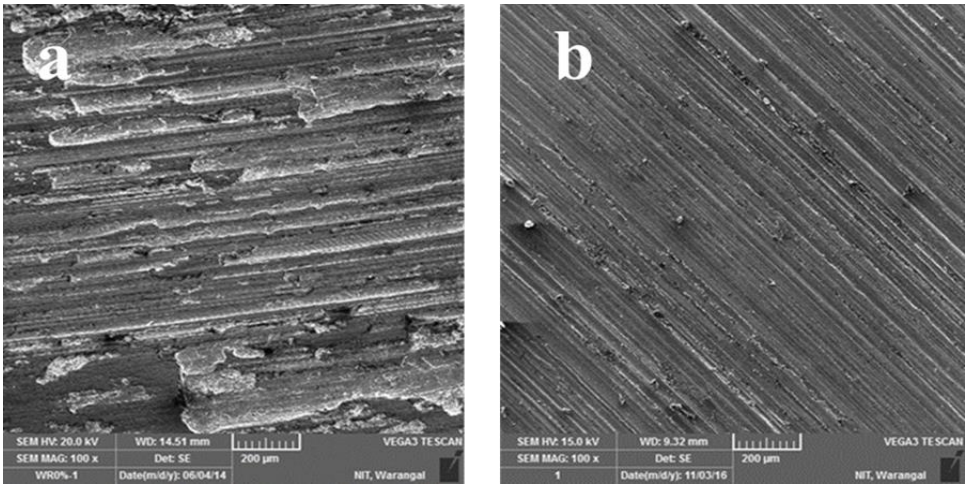

Fig. 4.15 SEM micrograph of the worn-out surface of (a) base material and (b) surface nanocomposite layer.

Fig. 4.15 shows the SEM micrograph of the worn-out surface of the surface nanocomposite and base material of 6061-T6 Al alloy to understand the mechanism of wear. Fig.4.15 it was observed that the coefficient of friction of base material (as-received Al alloy) was gradually increased much higher at initial stages during the process due to joining of the worn debris to the Al surface leads to abrasive wear mechanism and at later stages gets converted to adhesive wear mechanism.

4.2 Influence of Al_2O_3 and SiC on fabrication of composite by FSP

4.2.1 Introduction

The best condition obtained from the section 4.1 i.e. 1150 rpm tool rotational speed and 15 mm/min tool traverse speed was selected to fabricate the surface nanocomposites by varying volume percentage (2, 4 & 6) and reinforcements (Al_2O_3 & SiC).

4.2.2 Surface appearance of fabricated surface nanocomposite

Macroscopic appearances of the fabricated samples are shown in Fig. 4.16. All the composites were found to be defect free and the smoothness of the surface is varied concerning the volume percentage of the reinforcement as well as the type of reinforcement added. Al/Al_2O_3 surface composites exhibits very smooth surface finish than Al/SiC composites. Semi-circular onion ring like structure pattern was observed on the surface of the composites and there are no surface defects were observed [13]. Fig. 4.16(a), (b) and (c) shows the defect-free and smooth surface finished composites which were achieved at 2, 4 and 6 vol. % of Al_2O_3 fabricated by using single pass FSP. All the surface nanocomposites were fabricated at 1150 rpm as tool rotational speed and 15 mm/min as traverse speed. Rough surface finished composites were achieved with increase of reinforcement volume percentage into the base metal.

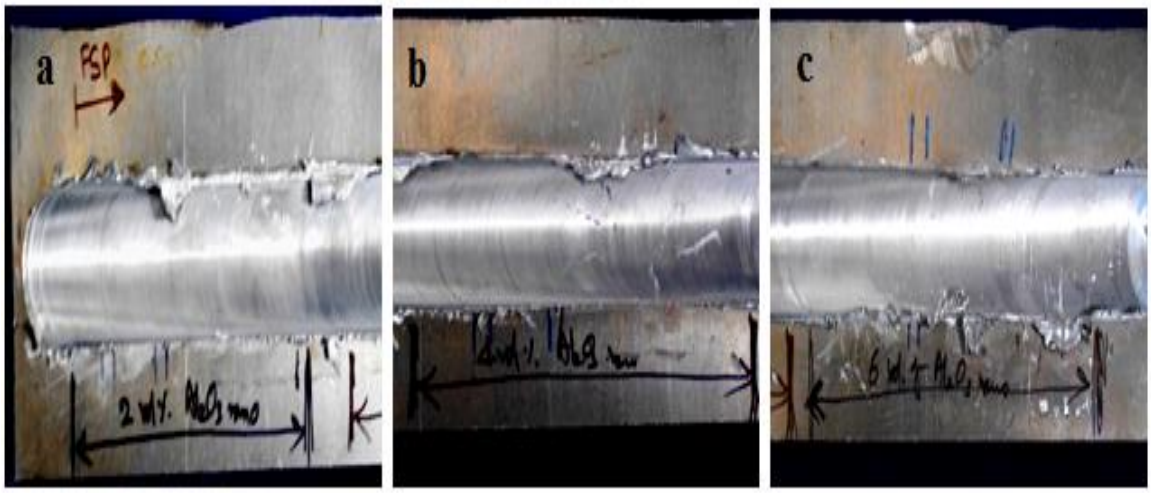

Fig. 4.16 Fabricated surface nano composites at 1150 rpm and 15 mm/min; (a) At 2 vol. % of Al_2O_3; (b) At 4 vol. % of Al_2O_3; (c) At 6 vol. % of Al_2O_3.

4.2.3 Microstructure

Fig. 4.17 shows various transitional zones formed during the fabrication of Al/Al_2O_3 surface nanocomposite. Those are stir zone (SZ) or nugget zone (NZ), thermo-mechanical affect zone (TMAZ) and heat affected zone (HAZ) and are shown in Fig. 4.17(a). Fine equiaxed grains are attributed in SZ due to dynamic recrystallization occurrence because of hot working process shown in 4.17(b). From Fig 4.17(c), coarsened grains and precipitates are observed at the TMAZ and more severely coarsened grain were observed at HAZ.

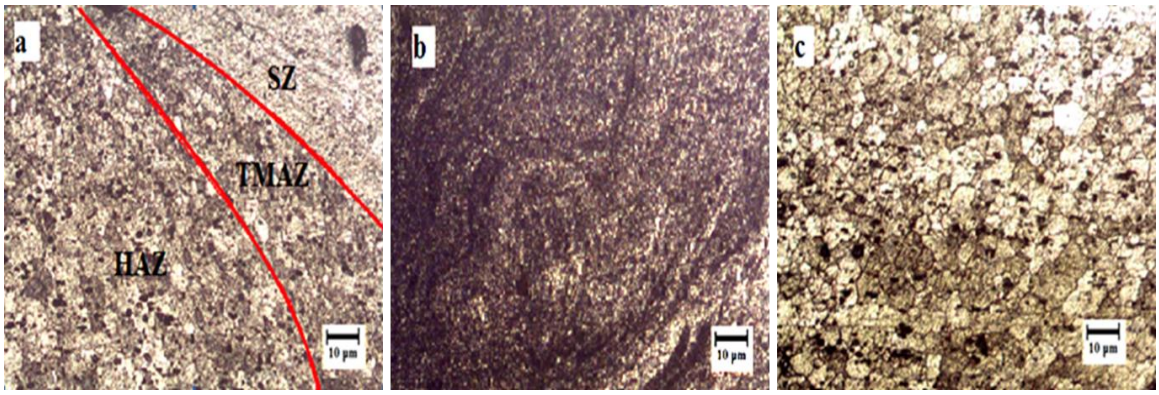

Fig. 4.17 Microstructures at various regions of fabricated Al/Al_2O_3 specimen. (a) transitional zones of composite; (b) fine grains at stir zone; (c) equiaxed grain formed at HAZ.

From the Fig. 4.18 it is clearly observed that a complete material flow of a surface nano composite occured during fabrication by FSP. Fig. 4.18(a) shows, microstructure of a SZ with full of Al_2O_3 particles, completely mixed with Al alloy by the means of tool pin. Here in mechanically mixed region (MMR), all the grains were fine coarsened because of dynamic crystallization caused by pinning effect. Onion ring like structures was obsered at SZ. From the Fig. 4.18(b) it is shown that white and dark layers, these layers are formed due to stirring action of the back edge of the pin, along the surface of the tool shoulder. An uni-axed grains are noticed in un-mixed region (UMR) shown in Fig. 4.18(c). This region is just beneath the bottom of the pin and the grain are uni-axed because of heat dissipation from the SZ. Fig. 4.18(d) reveals that banded structure consisting of alernatively lamellae of Al/Al_2O_3. Large equi-axed grains were spoted at HAZ shown in Fig. 4.18(e). From Fig. 4.18(f) it is observed that, a mixture of Al alloy and Al_2O_3 reinforcement like alternative vertex – like lamellae in severe induced plastic region (SIPR).

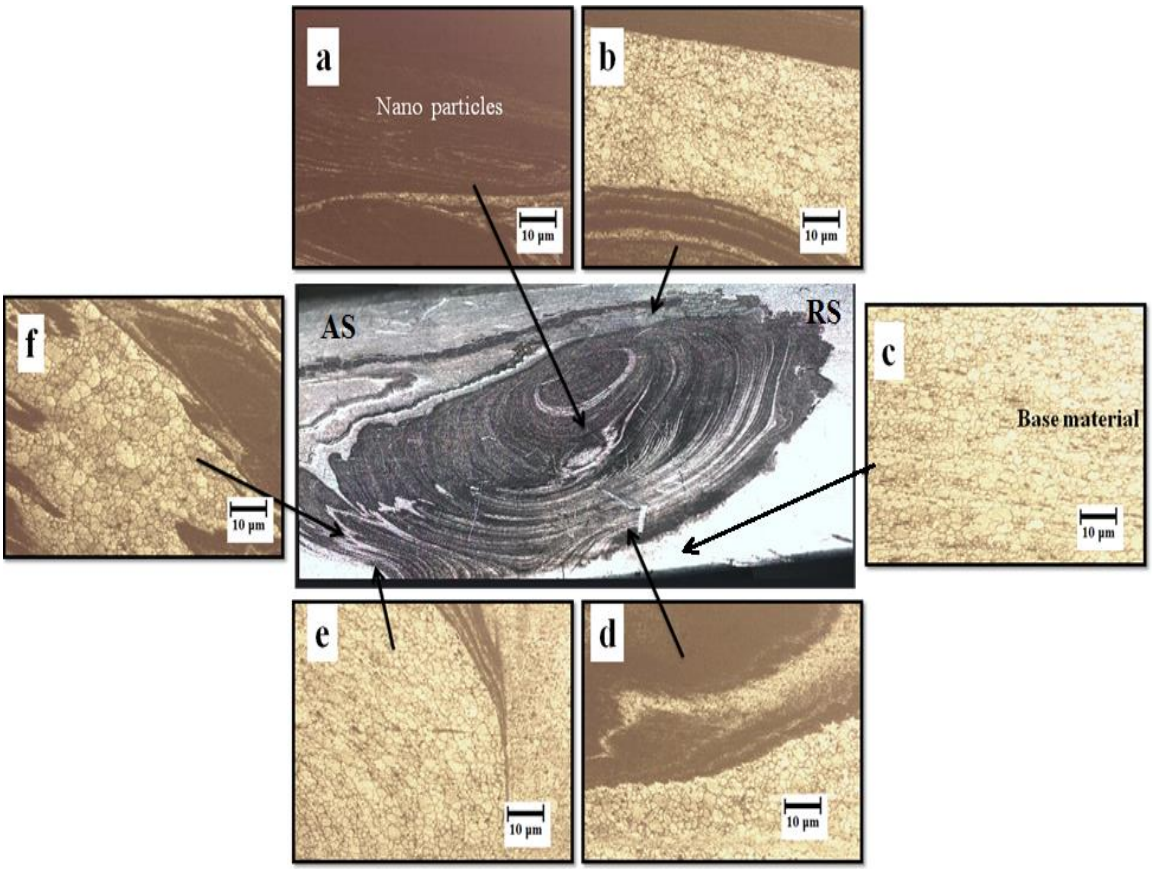

Fig. 4.18 Microstructure and material flow of fabricated surface nanocomposite: (a) microstructure and onion rings caused by MMR at the center of SZ with Al_2O_3 particles; (b) material is dragging towards AS from RS; (c) un-mixed region at bottom of pin; (d) material flow caused by the tool rotation at beneath the pin; (e) equiaxed grains formed at HAZ; (f) white and black flow bands were formed at SIPR.

From the SEM micrographs, a clear dispersion of the reinforcement particles was observed from the Fig. 4.19(a). From the Fig 4.19(b) it is observed that the reinforcement particles were occupied within the grains and at grain boundaries too. Most of the reinforcement particles were occupied on the boundaries of the grain shown in Fig. 4.19(c). From Figs. 4.19(d) it is observed that the mixing of reinforcement particle into the base material caused by pin. Transitional zone formation has taken place on the AS of processed region shown in Fig. 4.19(e). The size of the nanoparticles was increased more than doubled and led to agglomeration. Micro-cracks are initiated at the boundaries of the pin region along the flow pattern of the material as shown in 4.19(f) and (g).

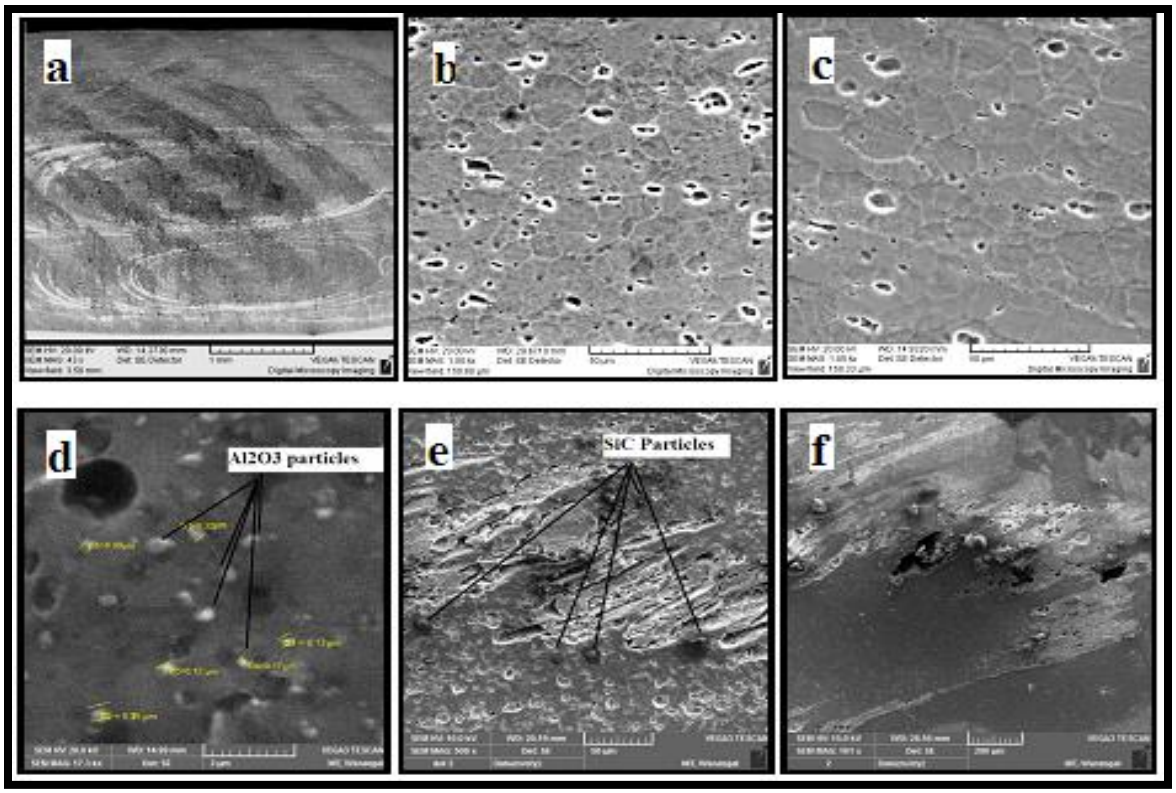

Fig. 4.19 SEM morphologies of fabricated surface nanocomposites: (a) processed region of fabricated surface nanocomposite; (b) Refined grain structure of Al/Al_2O_3 composite; (c) Microstructure of an Al/SiC composite; (d) Al/Al_2O_3 composite; (f) Defect formed during process; (g) Voids are formed during Al/Al_2O_3 composite at 6 vol.%.

Fig. 4.20 shows the micrographs of the surface nano composites fabricated by the FSP with different volume percentages of Al_2O_3 and SiC reinforcement particles at 1150 rpm tool rotational speed and 15 mm/min traverse speed. It is observed that the Al_2O_3 nano reinforcement particles at 2 vol.% are dispersed more uniformly in the SZ as compared to the 4 and 6 vol. % of nano reinforcement particles. Figs. 4.20(a) and (b) show at 2, 4 vol.% of Al_2O_3 nano reinforcement particles distributed in the SZ. With increasing the vol.% to 4 particle agglomerations occurred. Further increase in the volume percentage of reinforcement particles leads to defect formation a shown in Fig. 4.20(c). At 2 and 4 vol.% of Al_2O_3 the surface nanocomposites exhibited no defects but at 6 vol. %. defects were formed. With the increasing vol.% of reinforcement into the Al alloy, voids like defects were formed.

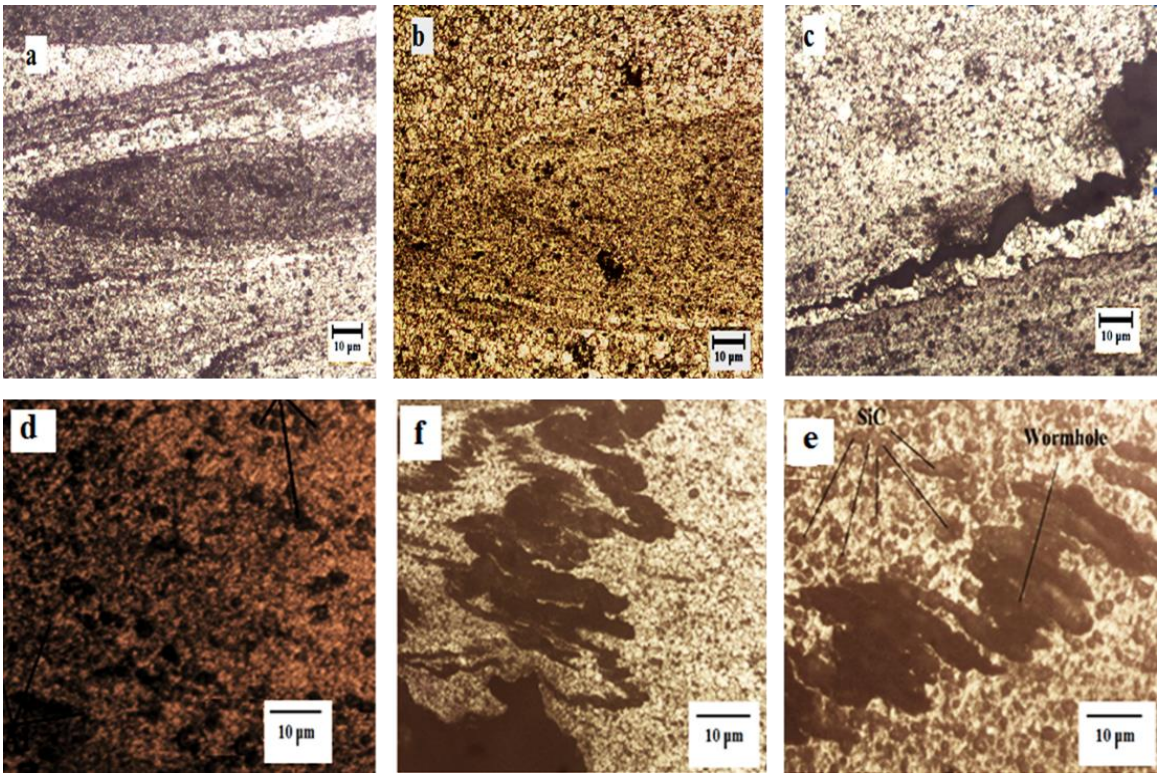

Fig. 4.20 Microstructures from varying volume percentage (vol.%) of reinforcement: Al/Al_2O_3 surface nanocomposite (a) 2 Vol.%; (b) 4 Vol.%; (c) 6 Vol.%. Al/SiC surface nanocomposite (d) 2 Vol.%; (e) 4 Vol.%; (f) 6 Vol.%.

Figs. 4.20(d), (e) and (f) show the fabricated Al/SiC surface nanocomposites. From Fig. (d) it is observed that, there are no defects formed at 2 vol.% of SiC and by increasing the vol.% of reinforcement to 4 and 6 the defects were observed. The defect formation does not only depend on the process parameters, tool geometry but also depends on reinforcement and its volume percentage. Small micro cracks are observed at 4 volume percentage of SiC reinforcement and voids, and a tunnel-like defect is observed at 6 volume percentage of reinforcement. Similar voids and tunneling like defects are observed in Al/Al_2O_3 composite with 6 volume percentage composites.

The defects are clearly shown in Fig. 4.20. Few researchers have studied the effect of SiC reinforcement particles on fabrication of Al/SiC composites [14]. They have produced a defect free composite with single pass FSP through a smaller amount volume percentage of SiC reinforcement (approx. 1 volume percentage). Here the volume percentage was increased up to 4 volume percentage of Al_2O_3 and 2 volume percentage of SiC by applying single pass FSP.

4.2.4 Scanning electron microscopy and energy dispersive spectroscopy analysis

By Energy Dispersive Spectroscopy (EDS) analysis, it was found that Al_2O_3 and SiC reinforcement particles are strengthening the Al matrix as shown in Figs. 4.21 and 4.22. From this analysis, the distribution of the reinforcement particles into the matrix can be observed. Figs. 4.21 and 4.22 reveals the existence of reinforcement particles (Al_2O_3 and SiC) into the matrix.

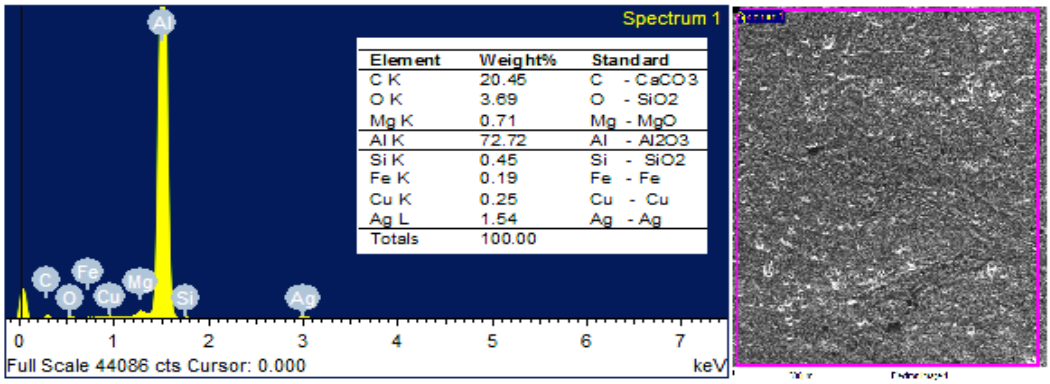

Fig. 4.21 EDS analysis of Al/Al_2O_3 surface nanocomposite.

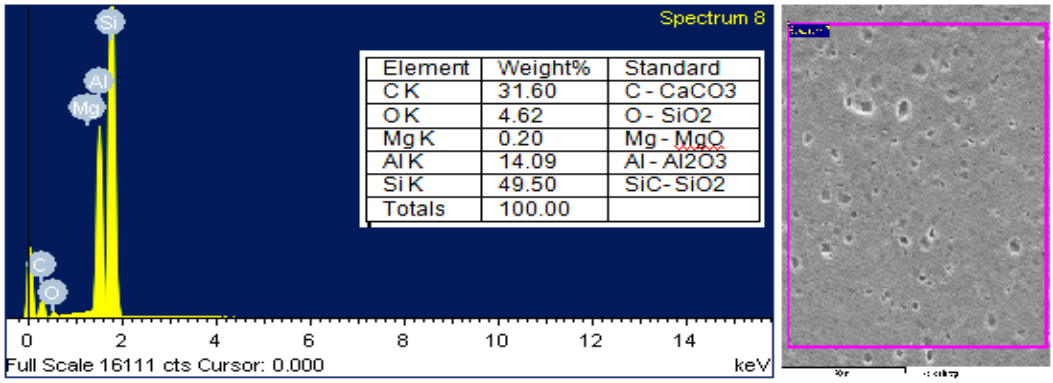

Fig. 4.22 EDS analysis of Al/SiC surface nanocomposite.

By using nano reinforcement particles the grain size was reduced and it became very fine because of the pinning effect. Better mechanical properties can be enhanced by reducing the grain size. The grain size was reduced to less than 200 nm successfully by applying nano reinforcement particles into the matrix shown in Fig. 4.23. The average agglomerated Al_2O_3 and SiC particle size is ~170 nm, much larger than the initial size ~50 nm. However, increase in

volume percentage from 2 to 4 and 6 of reinforcement particles increases the agglomeration, voids and tunnel defects on the advancing side of SZ.

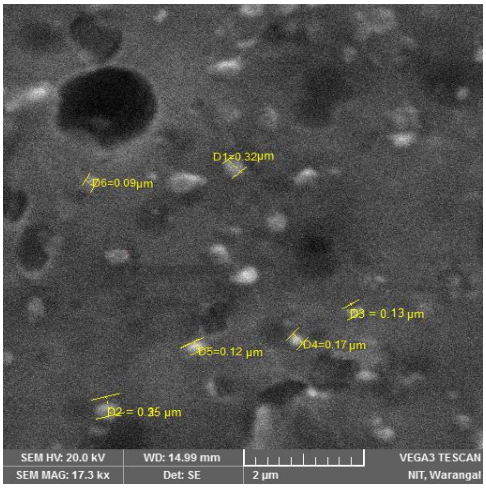

Fig. 4.23 Particles size measured after fabrication of surface composite through SEM analysis.

4.2.5 X-ray diffraction

X-ray diffraction (XRD) patterns of Al/Al_2O_3 and Al/SiC were shown in Figs. 4.42 and 4.25. From the XRD analysis, different phases were observed such as: Al_2O_3, Al_4Si, SiO_2 and $Mg_2Si_5Al_4O_{18}$. Fig. 4.25 shows the XRD patterns of fabricated composites. In the fabricated surface nanocomposite samples, the peaks of Al and SiC were identified. The identified peaks indicate that Aluminum and SiC were well mixed into the matrix during the fabrication process.

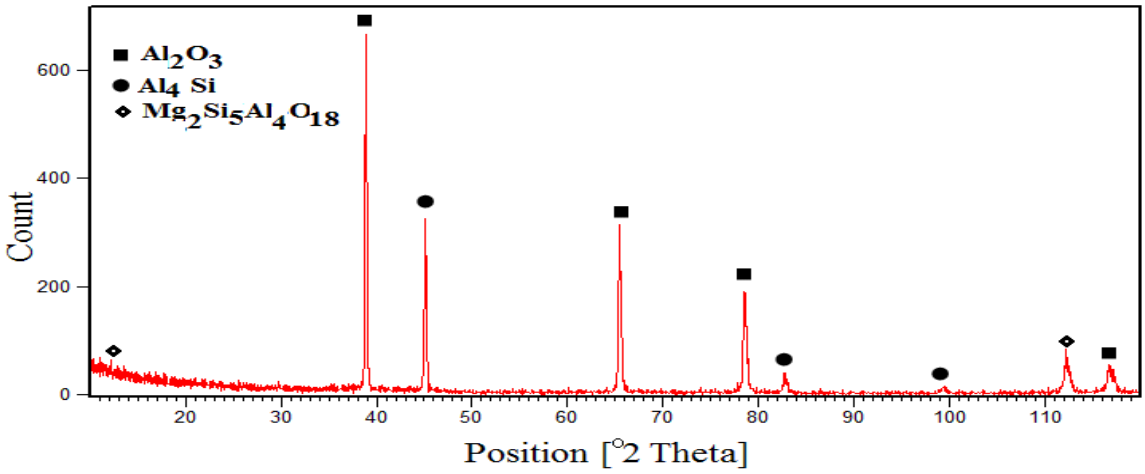

Fig. 4.24 XRD graph of Al/Al_2O_3 surface nanocomposite.

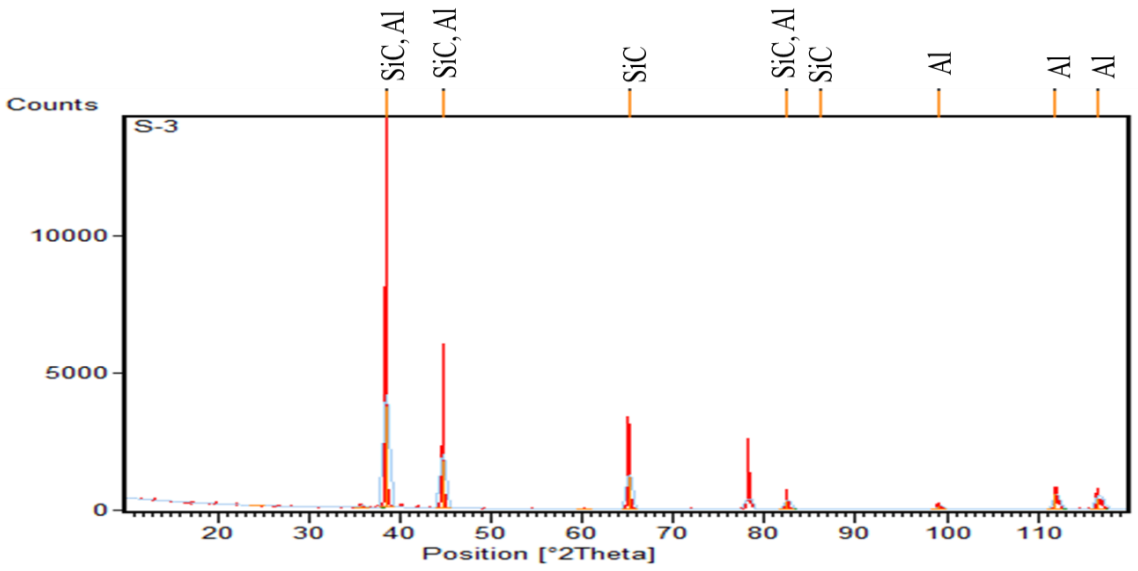

Fig. 4.25 XRD graph of Al/SiC surface nanocomposite.

4.2.6 Microhardness

Fig. 4.26 shows the microhardness variations in surface nanocomposite samples of Al/Al_2O_3 and Al/SiC with an increase in volume percentage of the reinforcement. This is attributed mainly because of microstructural enhancement due to FSP and strengthening mechanisms. Here the microhardness of the surface composites was increased based on strengthening mechanisms (Hall-Petch relation and Orowan theory) [15]. The dispersion of the SiC and Al_2O_3 reinforcement particles and the grain refinement of the matrix through FSP resulted in increase in microhardness. A clear microhardness divergence was observed between the SZ and the other transitional zones. The temperatures distribution during the FSP might be the reason for microhardness dissimilarity in transitional zones. The presence of reinforcement particles Al_2O_3 and SiC in the SZ, ageing and ultrafine grain structure improved the microhardness in the SZ [16]. Mainly in MMCs increased hardness was achieved basically due to nature of the reinforcement particles added and the uneven thermal expansion coefficient of reinforcement and matrix phases caused by dislocation [17].

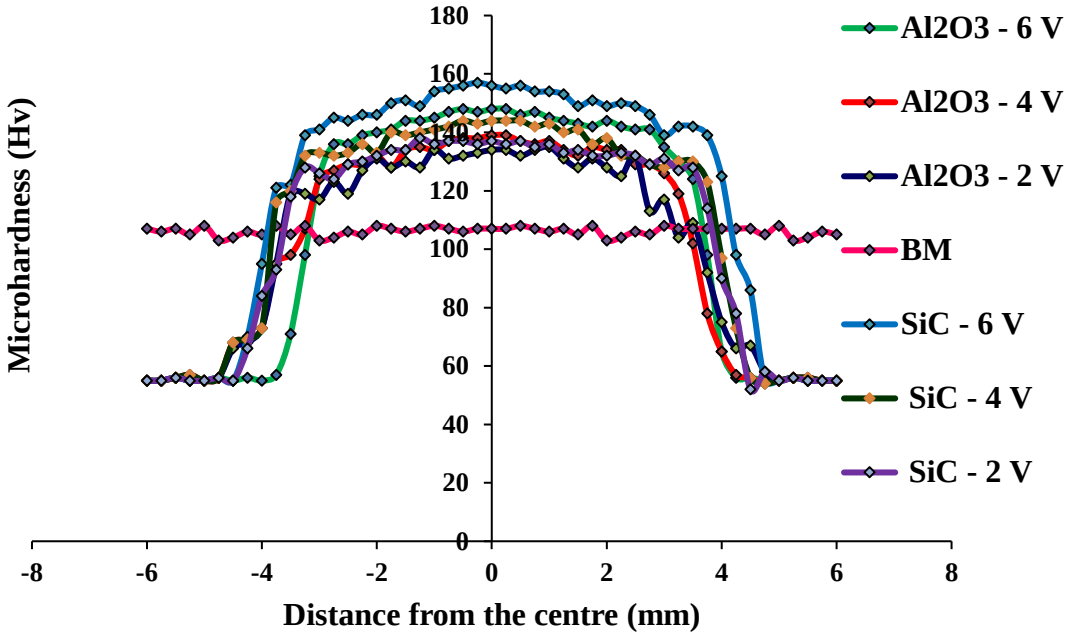

Fig. 4.26 Microhardness values of 2, 4 and 6 vol. % of Al/Al_2O_3 and Al/SiC composites fabricated at 1150 rpm with 15 mm/min.

Table 4.3 Microhardness values of samples.

Sample ID	Hardness (Hv)*
Base Material (BM)	107
2v- Al_2O_3	132
4v- Al_2O_3	139
6v- Al_2O_3	148
2v- SiC	137
4v- SiC	144
6v- SiC	156

*Avg. values of 3 samples

A clear microhardness inconsistency was noticed between the Al/Al_2O_3 and Al/SiC composites. Higher microhardness values were shown in Al/SiC composites than Al/Al_2O_3. At each level of volume percentage Al/SiC composites dominated the Al/Al_2O_3 composites. This may be due to the presence of hard ceramic and carbide particles of reinforcement. However, the

microhardness values attained by adding nano reinforcement particles are superior as compared to the base material shown in Table 4.3.

4.2.7 Tensile and fractography

The observed tensile properties (young's modulus (YS), ultimate tensile strength (UTS) and elongation (El)) of fabricated surface nanocomposites were shown in the Table 4.4. In summary, the tensile properties of the fabricated surface nanocomposites were decreased with the increase in volume percentage of the reinforcement into the matrix.

Many factors affect the determination of the tensile strength of MMCs. Most of them are (i) presence of defects in the deformation zone, (ii) improper mixing of reinforcement and base material, (iii) HAZ grain size and (iv) over ageing and dissolution of precipitation [18]. All the composites were tested for tensile to know the UTS, YS and %EL. Each sample was tested 3 times, and the average value of them is presented in Table. 4.4. The tensile tested fabricated samples were shown in Fig. 4.27. The surface nanocomposites show lower yield and tensile strength, as well as lower percentage elongation compared to the base metal. Fig. 4.28 shows the SEM fractography of the fabricated surface nanocomposite obtained at failure zone after the tensile test.

Fig. 4.27 Tensile tested samples of fabricated Al/Al_2O_3 and Al/SiC.

Table 4.4. Tensile strength properties of fabricated surface nanocomposites.

Sample	Ultimate tensile strength (UTS, MPa) *	Yield strength (YS, MPa) *	Percentage of elongation (%EL) *
Base Material	296	272	12.0
2v- Al_2O_3	176	102	9.4
4v- Al_2O_3	164	129	7.3
6v- Al_2O_3	152	95	5.2
2v- SiC	171	132	8.8
4v- SiC	157	118	4.9
6v- SiC	142	97	3.6

*Avg. values of 3 samples

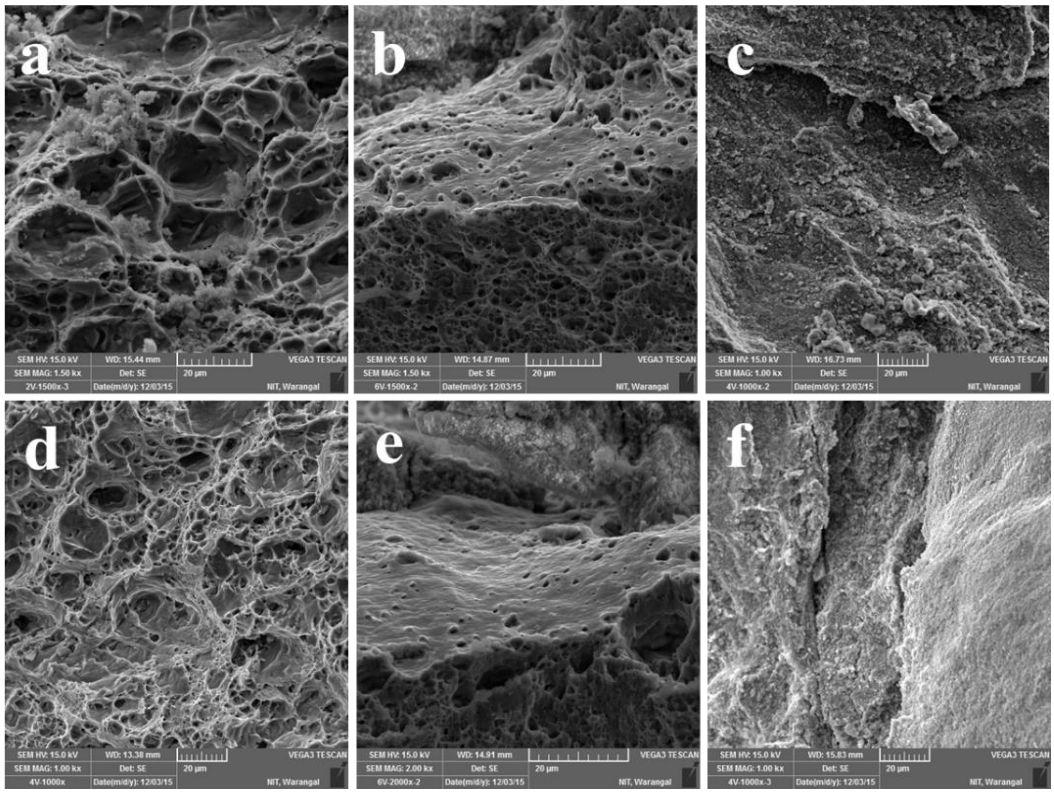

Fig. 4.28 SEM fractography's of (a) 2V-Al/Al_2O_3, (b) 4V-Al/Al_2O_3, (c) 6V-Al/Al_2O_3, (d) 2V-Al/SiC, (e) 4V-Al/SiC, (f) 6V-Al/SiC.

The FSPed surface nanocomposites shows finer dimples, which are associated with finer reinforcement of nanoparticles in the base material. The increase in dislocation density causes the reduction of elongation. The nano reinforced composites fracture morphologies shows the larger dimple size with reduced ductility. The existence of ceramic particles into the matrix reduces the moment of plasticized base material thus increased its brittleness to a certain extent. The failures were ductile type failure since the characteristic of fine dimples were observed. Cup and cone-like failure can be observed.

Figs. 4.28(a) and (b) show, SEM micrograph of fractured surface of the FSPed specimen with Al_2O_3 particles, represents a necked region. Furthermore, large, small and deep dimples are observed which indicate ductile nature of failure occurred. This can be attributed to the smaller grain size of this specimen that leads to more resistance against fracture. However, presence of large and small dimples together shows that dimpled rupture mechanism was not saturated and thus resistance against fracture was not very high. On the other hand, failure of this specimen occurred in the HAZ zone on the RS, where a lower amount of hardness was observed. Compared to the FSPed specimen with Al_2O_3 particles, the UTS and percentage elongation of all single-pass FSPed specimens with SiC particles are lower. In these specimens, fracture took place in the SZ where the crack nucleates in the interface of Al/SiC.

4.2.8 Wear properties of the fabricated Al/Al_2O_3 and Al/SiC surface nanocomposites

The relation between the coefficient of friction and sliding distance while changing the reinforcements like Al_2O_3 and SiC at 2, 4 & 6 volume percentages were shown in Figs. 4.29 and 4.30. A similar trend was observed on surface nanocomposites fabricated at different ratios of volume percentages. From the Fig. 4.29 it is clearly shown that the coefficient of friction between the surface fabricated at 2, 4 & 6 volume percentage of the Al/Al_2O_3 reinforcement samples and the disk was same during the process. The average coefficient of friction values revealed general tendency to decrease or increase with the amount of reinforcement added into the matrix material. The coefficient of friction between the disk and the sample surface was not affected by the volume percentage of the reinforcement but it was influenced by the reinforcement.

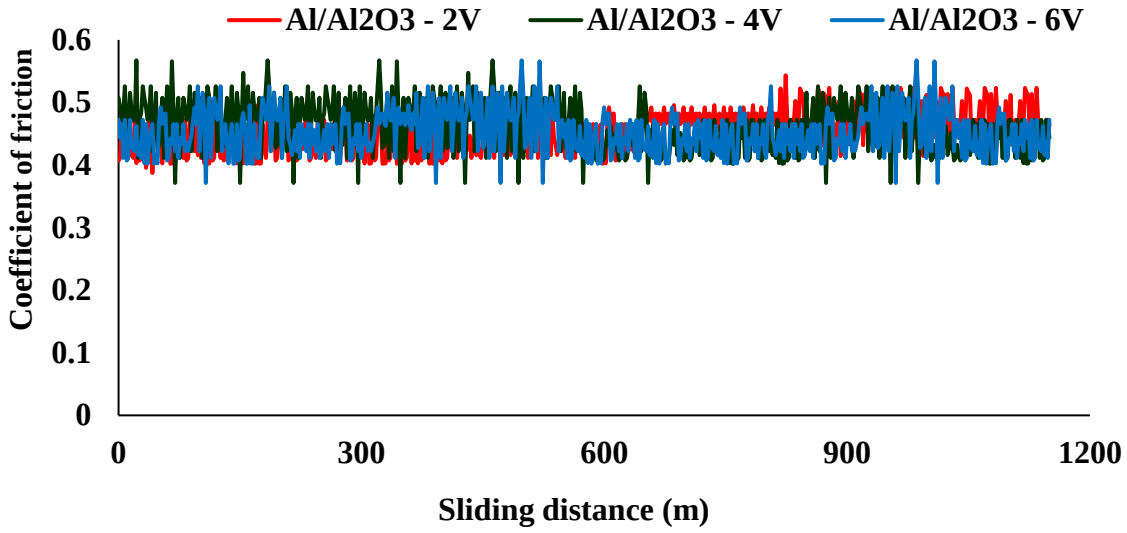

Fig. 4.29 Friction coefficient of the Al/Al_2O_3 composite as a function of sliding distances at an applied load of 20 N.

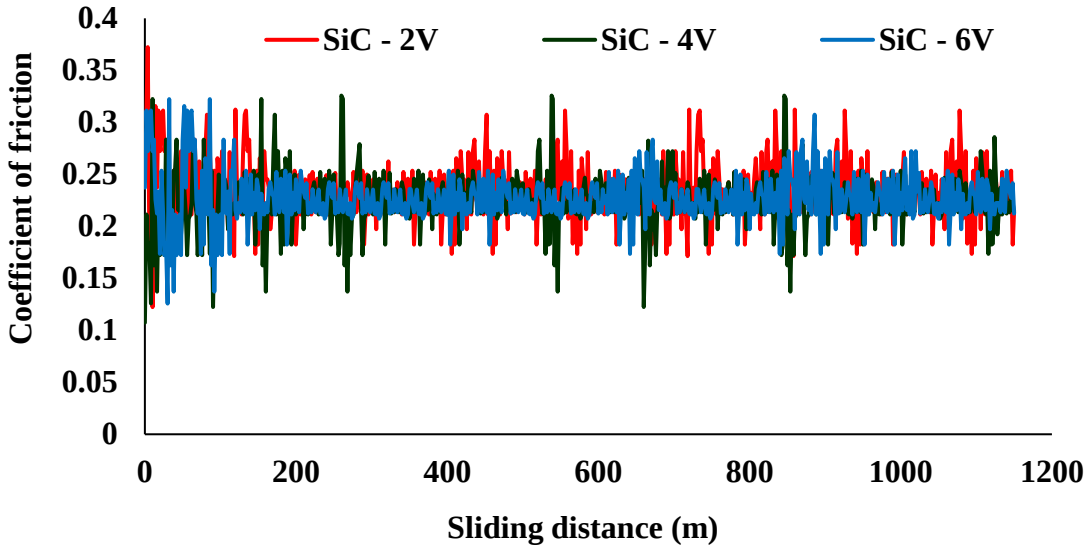

Fig. 4.30 Friction coefficient of the Al/SiC composite as a function of sliding distances at an applied load of 20 N.

Fig. 4.30 shows the coefficient of friction values obtained during the wear test of Al/SiC surface nanocomposites. From the Fig. 4.30 it is observed that, there is an increase of coefficient of friction at initial stage (lower sliding distances) of process may be due to higher frictional force to be required to avoid the adhesive contact among the sample surface and disc. The

average coefficient of friction for Al/Al_2O_3 is 0.4 and Al/SiC is 0.24 as shown in Figs. 4.29 and 4.30. It means the Al_2O_3 powder had a higher frictional coefficient over SiC under the same circumstances. Hence it is observed that, the fabricated surface nanocomposite with SiC reinforcement exhibits lower coefficient of friction than Al_2O_3 reinforced composites.

Figs. 4.31(a) - (f) show the wear morphology of Al/Al_2O_3 and Al/SiC surface nanocomposites tested at same conditions of load and distance. The effect of the coefficient of friction can be observed through the Figs. 4.31(a) - (f). A clear view of grooves can be observed on the surface of the nanocomposite of Al/SiC sample than Al/Al_2O_3 sample.

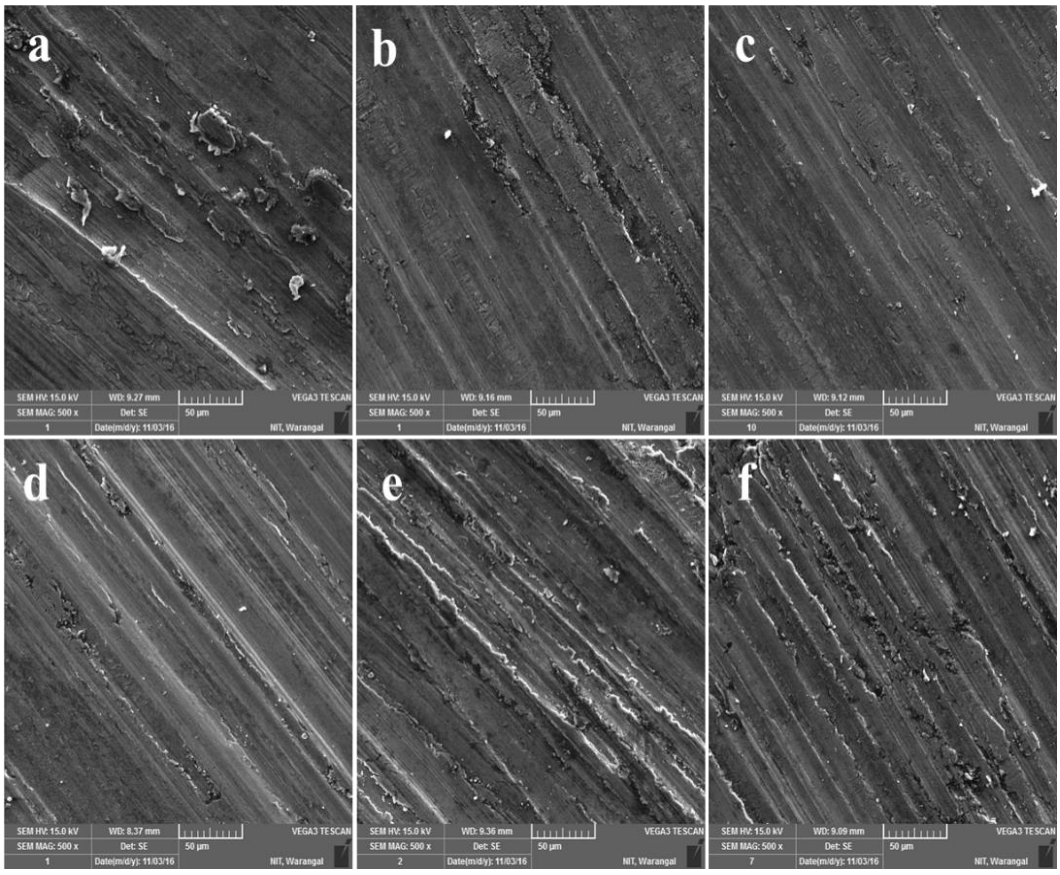

Fig. 4.31 SEM micrographs of worn surfaces of fabricated surface nanocomposites (a) 2V-Al/Al_2O_3, (b) 4V-Al/Al_2O_3, (c) 6V-Al/Al_2O_3, (d) 2V-Al/SiC, (e) 4V-Al/ SiC, (f) 6V-Al/ SiC.

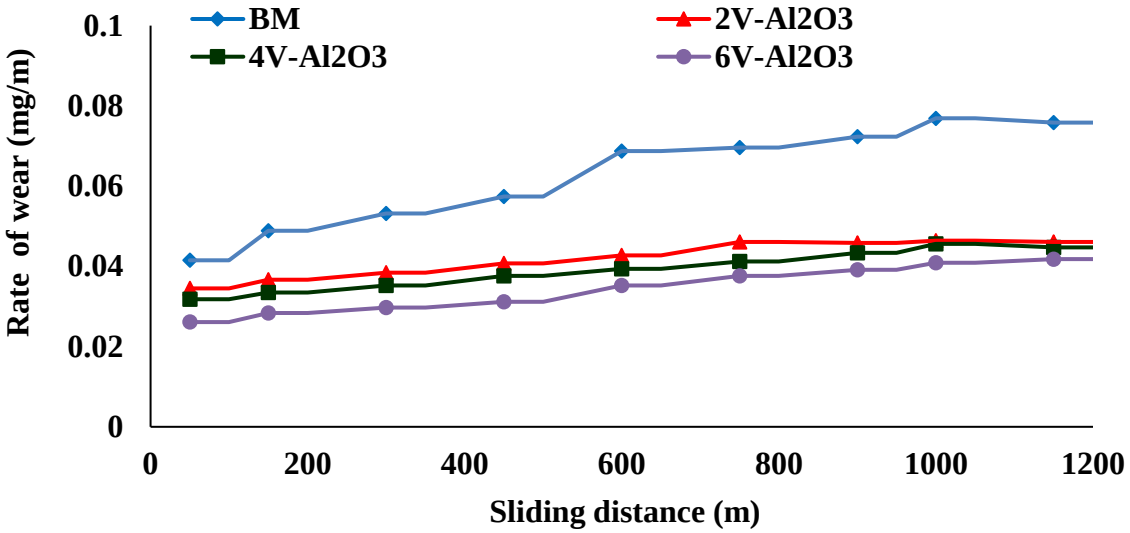

Fig. 4.32 Rate of wear of 2, 4 & 6 Vol.% of Al/Al_2O_3 surface nanocomposite.

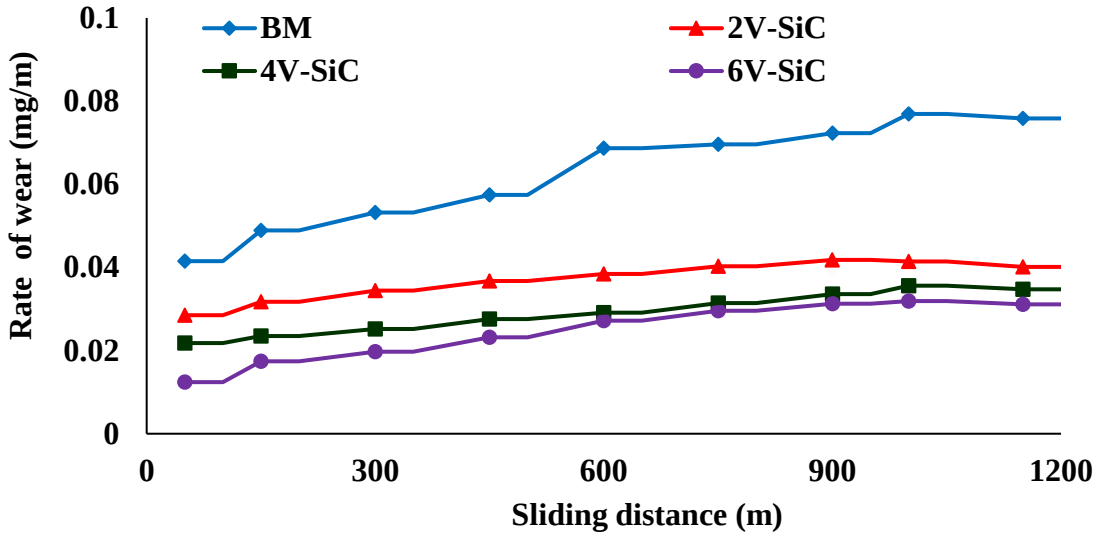

Fig. 4.33 Rate of wear of 2, 4 & 6 Vol.% of Al/SiC surface nanocomposite.

The variations in the measured rate of wear versus sliding distance of Al/Al_2O_3 and Al/SiC with varying volume percentage of reinforcements are shown in Figs. 4.32 and 4.33. The change in wear weight loss of sample versus sliding distance of Al/Al_2O_3 and Al/SiC surface nanocomposite fabricated at various volume percentages of reinforcements are shown in Figs. 4.34 and 4.35. The fabricated surface nanocomposites exhibit lower weight loss than compared with base material.

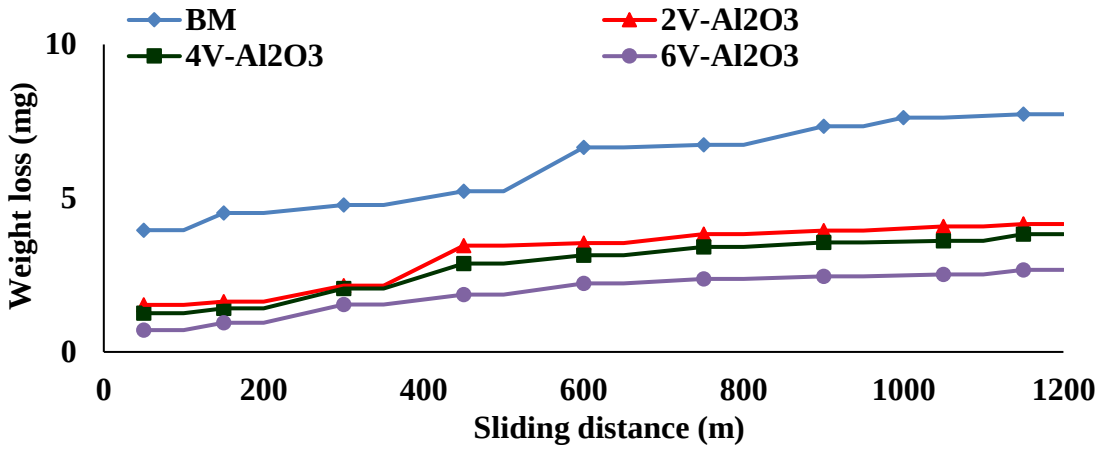

Fig. 4.34 Weight loss with sliding distance for base material and Al/Al_2O_3 surface nanocomposites.

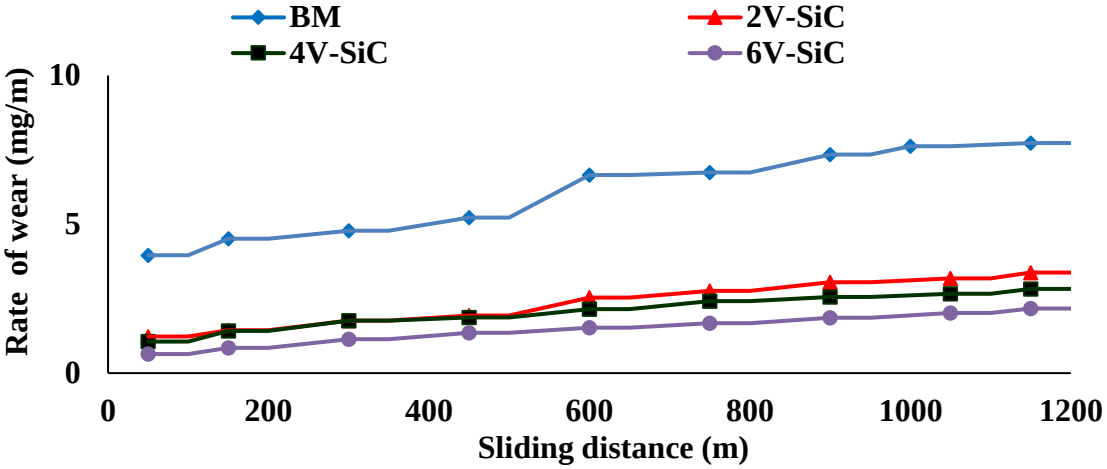

Fig. 4.35 Weight loss with sliding distance for base material and Al/SiC surface nanocomposites.

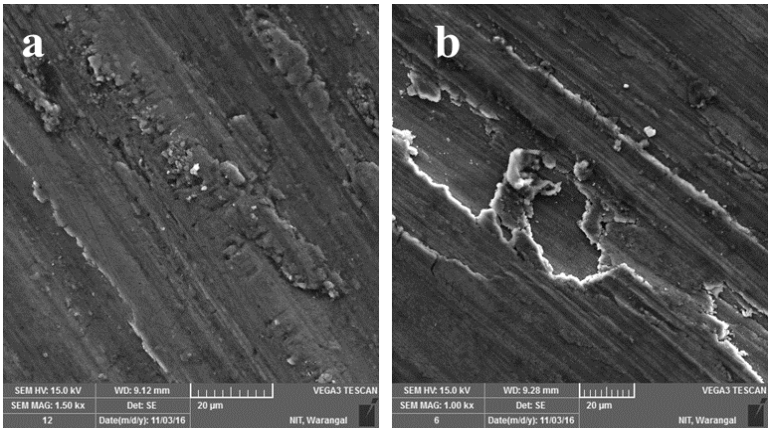

Fig. 4.36 Worn surfaces of (a) Al/SiC and (b) Al/Al_2O_3 surface nanocomposites.

The fabricated Al/Al_2O_3 and Al/SiC surface nanocomposites shows superior wear resistance properties over base material. The addition of higher reinforcement particles into the matrix resulted in decrease of wear rate. The more amount of added reinforcement particles into the matrix reduces the wear rate of the composites with respect to the sliding distance. At the side of extended sliding distance, the weight loss of the surface nanocomposites become very less shown in Fig. 4.36(a) and (b).

4.3 Implementation of multi hole and multi groove techniques for fabrication of composites by FSP.

4.3.1 Introduction of multi hole technique

From the single groove technique, maximum volume percentage of reinforcement which can be achieved with Al_2O_3 is 4 vol.% and SiC is 2 vol.%. To improve the surface composite region and volume percentage of reinforcement, single groove technique is not appropriate due to increasing groove dimensions leads to increase in defect formation in the surface composites. To overcome these limitations new techniques such as multi hole and multi groove were implemented to fabricate the surface composite. The basis for fabrication and characterization of the surface composites using these techniques, the results of section 4.3.2 and 4.3.3 were considered.

In this research work a new technique is implemented to improve the composite region up to processed region called multi hole technique. Initially a double series holes were made on the pin region and later the holes were extended on the shoulder region towards advancing side of the tool. By using this technique, the volume percentage of the reinforcement can be adjusted by changing the dimensions of the hole. Here, the diameter of the hole is taken as 1.5 mm and 2 mm, where depth of the hole is varied from 1 mm to 3.5 mm in the pin region and 1 mm in shoulder region.

Table 4.5 Detailed experimental sequence of multi hole technique.

Sample ID	Composite	Composite region	Dimensions (mm)		No. of Holes	
			Pin	Shoulder	Pin	Shoulder
A1	Al + Al_2O_3	P	D = 1.5, Dh = 1		32	
A2	Al + Al_2O_3	P	D = 1.5, Dh = 2		32	
A3	Al + Al_2O_3	P	D = 1.5, Dh = 3		32	
A4	Al + Al_2O_3	P	D = 1.5, Dh = 3.5		32	
B1	Al + Al_2O_3	P + S	D = 1.5, Dh = 1	D = 1.5, Dh = 1	32	32
B2	Al + Al_2O_3	P + S	D = 1.5, Dh = 2	D = 1.5, Dh = 1	32	32
B3	Al + Al_2O_3	P + S	D = 1.5, Dh = 3	D = 1.5, Dh = 1	32	32
B4	Al + Al_2O_3	P + S	D = 1.5, Dh = 3.5	D = 1.5, Dh = 1	32	32
C1	Al+ SiC	P	D = 1.5, Dh = 1		32	
C2	Al+ SiC	P	D = 1.5, Dh = 2		32	
C3	Al+ SiC	P	D = 1.5, Dh = 3		32	
C4	Al+ SiC	P	D = 1.5, Dh = 3.5		32	
D1	Al+ SiC	P + S	D = 1.5, Dh = 1	D = 1.5, Dh = 1	32	32
D2	Al+ SiC	P + S	D = 1.5, Dh = 2	D = 1.5, Dh = 1	32	32
D3	Al+ SiC	P + S	D = 1.5, Dh = 3	D = 1.5, Dh = 1	32	32
D4	Al+ SiC	P + S	D = 1.5, Dh = 3.5	D = 1.5, Dh = 1	32	32
E1	Al/Al_2O_3 + SiC	P	D = 1.5, Dh = 1		32	
E2	Al/Al_2O_3 + SiC	P	D = 1.5, Dh = 2		32	
E3	Al/Al_2O_3 + SiC	P	D = 1.5, Dh = 3		32	
E4	Al/Al_2O_3 + SiC	P	D = 1.5, Dh = 3.5		32	
F1	Al/Al_2O_3 + SiC	P + S	D = 1.5, Dh = 1	D = 1.5, Dh = 1	32	32
F2	Al/Al_2O_3 + SiC	P + S	D = 1.5, Dh = 2	D = 1.5, Dh = 1	32	32
F3	Al/Al_2O_3 + SiC	P + S	D = 1.5, Dh = 3	D = 1.5, Dh = 1	32	32
F4	Al/Al_2O_3 + SiC	P + S	D = 1.5, Dh = 3.5	D = 1.5, Dh = 1	32	32

P = Pin region; P+ S = Pin + Shoulder region; D = Diameter of the hole; Dh = Depth of the hole.

Table 4.6 Detailed experimental sequence of multi hole technique.

Sample ID	**Composite**	**Composite region**	**Dimensions (mm)**		**No. of Holes**	
			Pin	Shoulder	Pin	Shoulder
G1	Al + Al_2O_3	P	D = 2.0, Dh = 1		32	
G2	Al + Al_2O_3	P	D = 2.0, Dh = 2		32	
G3	Al + Al_2O_3	P	D = 2.0, Dh = 3		32	
G4	Al + Al_2O_3	P	D = 2.0, Dh = 3.5		32	
H1	Al + Al_2O_3	P + S	D = 2.0, Dh = 1	D = 2.0, Dh = 1	32	32
H2	Al + Al_2O_3	P + S	D = 2.0, Dh = 2	D = 2.0, Dh = 1	32	32
H3	Al + Al_2O_3	P + S	D = 2.0, Dh = 3	D = 2.0, Dh = 1	32	32
H4	Al + Al_2O_3	P + S	D = 2.0, Dh = 3.5	D = 2.0, Dh = 1	32	32
I1	Al+ SiC	P	D = 2.0, Dh = 1		32	
I2	Al+ SiC	P	D = 2.0, Dh = 2		32	
I3	Al+ SiC	P	D = 2.0, Dh = 3		32	
I4	Al+ SiC	P	D = 2.0, Dh = 3.5		32	
J1	Al+ SiC	P + S	D = 2.0, Dh = 1	D = 2.0, Dh = 1	32	32
J2	Al+ SiC	P + S	D = 2.0, Dh = 2	D = 2.0, Dh = 1	32	32
J3	Al+ SiC	P + S	D = 2.0, Dh = 3	D = 2.0, Dh = 1	32	32
J4	Al+ SiC	P + S	D = 2.0, Dh = 3.5	D = 2.0, Dh = 1	32	32
K1	Al/Al_2O_3 + SiC	P	D = 2.0, Dh = 1		32	
K2	Al/Al_2O_3 + SiC	P	D = 2.0, Dh = 2		32	
K3	Al/Al_2O_3 + SiC	P	D = 2.0, Dh = 3		32	
K4	Al/Al_2O_3 + SiC	P	D = 2.0, Dh = 3.5		32	
L1	Al/Al_2O_3 + SiC	P + S	D = 2.0, Dh = 1	D = 2.0, Dh = 1	32	32
L2	Al/Al_2O_3 + SiC	P + S	D = 2.0, Dh = 2	D = 2.0, Dh = 1	32	32
L3	Al/Al_2O_3 + SiC	P + S	D = 2.0, Dh = 3	D = 2.0, Dh = 1	32	32
L4	Al/Al_2O_3 + SiC	P + S	D = 2.0, Dh = 3.5	D = 2.0, Dh = 1	32	32

P = Pin region; P+S = Pin + Shoulder region; D = Diameter of the hole; Dh = Depth of the hole.

4.3.2 Surface appearance of fabricated surface nanocomposite and macrostructure

From the Fig. 4.37 it is observed that, the fabricated surface nanocomposite surface was very smooth and semicircular patterns with exit hole at the end of the process. Figs. 4.38 and 4.39 show that the cross-sectioned microstructure of the fabricated surface nanocomposites. All the fabricated composites were visually examined and it is revealed that, no obvious defects were found on the surface of the composite, indicating that fine structured surface composites were obtained. A great mixture of reinforcement particles was observed in the fabricated surface nano composites shown in Figs. 4.38 and 4.39. This may be due to the large dimensions of the holes and it leads to increase in volume percentage of the reinforcement in the matrix.

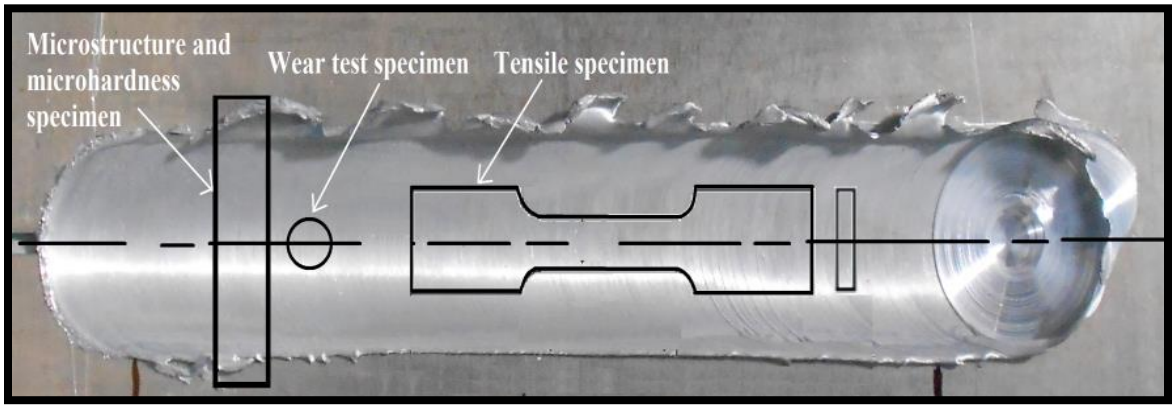

Fig. 4.37 Schematic diagram of selection of sample for testing

Fig.4.38 and 4.39 shows, the macrostructure of surface nanocomposites fabricated with multi hole technique. The samples fabricated with diameter of hole taken as 1.5 mm by changing the depths as 1, 2, 3 and 3.5 mm are shown in Figs. 4.38. By increasing the diameter of the hole from 1.5 to 2.0 mm and varying the depth of the hole as 1, 2, 3 and 3.5 mm the fabricated surface nano composites are shown in Fig. 4.39.

Figs. 4.38 and 4.39 show, the increased surface nanocomposite region from SZ to processed region. The dispersion of the reinforced particles in the processed region was good where composites made with the hole on pin + shoulder region. The composite region was successfully increased from pin region to complete processed region and the amount of the volume percentage was increased by applying the multi hole technique.

Multi hole technique (Pin region)	Multi hole technique (Pin + Shoulder region)
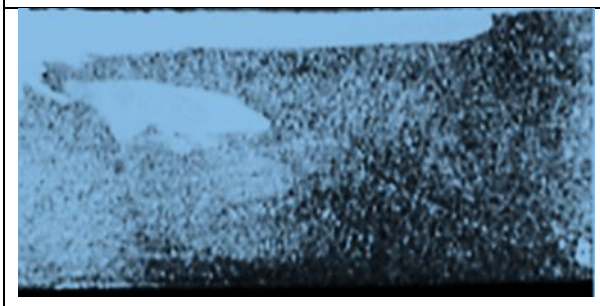	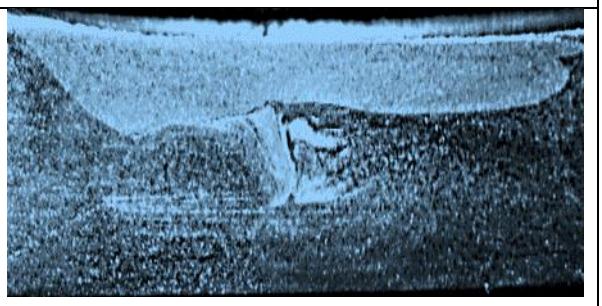
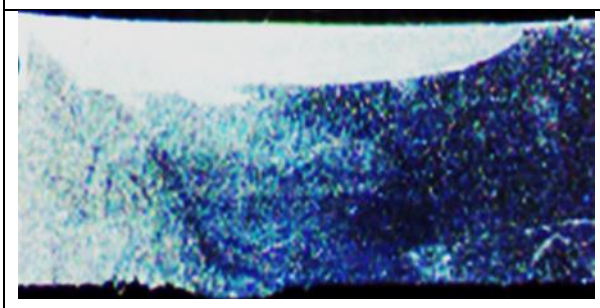	
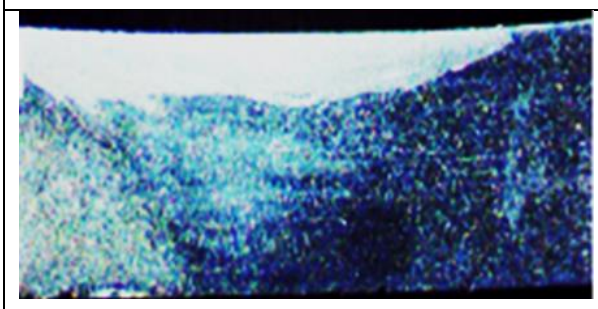	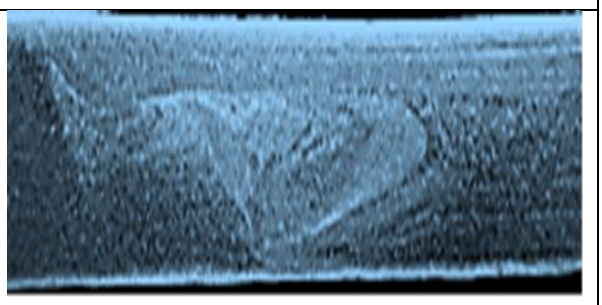
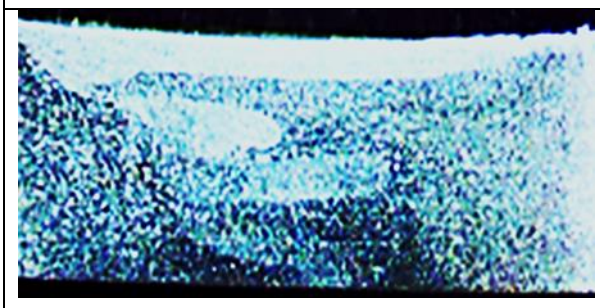	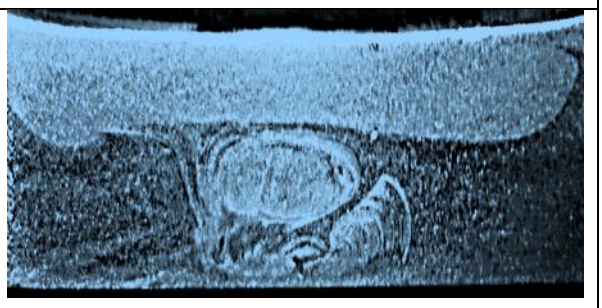

Fig. 4.38 Macrostructure of surface nano composites fabricated with multi hole technique (diameter of hole D = 1.5 mm).

Multi hole technique (Pin region)	Multi hole technique (Pin + Shoulder region)
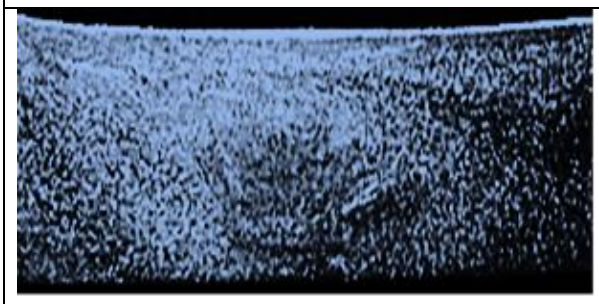	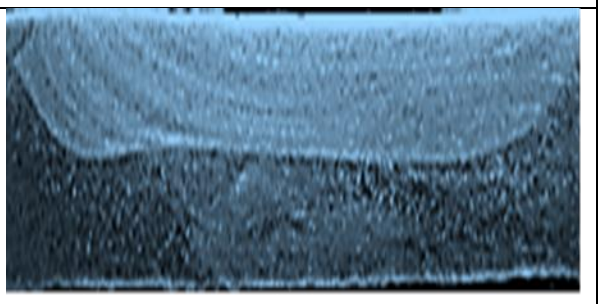
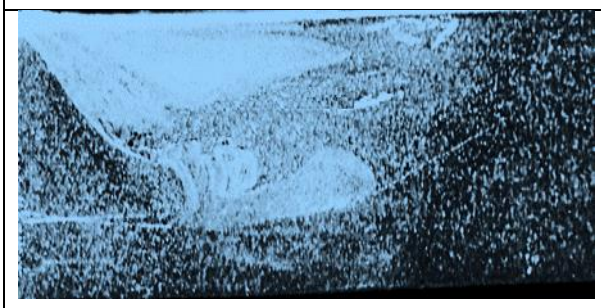	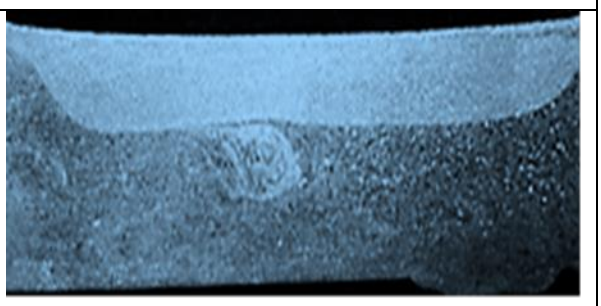
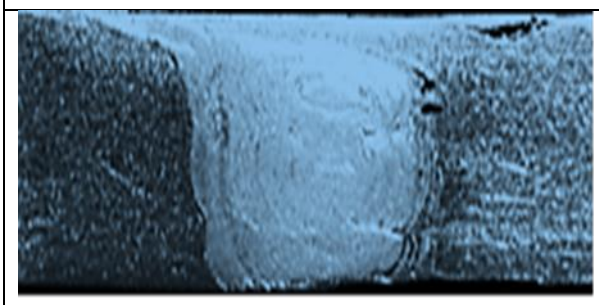	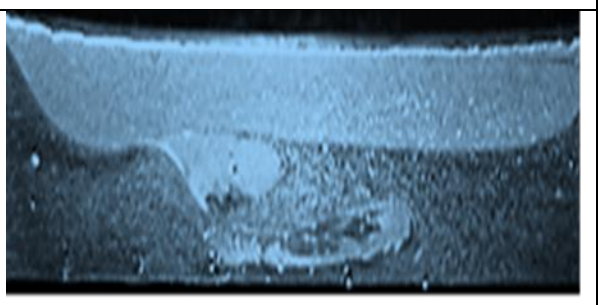
	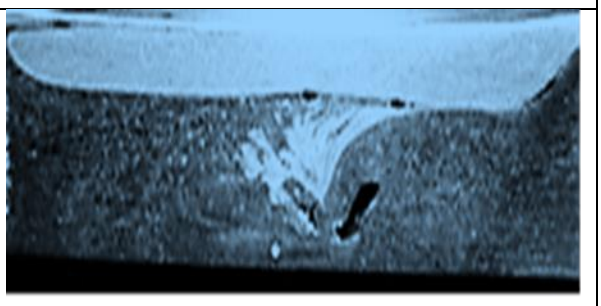

Fig. 4.39 Macrostructure of surface nano composites fabricated with multi hole technique (diameter of hole D = 2.0 mm).

4.3.3 Microstructure

Fig. 4.40 shows the microstructure of fabricated surface nanocomposites with varying depth of the hole from 1 – 3.5 mm. The increase in depth of the hole increases the quantity of reinforcement simultaneously which results in the richer and even distribution of the reinforcement into the processed.

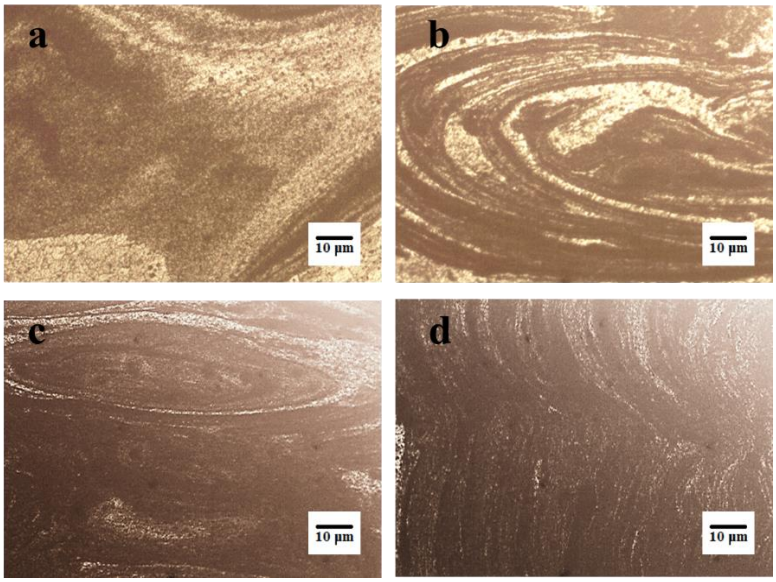

Fig. 4.40 Microstructures of fabricated surface nano composites by multi hole technique at different depth of the holes; (a) Dp = 1 mm, (b) Dp = 2 mm, (c) Dp = 3 mm, (d) Dp = 3.5 mm.

With the increasing depth of the hole the volume percentage of the reinforcement was increased. From Fig. 4.40(a) shows, the reinforcement particles are well distributed in the SZ at d = 1 mm. Very light white and dark bands can be seen from the composite fabricated at d = 1 mm. The amount of the reinforcement particles was incorporated with the increasing depth of hole from1 to 2mm shown in Fig. 4.40(b). Increase in volume percentage of reinforcement increases the richness of reinforcement particles into the SZ and forms more dark and white bands. Figs. 4.40(c) and (d) show the rich amount of the reinforcement particles takes place with increasing depth of the hole from 3 to 3.5 mm. Same kind of material flow was observed in all fabricated surface nanocomposite of A/Al_2O_3, Al/SiC and Al (Al_2O_3+SiC). Increasing the dimensions of the hole leads to increase in the volume percentage of the reinforcement into the SZ.

Microscopic examinations unveil that the process variables have a significant impact on the formation of surface nanocomposites. The nano reinforcement particles spread more usually and unvaryingly in the nugget zone (NZ) or stir zone (SZ) for all volume percentages of SiC and Al_2O_3 nano reinforcements by applying the single FSP pass. The mixture (reinforcement and matrix material) of the plasticized material primarily yield from advancing side (AS) and travels towards retreating side (RS). At advancing of the tool, the material undergoes plasticized to forges towards the bottom of the pin. With the dynamic stirring action of the tool directs the packed reinforcement to mix with the plasticized matrix to form the composite. A good mixture of the reinforcement particles with the matrix was observed in the fabricated composite.

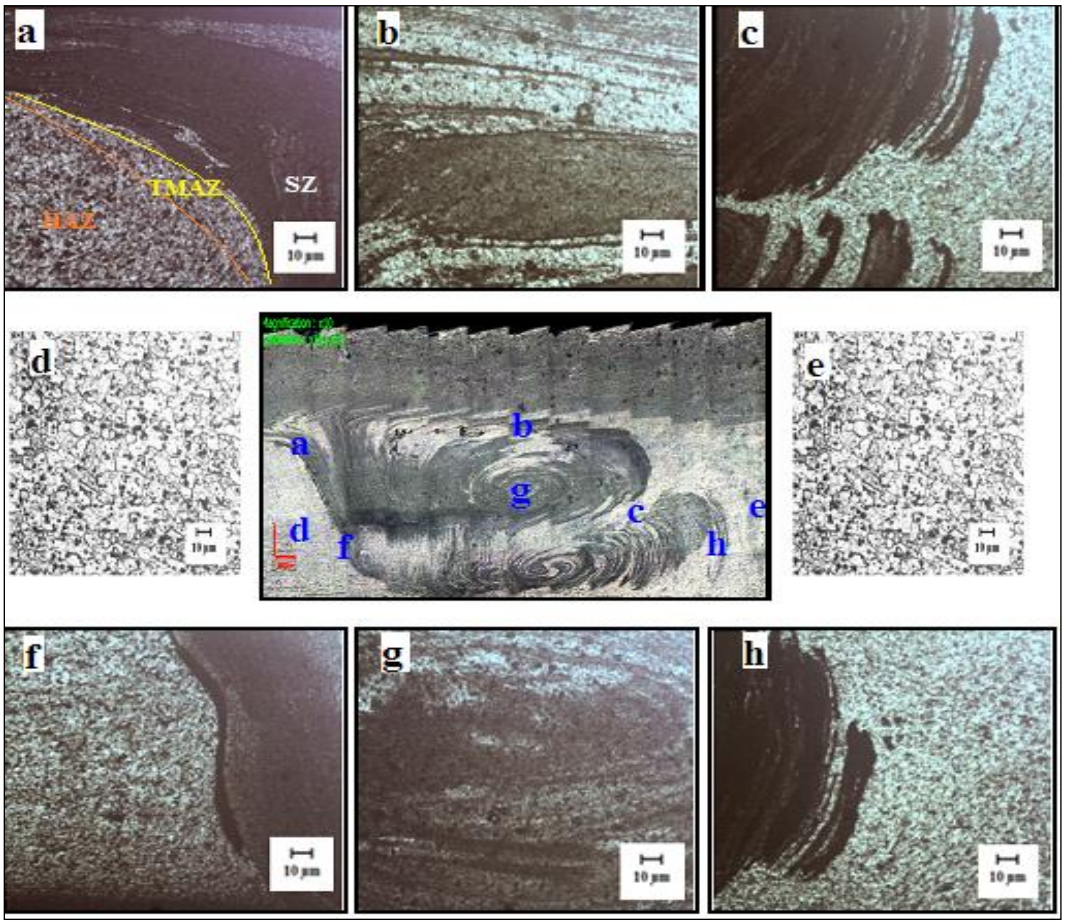

Fig. 4.41 Microstructures of fabricated composites: (a) Transitional zones, (b) Shoulder Influenced region, (c) material flow taken short turn at RS, (d) HAZ region on AS, (e) HAZ on RS, (f) Plasticized material flow forged by shoulder of the tool, (g) Stir zone, (h) material flow at RS.

The microstructures of Al/Al_2O_3 and Al/SiC fabricated composites taken at various regions within the processed region are shown in Fig. 4.41. The composites produced by applying groove technique, Al_2O_3 reinforcement particles are effectively dispersed in the SZ than SiC. It is hard to obtain even distribution of reinforcement across the SZ using single groove technique. Different flow patterns can be observed in the composite fabricated with multi hole method and are shown in Fig. 4.41. From the Fig 4.41(a), it is detected that the material is dragged from the top surface of the material from the RS into AS by the tool shoulder. The concave geometry of the tool and large downward forces helps the material to easily flow towards SZ from the upper layer of the material. Transitional zones (Stir zone (SZ), Thermo-mechanical heat affected zone (TMAZ) and Heat affect zone (HAZ)) are formed during the plasticization of material [16]. A non-uniform mixture of a surface composite layer can be observed from Fig. 4.41(b). Tool rotational speed and transverse speed causes to form dark and white colored bands during the process. Fig. 4.41(c) shows, the flow of material on the RS. A quick return of material flow takes place during the process leads to a formation of onion ring like structures. More number of onion rings forms at high tool rotational speeds with low traverse speeds. Fig 4.41(d) and (e) shows the HAZ regions formed during the process on AS and RS. It was clearly seen that grain refinement occurred during the process. Large sizes of grains were observed at the HAZ region. A similar way of grain growth takes place on both sides of the processed region and noticed that the size of the grain was increased much large like elongated grain while moving towards the base metal (BM) region. The geometry of the tool pin is incredibly significant in plasticization of material flow and its trend inside the deformation zone. At this point, the geometry of tool and pin is flexible to allow the rich mixture of reinforcement with matrix into the SZ which is shown in Fig. 4.41(f). At the center of the SZ formation of onion ring-like structure can be seen in Fig. 4.41(g). Fig. 4.41(h) shows that the material is drawn towards the surface on the RS.

Figs. 4.42 and 4.43 show the material flow pattern of the fabricated surface nanocomposites with multi hole technique. Fig. 4.42 shows the flow pattern of composite with the multi parallel holes technique where the holes are made within the pin region. Fig. 4.43 shows the flow pattern of composite with multi hole technique where the multi parallel holes were made on both pin region and shoulder region. From the Figs. 4.42 and 4.43 it is clearly shown that, the distribution of the reinforcement particles was taken more effectively into the SZ.

With the addition of multi parallel holes into the shoulder region shows more effective dispersion of reinforcement particles into the shoulder driven region shown in Fig. 4.43. By applying this technique, the distribution of the reinforcement particles into the processed region is more effective than previous technique.

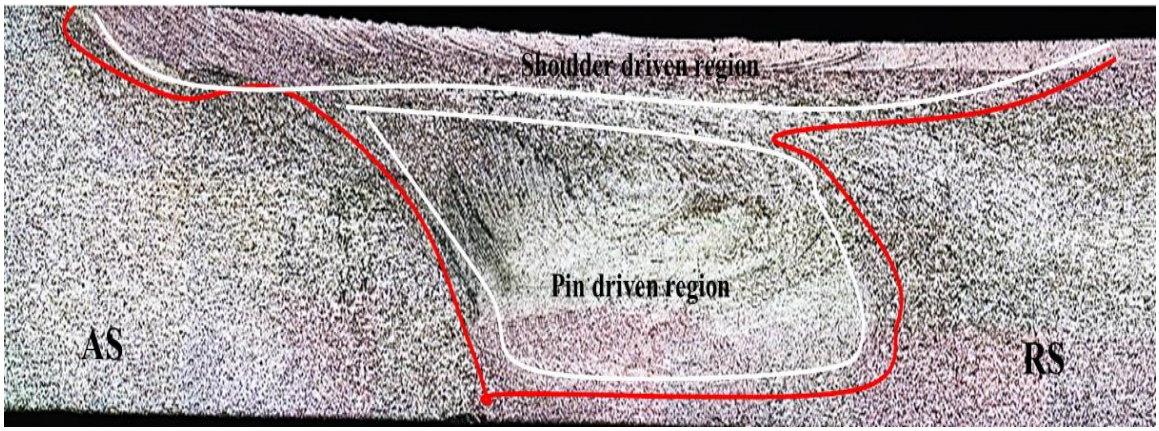

Fig. 4.42 Flow pattern of surface nanocomposite fabricated by FSP with multi hole technique at pin region.

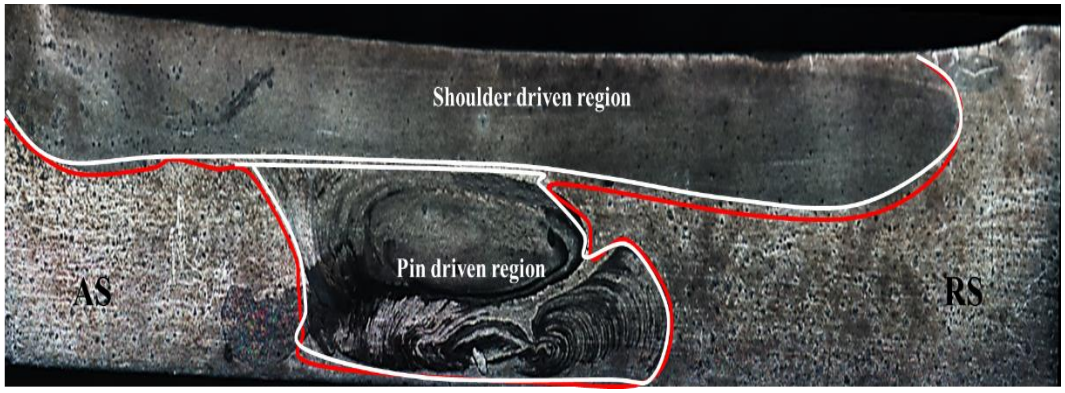

Fig. 4.43 Flow pattern of surface nanocomposite fabricated by FSP with multi hole technique at pin and shoulder region.

4.3.4 Microhardness

To find out the effect of multi hole technique (pin region and pin with shoulder region) on the microhardness properties of fabricated surface nanocomposite all the samples were tested and their values are presented as shown in Tables.

Table 4.7. Microhardness survey of surface nanocomposite produced by multi hole technique (D = 1.5 mm).

Sample ID	Microhardness (Hv)
A1	113.8
A2	126.4
A3	132.5
A4	140.8
B1	121.8
B2	127.4
B3	136.9
B4	141.5
C1	119.8
C2	132.9
C3	139.6
C4	143.6
D1	128.5
D2	134.8
D3	140.5
D4	147.3
E1	115.9
E2	129.5
E3	135.6
E4	141.3
F1	124.6
F2	131.9
F3	138.1
F4	143.8

Table 4.8 Microhardness survey of surface nanocomposite produced by multi hole technique (D = 2.0 mm).

Sample ID	Microhardness (Hv)
G1	129.1
G2	135.4
G3	141.3
G4	146.3
H1	137.6
H2	145.9
H3	149.3
H4	154.2
I1	131.1
I2	139.8
I3	148.2
I4	154.3
J1	143.6
J2	154.1
J3	159.7
J4	162.5
K1	130.3
K2	134.2
K3	145.9
K4	151.2
L1	138.7
L2	147.1
L3	152.8
L4	156.6

Figs. 4.44, 4.45, 4.46 and 4.47 show the microhardness graphs of fabricated surface nanocomposites at different composition of reinforcement regions and with varying diameter of hole. Tables 4.5 and 4.6 show the microhardness values of fabricated surface nanocomposites with multi hole technique having diameter of the hole as 1.5 mm and 2 mm. Figs. 4.44 and 4.46 show the microhardness graphs of surface nanocomposites fabricated with multi hole technique (holes made in pin region) and Figs. 4.45 and 4.47 show the microhardness graphs of the samples produced with multi hole technique (holes made in pin and shoulder region). The samples A1 to B4 and G1 to H4 are produced with the addition of Al_2O_3 reinforcement. The sample C1 to D4 and I1 to J4 are produced with the addition of SiC reinforcement. The samples E1 to F4 and K1 to L4 are produced with hybrid reinforcement (Al_2O_3+SiC).

Fig. 4.44 shows the microhardness graphs of the composites (Al/Al_2O_3, Al/SiC & Al/Al_2O_3 + SiC) produced with hole diameter of 1.5 mm with changing depth of 1, 2, 3 & 3.5 mm at pin region and keeping diameter and depth 1 mm constant on shoulder region. Similarly, Fig. 4.46 gives the microhardness values of composites but the diameter of the hole is changed as 2 mm on pin region as well as shoulder region too. With the increase of hole diameter 1.5 to 2 mm, the addition quantity of the reinforcement particles was increased and it helps to disperse the reinforcement particles into the processed region more uniformly.

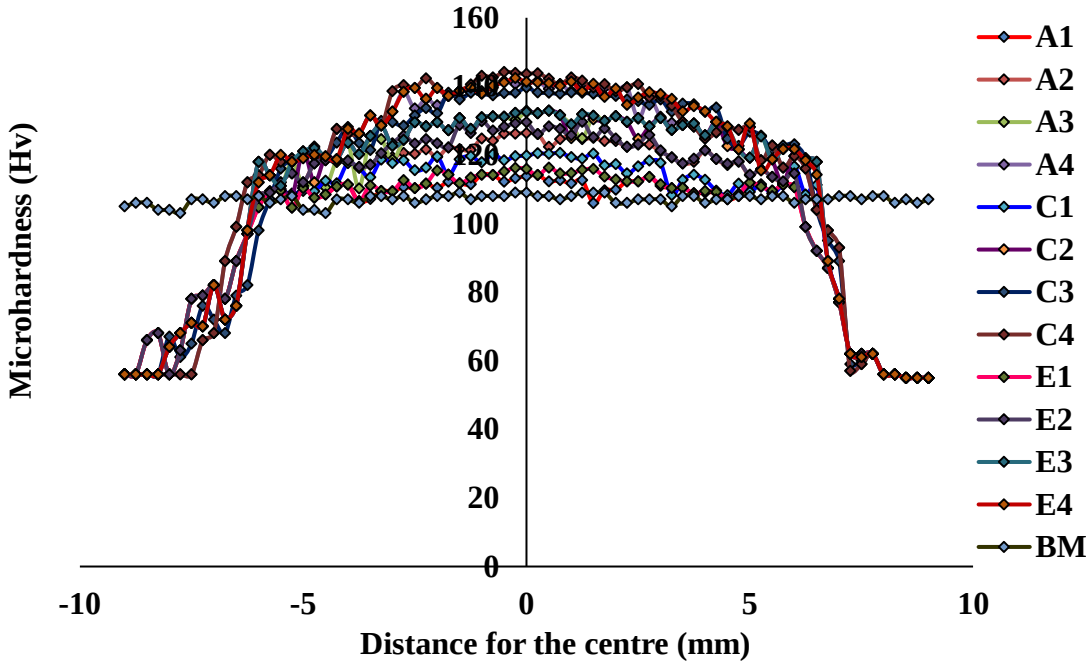

Fig. 4.44 Microhardness survey of fabricated surface nanocomposites (pin region).

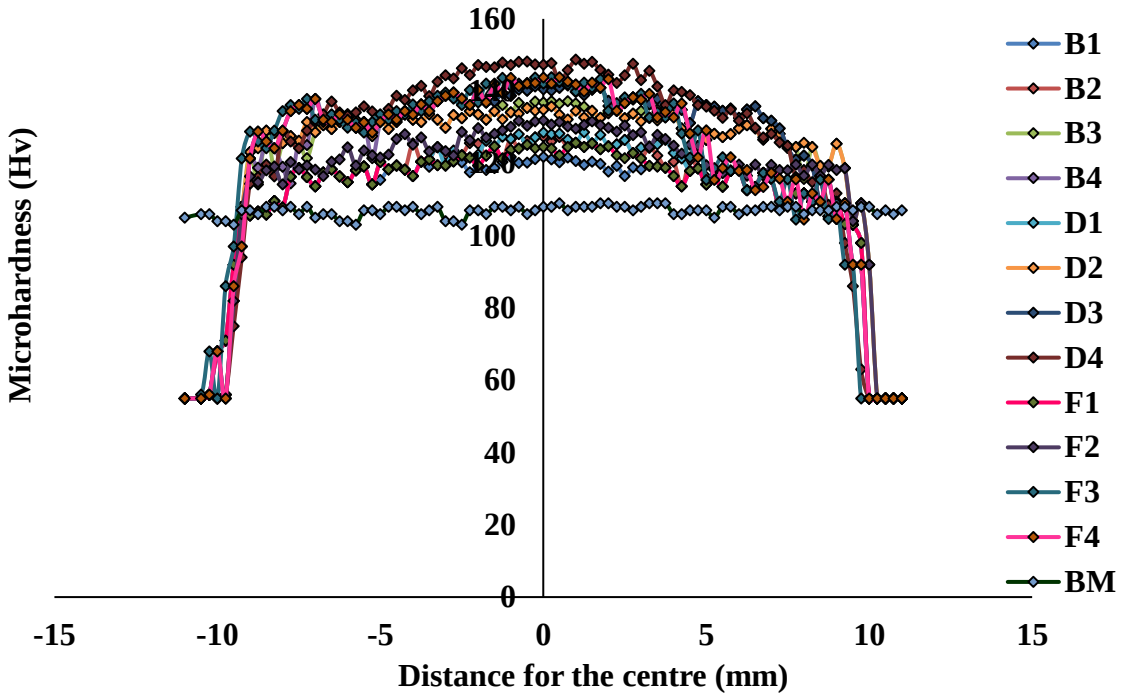

Fig. 4.45 Microhardness survey of fabricated surface nanocomposites (pin + shoulder region).

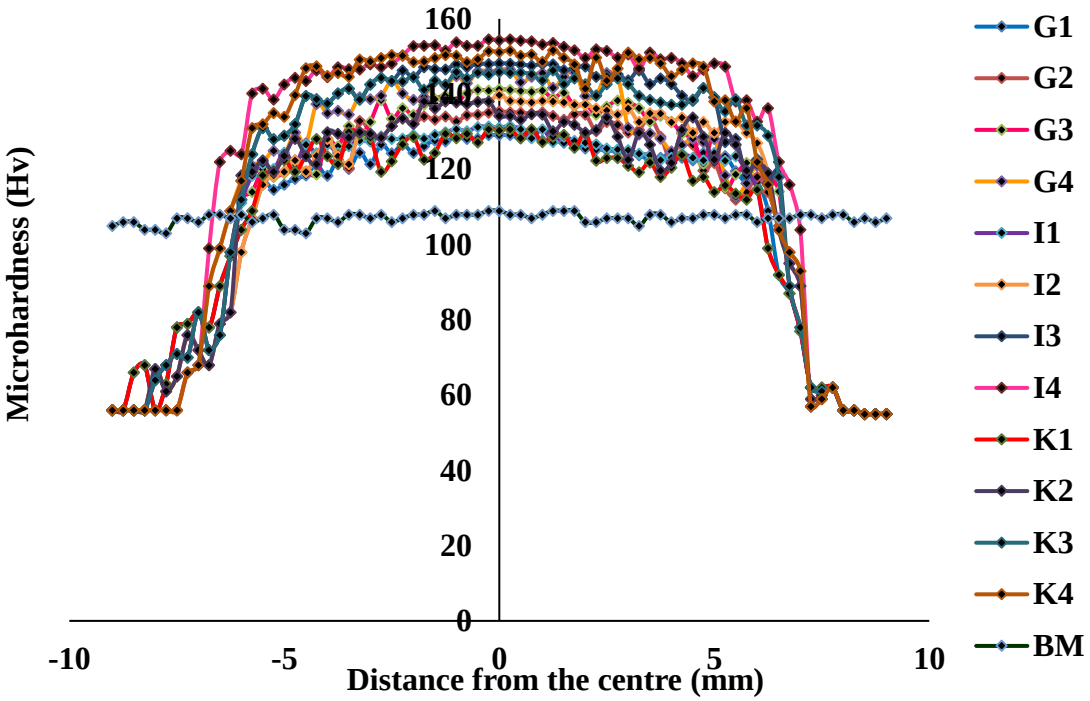

Fig. 4.46. Microhardness survey of fabricated surface nanocomposites (pin region) with diameter of hole is 2.0 mm.

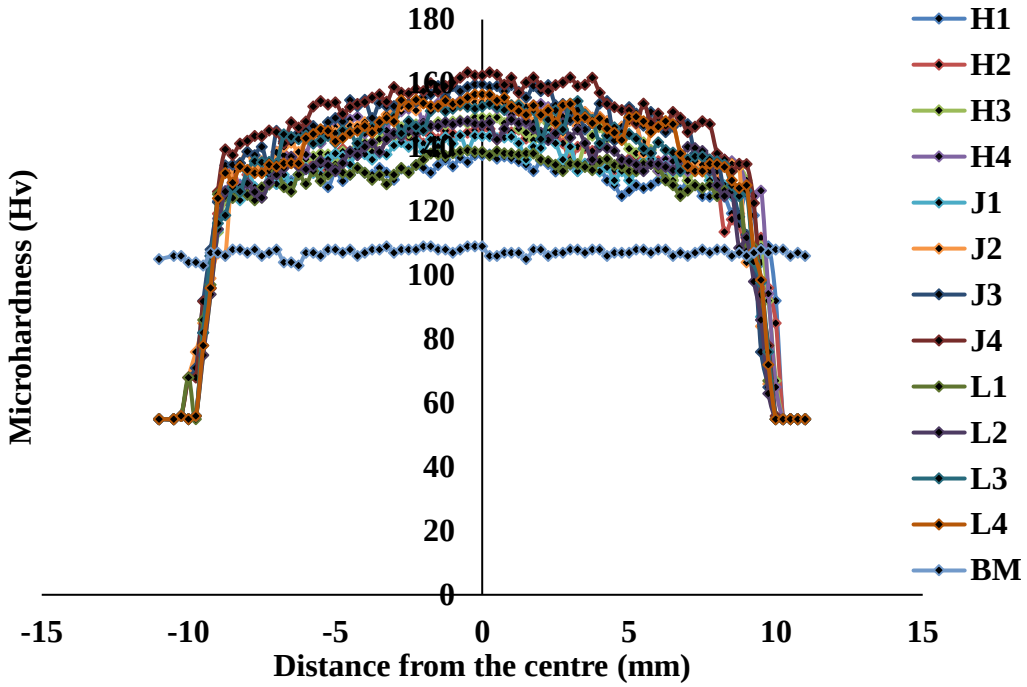

Fig. 4.47. Microhardness survey of fabricated surface nanocomposites (pin + shoulder region) with diameter of hole is 2.0 mm.

From the Fig. 4.44 it is clearly observed that the reinforcement particles (Al_2O_3, SiC & Hybrid) are distributed entirely in the SZ. According to the Hall–Petch equation, high strength and hardness are associated with grain size. Here, the reinforcement particles are occupied at the interfaces of grains and grain boundaries and there were restricted the grain growth which resulted increase in microhardness of the composites. With the addition of reinforcement particles, the microhardness values of the composites were increased much higher than as received base material. There is a slight variation of microhardness values were observed from the microhardness graphs due to some agglomeration of reinforcement particles occurred in the processed region. On the other side, microhardness values at RS shows higher values than the values presented on AS. The same kind of results were observed in all the microhardness graphs shown in Figs. 4.44, 4.45, 4.46 and 4.47.

Figs. 4.45 and 4.47 shows the microhardness graphs of samples B1-B4, D1-D4, F1-F4, H1-H4, J1-J4 and L1-L4. From these graphs it is observed that, the hardness region up to processed region was increased than compared with Figs. 4.46 and 4.48. The multi hole technique (pin + shoulder region) gives effective results and improves the surface composite

region up to processed region. The samples made with the reinforcement of Al_2O_3 and hybrid shows lower values than sample made with SiC reinforcement but compared with base material all the fabricated samples exhibited superior values. From all the microhardness graphs (Figs. 4.44, 4.45, 4.46 and 4.47) higher microhardness values are obtained with the sample of J4 i.e.162.5 Hv (Al/SiC). From the microhardness analysis it is concluded that, the distribution of the reinforcement particles into the SZ and processed region were excellent with superior microhardness values.

4.3.5 Tensile and fractography

To know the strength of the metal or material, tensile test will give the proper results. Here tensile test was performed from the samples fabricated with added multiple reinforcement and with multi hole technique by FSP. All the tensile tested samples were shown in Fig. 4.48. Tables 4.9 and 4.10 show the values of tensile tested samples of A1 to L4. Table 4.9 shows the tensile test results of the sample fabricated with multi hole technique having hole diameter of 1.5 mm and the graphical representation of these values are shown in Fig. 4.49. Similarly, Table. 4.10 shows the tensile test results of the sample fabricated with multi hole technique having diameter of the hole is 2 mm and the graphical representation of these values are shown from the Fig. 4.51. From the Figs. 4.49 and 4.50 it is observed that, the fabricated surface nanocomposites show lower tensile values than base material.

Fig. 4.48 Tensile tested samples of fabricated surface nanocomposites.

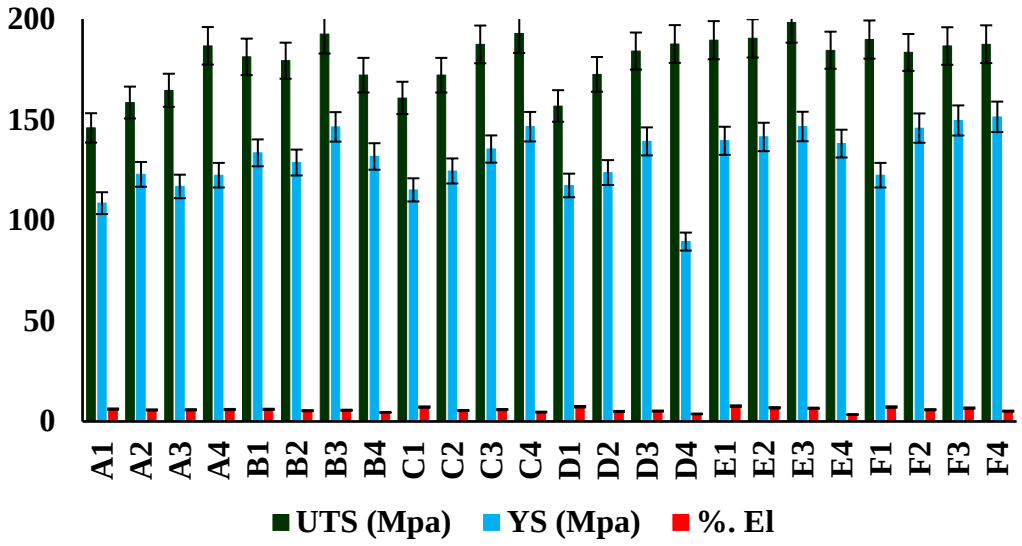

Fig. 4.49 Tensile properties of fabricated surface nanocomposites (D = 1.5 mm) of 3 measurements.

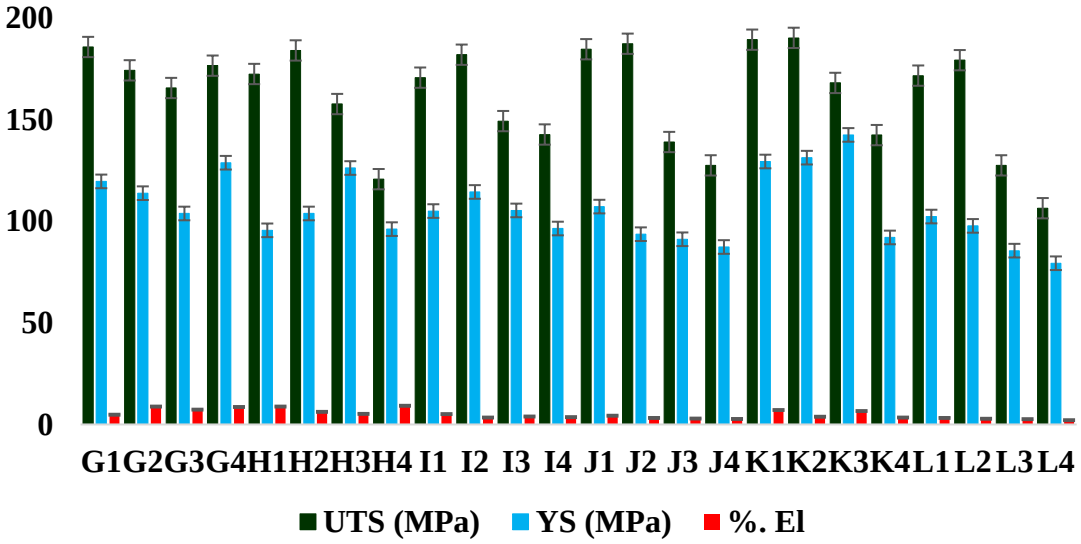

Fig. 4.50 Tensile properties of fabricated surface nanocomposites (D = 2.0 mm) of 3 measurements.

Table 4.9. Tensile properties of surface nano composites fabricated by multi hole technique at D = 1.5 mm.

Sample ID	Ultimate tensile strength (UTS, MPa) *	Yield strength (YS, MPa) *	Percentage of elongation (%EL) *
A1	145.9	108.5	6.14
A2	158.5	122.8	5.72
A3	164.6	116.8	5.82
A4	186.7	122.4	5.93
B1	181.2	133.5	6.02
B2	179.3	128.7	5.36
B3	192.5	146.4	5.56
B4	172.1	131.7	4.48
C1	160.8	115.1	7.12
C2	172.1	124.5	5.42
C3	187.4	135.4	5.89
C4	192.8	146.5	4.64
D1	156.8	117.3	7.32
D2	172.5	123.7	4.98
D3	184.1	139.2	5.16
D4	187.6	89.4	3.73
E1	189.5	139.5	7.62
E2	190.4	141.4	6.78
E3	198.2	146.6	6.54
E4	184.5	138.1	3.43
F1	189.8	122.4	7.15
F2	183.4	145.8	5.83
F3	186.6	149.6	6.61
F4	187.5	151.4	5.12

Table 4.10. Tensile properties of composites fabricated by multi hole technique at D = 2.0 mm.

Sample	Ultimate tensile strength (UTS, MPa) *	Yield strength (YS, MPa) *	Percentage of elongation (%EL) *
G1	185.9	119.7	4.8
G2	174.4	113.9	8.8
G3	165.7	103.9	7.3
G4	176.7	128.9	8.6
H1	172.6	95.6	8.8
H2	184.2	103.9	6.2
H3	157.8	126.3	5.2
H4	120.8	96.2	9.2
I1	170.8	105.1	5.1
I2	182.1	114.5	3.4
I3	149.4	105.4	3.9
I4	142.8	96.5	3.6
J1	184.8	107.3	4.3
J2	187.5	93.7	3.2
J3	139.1	91.2	2.9
J4	127.6	87.4	2.7
K1	189.5	129.5	7.1
K2	190.4	131.4	3.8
K3	168.2	142.6	6.6
K4	142.5	92.1	3.4
L1	171.8	102.4	3.2
L2	179.4	97.8	2.8
L3	127.6	85.6	2.6
L4	106.5	79.4	2.1

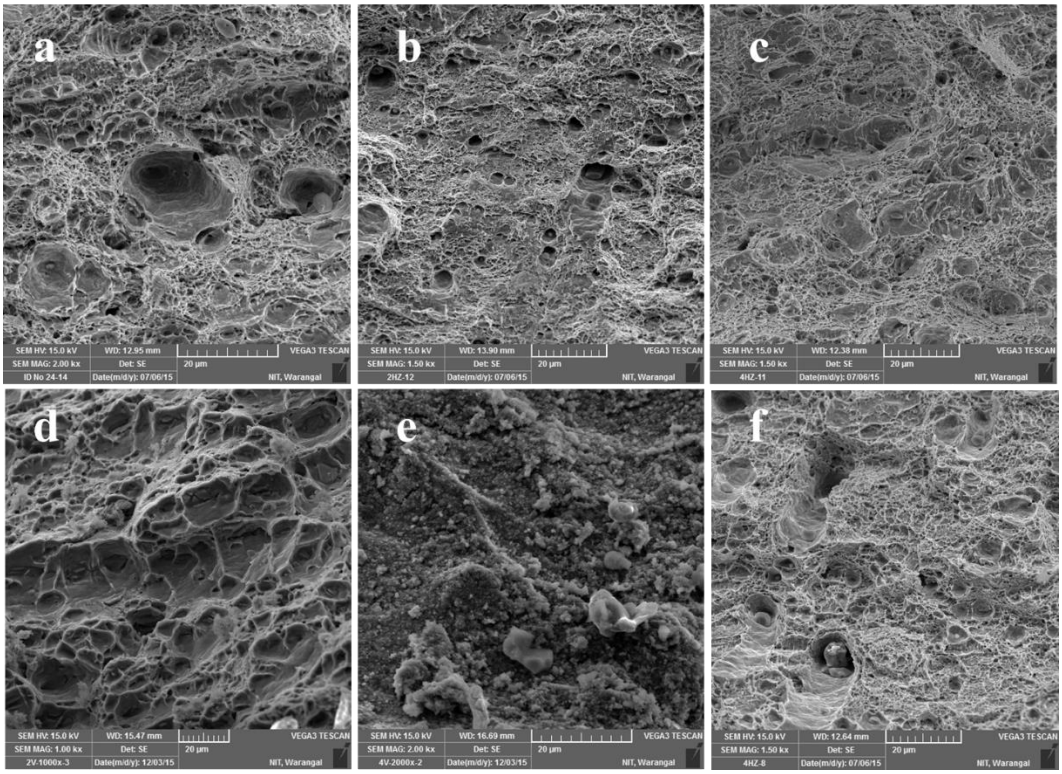

Fig. 4.51 SEM fractography images of fabricated surface nanocomposites with pin region and pin + shoulder region: (a) Al/Al_2O_3 (pin region); (b) Al/SiC (pin region); (c) Al/Al_2O_3 + SiC (pin region); (d) Al/Al_2O_3 (pin + shoulder region); (b) Al/SiC (pin + shoulder region); (c) Al/Al_2O_3 + SiC (pin + shoulder region).

From the fractography analysis of SEM micrographs it is revealed that, the failure occurred in the form of ductile nature in Al/Al_2O_3 composites, little bit brittle nature in Al/SiC composites and the combination of brittle and ductile failure occurred in hybrid composites (Al/Al_2O_3+SiC). Figs. 4.51(a) and (d) show, ductile nature (large dimples were observed) of failure of Al/Al_2O_3 composites. Figs. 4.51(b) and (e) show the fractography micrographs of Al/SiC composites. The failure of the composites shown little bit brittle nature due to the presence of SiC reinforcement particles. Figs. 4.51(c) and (f) show a mixed nature of failure in hybrid composites. The presence of Al_2O_3 and SiC particles may cause this type of failure. All the fabricated surface nanocomposites with multi hole technique resulted in similar kind of failures.

It is revealed that, UTS, YS and %EL of all the above surface nanocomposites are lower than the as-received Al alloy. This is due to the presence of reinforcement particles that could be restricting the grain boundary sliding and dislocations which leads to deteriorate the tensile properties [67] and loss of precipitations during FSP [70,72].

4.3.6 Wear

Addition of reinforcement particles into the matrix material results in increasing wear and mechanical properties of fabricated composite (metal matrix composite). In order to find out the wear mechanism of fabricated composites conduct of wear test is necessary. For that all the fabricated samples (Al/Al_2O_3, Al/SiC and hybrid) were tested under constant load (20 N) with varying sliding distance. After conducting wear test, the samples were observed under SEM to study the wear characteristic of samples.

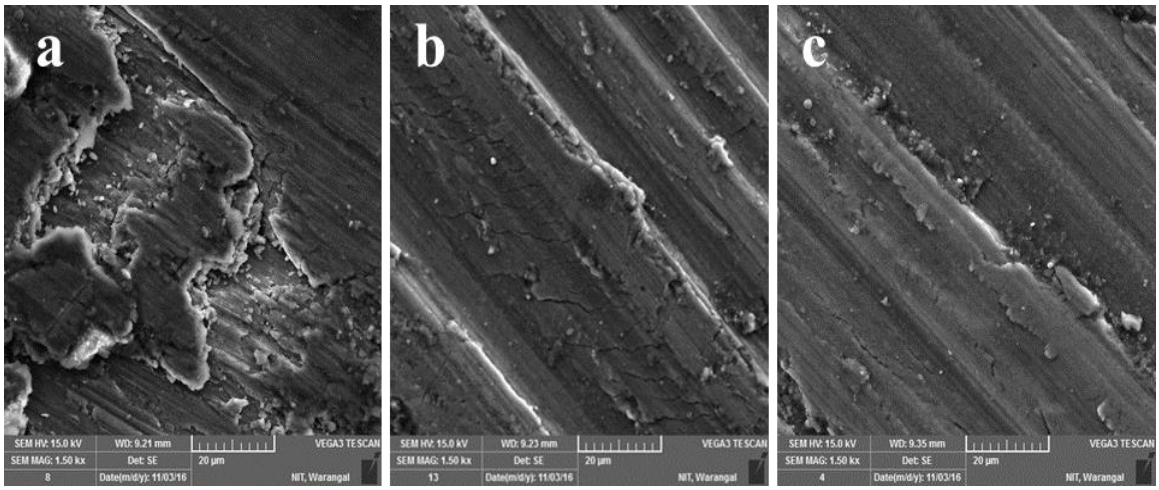

Fig. 4.52 SEM micrographs of the worn surface of surface nano composites and hybrid surface nanocomposite: (a) Al/Al_2O_3, (b) Al/SiC and (c) Al/(Al_2O_3+SiC).

Fig. 4.52 shows the worn-out surfaces of fabricated surface nanocomposites (Al/Al_2O_3, Al/SiC and Al/Al_2O_3+SiC). The samples fabricated with Al_2O_3 at different composition shows similar results with slight variation to that of SiC and Hybrid (Al_2O_3 + SiC) composites too. Here Fig. 4.52(a) shows the worn-out surface of the sample fabricated with the addition of Al_2O_3 reinforcement particles, Fig. 4.52(b) shows the worn-out surface of the composite fabricated with the addition of SiC particles and Fig. 4.52(c) shows the worn-out surface of the composite fabricated with the addition of hybrid (Al_2O_3 + SiC) reinforcement. Fig. 4.52(a) shows, the worn-

out surface of Al/Al_2O_3 composite and it is evident from removal of a surface layer in the form of small fragments where the crack is generated. This kind of fragment formation occurred throughout the worn-out surface of the sample which increases the tendency of removal of material from the surface. Fig. 4.52(b) shows, the worn-out surface of Al/SiC composite. There are several parallel grooves like structure observed on the surface due to the presence of SiC particles. During the test, the SiC particles acts like blockades to prevent the larger material removal from the composite surface and forms like parallel grooves. Fig. 4.52(c) shows, the worn-out surface of hybrid composite. From the Fig. 4.52(c) it is observed that the combination of Al_2O_3 and SiC reinforcement gives best result in the form of less removal of material from the composite surface. Individual properties of Al_2O_3 and SiC particle showed completely different kind of worn-out surfaces but when they were combined as one they exhibited superior properties than individual properties of reinforcement because Al_2O_3 acts like solid lubricant and SiC acts like load bearing particles.

The graphical representation of wear rate versus sliding distance of fabricated composites shown in Fig. 4.53. From the graph, it is clearly seen that, rate of wear of the base material is very high than compared with fabricated composites and it is almost more than twice of the composites. From the Fig. 4.53 it is observed that, the fabricated composites have excellent wear resistance properties than base material. Hybrid composite (avg. 0.0321 mg/m) shows good wear resistance properties than Al/Al_2O_3 (avg. 0.0404), Al/SiC (avg. 0.0359 mg/m) and base material (avg. 0.0627). Fig. 4.54 shows the graphical representation of weight loss of the material versus sliding distance. From the Fig. 4.54 it is observed that large amount of the material is removed from the base material due to high amount of frictional heat is generated at rubbing surface between the hard disk and soft base material. Initially the wear rate of base material is twice that of the composite but later with increasing sliding distance it was gradually increased. At the extent period of sliding distance, the loss of material from the surface is decreased than initial stage of test. This may be due to the formation of a surface layer (debris of removal material) between the sample and disk. The fabricated surface nanocomposites exhibited superior wear resistance properties than base material and it is shown evidently from the Fig. 4.54. Hybrid surface nanocomposites showed excellent wear resistant property than Al/Al_2O_3 and Al/SiC composites. The weight loss of the hybrid surface nanocomposite (avg. 2.14 mg) is less than Al/Al_2O_3 (avg. 3.16 mg), Al/SiC (2.61 mg) and base material (avg. 6.06 mg).

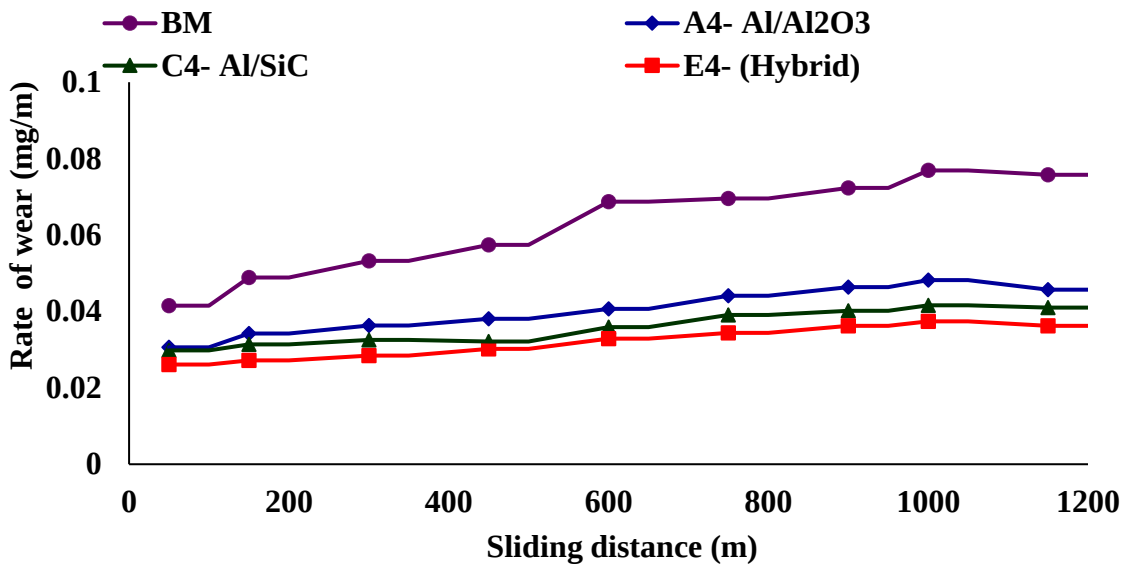

Fig. 4.53 Change in the rate of wear with sliding distance for the composites produced by multi hole technique.

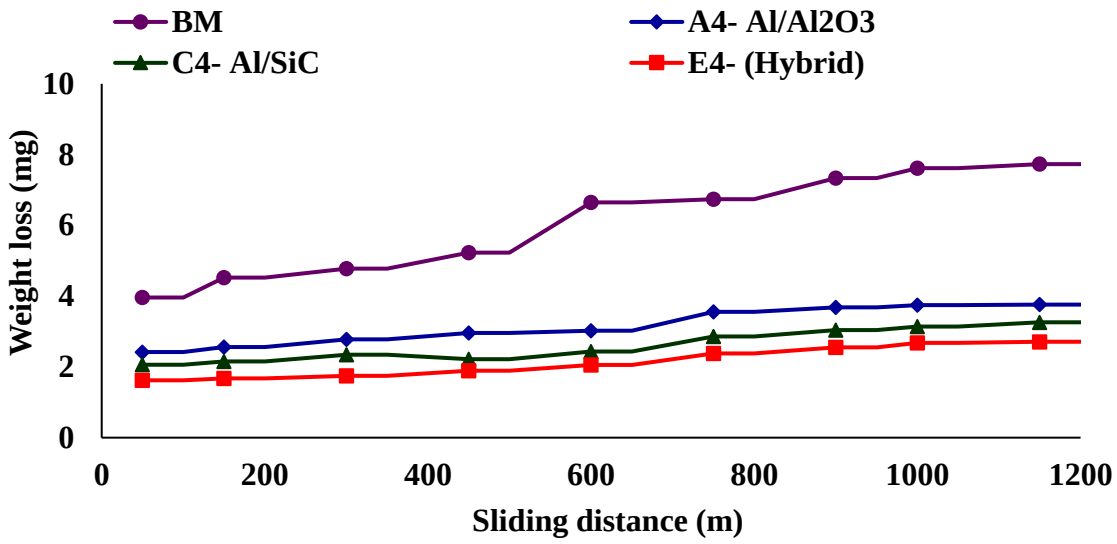

Fig. 4.54 Change in the weight loss with sliding distance for the composites produced by multi hole technique.

4.3.7 Introduction of Multi groove technique

A novel technique is used to develop a surface nanocomposite with high volume percentage of reinforcement into the matrix material. Initially grooves were made with in the pin region to study the nature of the material flow and the dispersion of the reinforcement particles into the matrix. In previous investigation, a single groove is made along the center line to add the reinforcement into the base material.

To increase the reinforcement volume percentage, the groove dimensions are to be change per the volume percentage of reinforcement. This leads to increase in the defect formation during the fabrication of high volume percentage of composites. So, to avoid the defect formation and increase the volume percentage of reinforcement a novel technique called multi groove technique was implemented to fabricate successful surface nanocomposites with single pass FSP. Fig. 4.49 shows the multi grooves were made on the advancing side of the center of line and the number of the grooves made depends on the tool pin. Here four grooves were made on AS with in the pin region to produce surface composite. The width of the groove (w) is kept as constant and depth (d) is changed to increase the volume percentage of reinforcement. Here, the width of the groove is 0.5 mm as mentioned above for all the regions but the depth of the shoulder is restricted up to 1 mm only.

Further increase in depth in the shoulder region leads to defect formation. Selected process parameters for conducting the experiments were shown in Table. 4.11. Selected concave shoulder taper cylindrical threaded tool having 24 mm shoulder diameter tool geometry was used to fabricate the surface composites. A detailed list of sequence of experiments are listed in Table. 4.11.

Table 4.11 Detailed experimental sequence of multi groove technique.

Sample ID	Composite	Composite region	Dimensions (mm)		No. of grooves	
			Pin	Shoulder	Pin	Shoulder
T1	Al + Al_2O_3	P	W = 0.5, Dg = 1		4	
T2	Al + Al_2O_3	P	W = 0.5, Dg = 2		4	
T3	Al + Al_2O_3	P	W = 0.5, Dg = 3		4	
U1	Al + Al_2O_3	P + S	W = 0.5, Dg = 1	W = 0.5, Dg = 1	4	4
U2	Al + Al_2O_3	P + S	W = 0.5, Dg = 2	W = 0.5, Dg = 1	4	4
U3	Al + Al_2O_3	P + S	W = 0.5, Dg = 3	W = 0.5, Dg = 1	4	4
V1	Al+ SiC	P	W = 0.5, Dg = 1		4	
V2	Al+ SiC	P	W = 0.5, Dg = 2		4	
V3	Al+ SiC	P	W = 0.5, Dg = 3		4	
W1	Al+ SiC	P + S	W = 0.5, Dg = 1	W = 0.5, Dg = 1	4	4
W2	Al+ SiC	P + S	W = 0.5, Dg = 2	W = 0.5, Dg = 1	4	4
W3	Al+ SiC	P + S	W = 0.5, Dg = 3	W = 0.5, Dg = 1	4	4
X1	Al + Al_2O_3 + SiC	P	W = 0.5, Dg = 1		4	
X2	Al + Al_2O_3 + SiC	P	W = 0.5, Dg = 2		4	
X3	Al + Al_2O_3 + SiC	P	W = 0.5, Dg = 3		4	
Y1	Al + Al_2O_3 + SiC	P + S	W = 0.5, Dg = 1	W = 0.5, Dg = 1	4	4
Y2	Al + Al_2O_3 + SiC	P + S	W = 0.5, Dg = 2	W = 0.5, Dg = 1	4	4
Y3	Al + Al_2O_3 + SiC	P + S	W = 0.5, Dg = 3	W = 0.5, Dg = 1	4	4

P = Pin region; P+S = Pin + Shoulder region; W = Width of the groove; Dg = Depth of the groove.

4.3.8 Macrostructure

The fabricated surface nanocomposites show defect free and smooth surface finished composites. A common exist hole was found in all fabricated composites and a small amount of flash was observed along boundaries of the processed region. The surface finish of the fabricated composites was varied with the addition of Al_2O_3, SiC and Al_2O_3 + SiC (Hybrid) nano

reinforcements. The fabricated Al/SiC composite surface finish was found to be rough as compared to Al/Al_2O_3 and Al/Al_2O_3 + SiC composites.

4.3.9 Microstructure

To study the effect of multi groove technique on material flow and defect formation, all the samples were examined by using stereo zoom microscope. Fig. 4.55 shows the various micrographs of fabricated samples. By using novel technique (multi groove) all samples were fabricated.

The samples made with multi groove technique (pin region) shows a clear distribution of reinforcement particles into the SZ and the samples made with multi groove technique (pin + shoulder region) shows the distribution of the reinforcement occurred at processed region. By changing the reinforcement particles, it is not going to affect the dispersion of the particles into the SZ as well as processed region. The same material flow was observed in all fabricated surface nanocomposites with different reinforcements like Al_2O_3, SiC and hybrid (Al_2O_3 + SiC).

Fig. 4.56 shows the SEM micrographs taken at various regions of composites. Fig. 4.56(a) shows the fabricated Al/Al_2O_3 surface nanocomposite, Fig. 4.56(b) shows Al/SiC surface nanocomposite and Fig. 4.56(c) shows Al/Al_2O_3 +SiC (hybrid) surface nanocomposite. From all the SEM micrographs reveals that, the good dispersion of reinforcement particles takes place. In all the Fig. 4.56 agglomeration of the particle is observed.

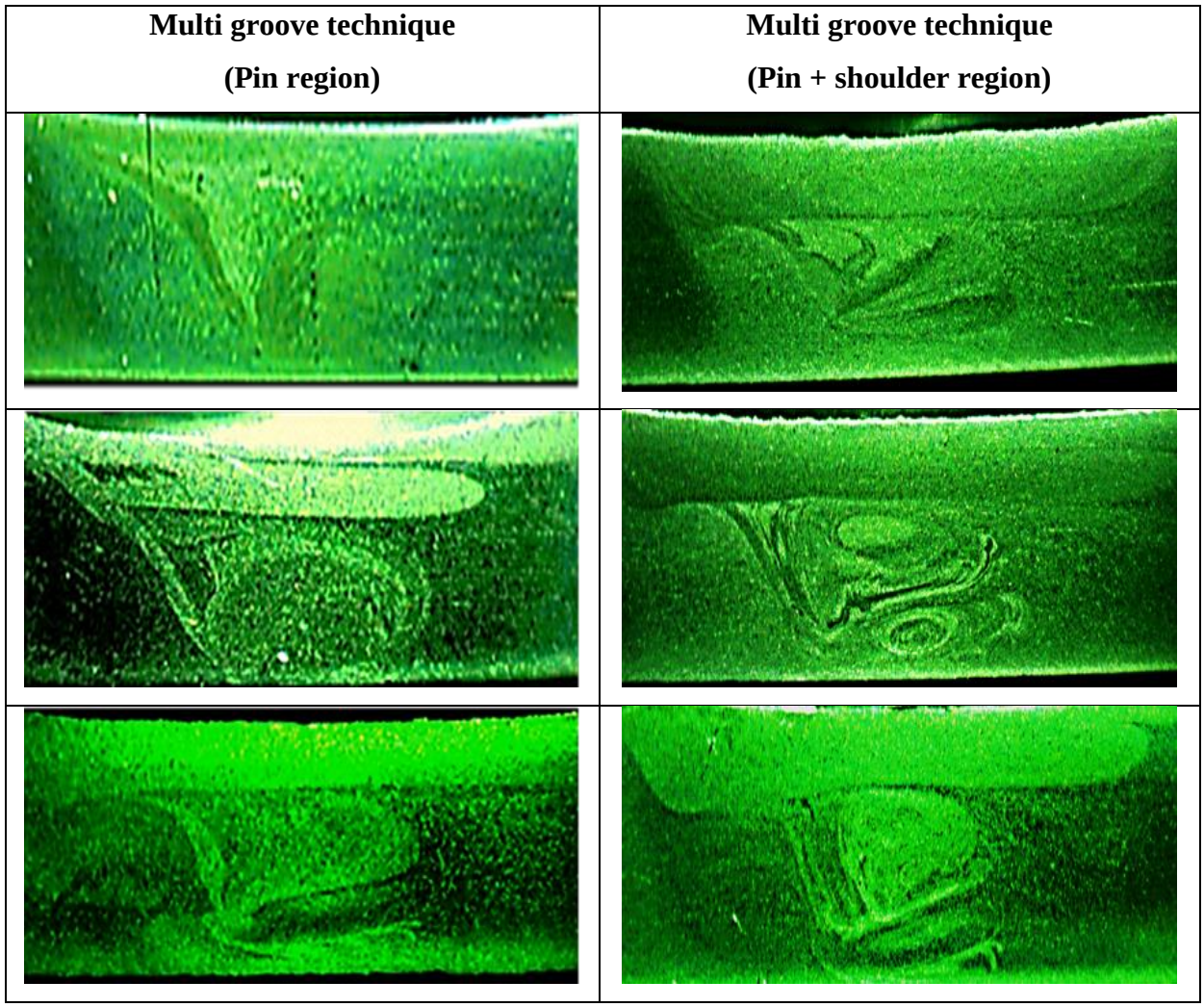

Fig. 4.55 Macrostructures of fabricated samples with pin region and pin + shoulder region.

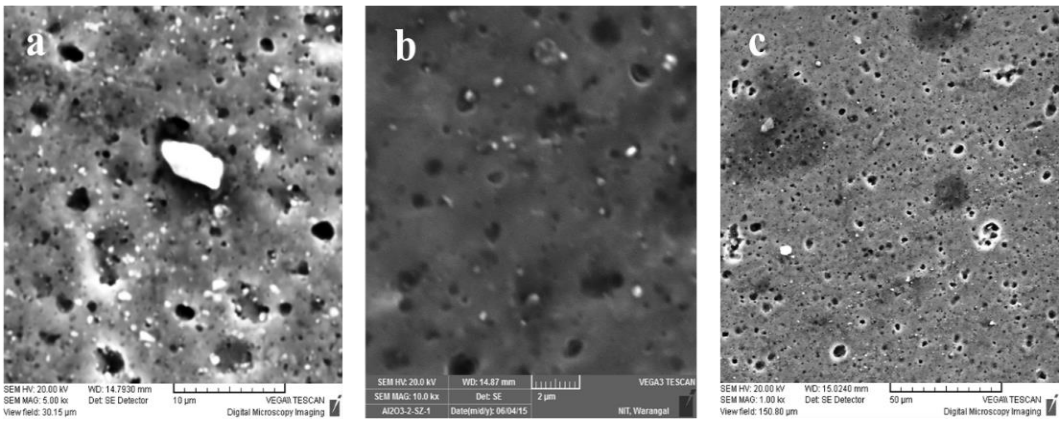

Fig. 4.56 SEM micrograph of fabricated surface nanocomposite: (a) Al/Al_2O_3, (b) Al/SiC, (c) $Al/(Al_2O_3+SiC)$.

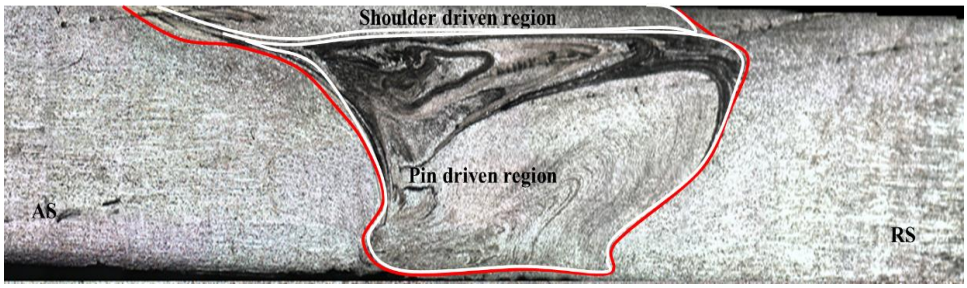

Fig. 4.57 Flow pattern of fabricated surface nanocomposite with multi groove technique (pin region) by FSP.

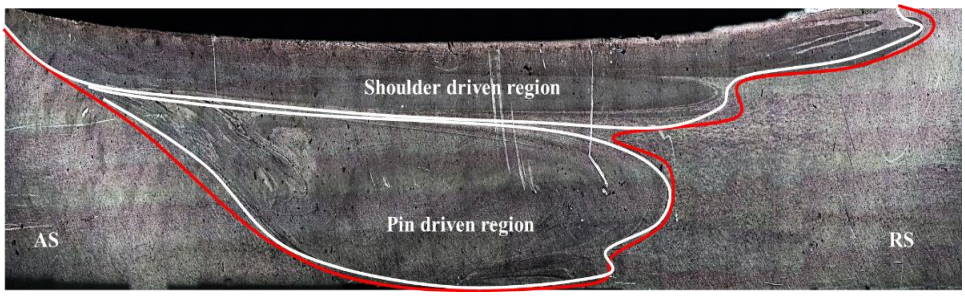

Fig. 4.58 Flow pattern of fabricated surface nanocomposite with multi groove technique (pin and shoulder region) by FSP.

Multi groove technique is one of the best technique to improve the surface composite region and it is clearly seen through the flow patterns of the fabricated surface nanocomposites shown in Figs. 4.57 and 4.58. The dispersion of the reinforcement particles into the processed was restricted to pin driven region shown in Fig. 4.57. From the Fig. 4.58 it is observed that, the reinforcement particles are widely distributed throughout the processed region. It means, making of multi groove on shoulder contact region gives more effective results than groove made in pin region.

4.3.10 Microhardness

A superior microhardness values are achieved with the composites produce by using multi groove technique. Figs. 4.59 and 4.60 give a complete detail of microhardness values obtained at pin region and pin + shoulder region. The dispersion of the reinforced particles can be seen from the microhardness graphs. The increase in composite region shows good microhardness values than groove made only in pin region. The composites made with SiC

reinforcement particles exhibited higher microhardness values than compared with the Al/Al_2O_3 and hybrid composites. Mainly in MMC increased hardness was achieved basically due to nature of the reinforcement particles added and the uneven thermal expansion coefficient of reinforcement and matrix phases caused by dislocation [23]. A clear hardness disparity was noticed between the Al/Al_2O_3, Al/SiC and Al/Al_2O_3+SiC (hybrid) composites. Higher hardness values were shown in Al/SiC composites than Al/Al_2O_3 and hybrid composites. At each level of volume percentage Al/SiC composites dominated the Al/Al_2O_3 and hybrid composites. It may be due to the presence of hard ceramic and carbide particles of reinforcement.

Table 4.12 Microhardness values of surface nanocomposites produced by multi groove technique.

Sample ID	Microhardness (Hv)*
T1	129.3
T2	138.5
T3	146.6
U1	140.4
U2	149.1
U3	153.3
V1	134.3
V2	146.5
V3	150.5
W1	145.4
W2	151.9
W3	163.4
X1	135.4
X2	142.8
X3	149.1
Y1	143.7
Y2	151.9
Y3	158.2

*Average of 3 samples.

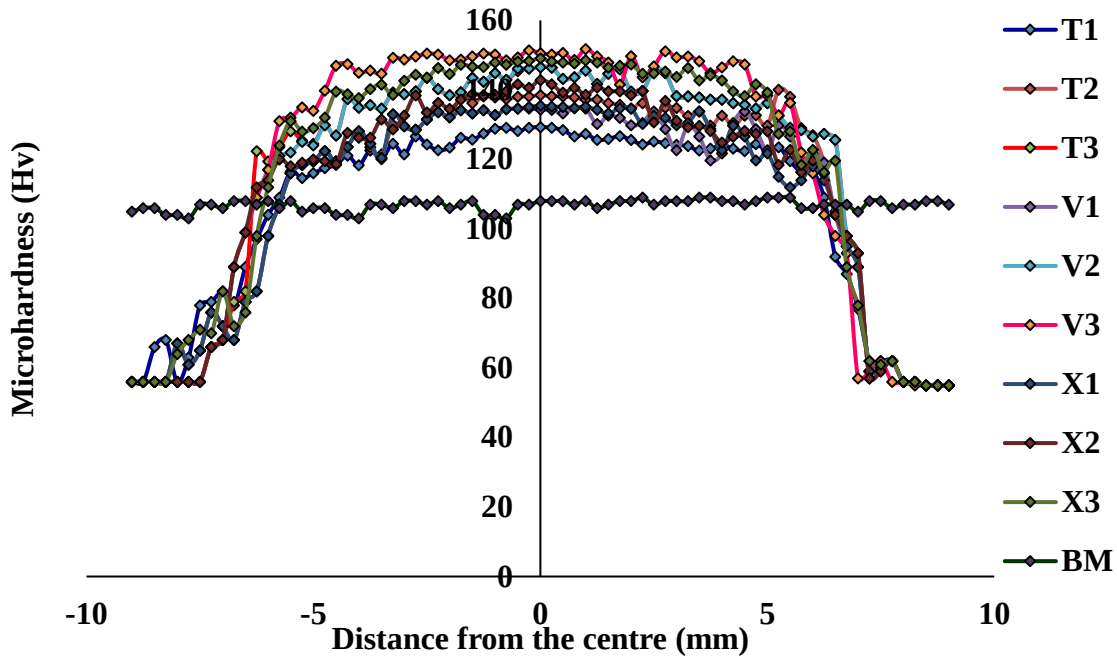

Fig. 4.59 The microhardness survey of surface nanocomposites fabricated with multi groove technique at pin region.

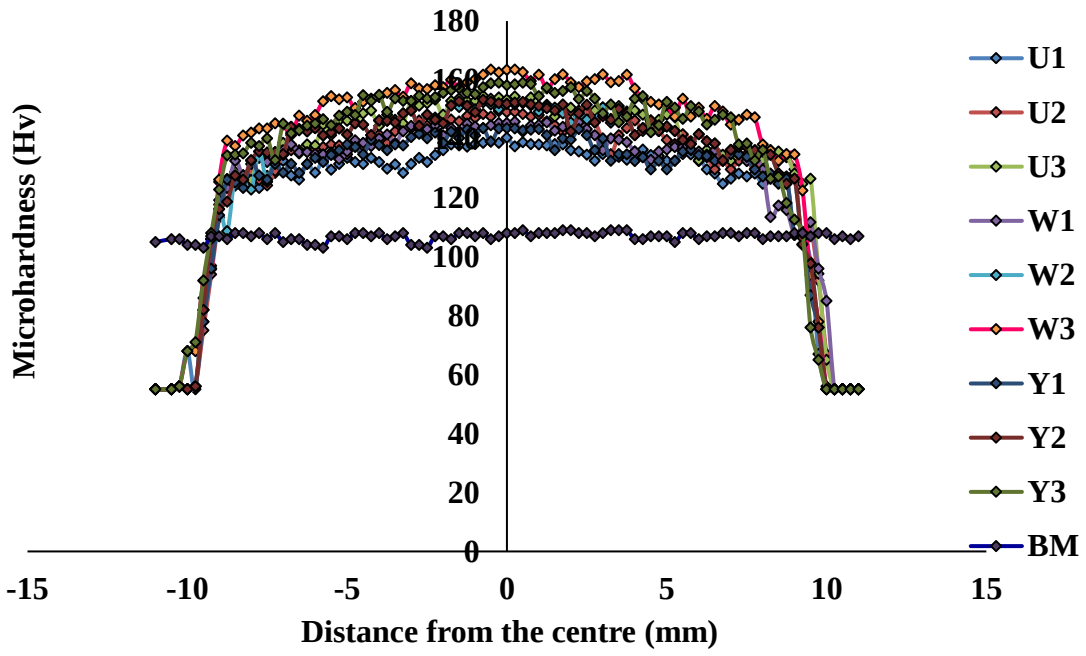

Fig. 4.60 The microhardness survey of surface nanocomposites fabricated with multi groove technique at pin + shoulder region.

4.3.11 Tensile and fractography

Tensile test was conducted to know the strength of the composites under room condition using universal testing machine. Each sample was tested (an average of three samples of each composite) under same conditions and the results were drawn. The tensile tested samples were shown in Fig. 4.61. Almost all the samples were failed at the middle of the composite in the form of cup and cone shape. After that samples were examined under SEM for fractography analysis.

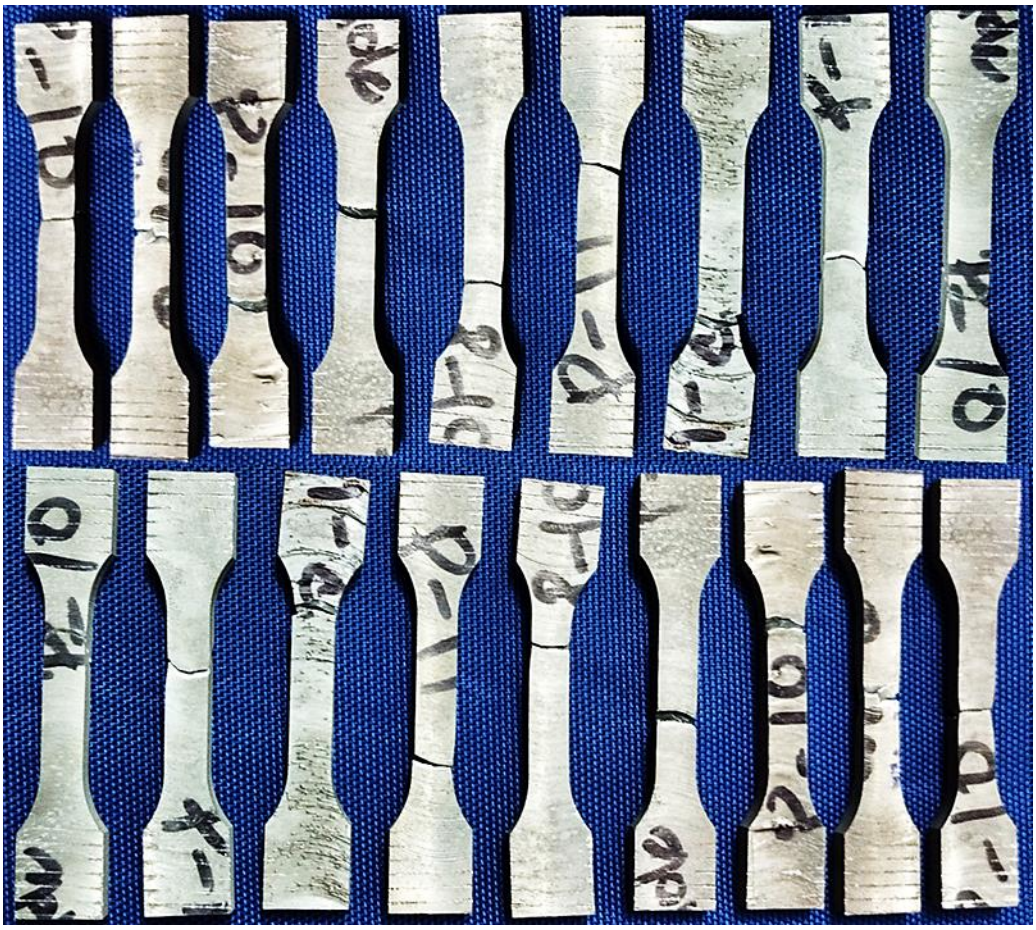

Fig. 4.61 Tensile tested samples of surface nanocomposites.

Table 4.13 shows the tensile tested results of the composites. From the results it is observed that, the composite fabricated with the combination of Al_2O_3 and SiC reinforcement shows superior tensile properties than compared with Al/Al_2O_3 and Al/SiC composites. Fig. 4.62 shows graphical representation of tensile tested values of composites. Fig. 4.63 shows the SEM micrographs of fractured surfaces of composites.

Table 4.13 Tensile properties of surface nanocomposites fabricated by multi groove technique.

Sample ID	Ultimate tensile strength (UTS, MPa) *	Yield strength (YS, MPa) *	Percentage of elongation (%EL) *
T1	182.4	125.7	7.32
T2	186.6	138.3	7.41
T3	191.1	130.4	6.53
U1	182.5	136.7	5.29
U2	133.7	121.7	3.67
U3	168.5	116.5	4.51
V1	175.6	132.4	5.21
V2	152.2	98.4	4.92
V3	164.5	103.1	5.26
W1	157.6	118.4	5.21
W2	194.5	123.6	7.12
W3	195.4	137.2	5.98
X1	185.4	116.4	6.72
X2	192.1	129.6	4.24
X3	194.3	122.5	4.36
Y1	192.9	134.2	5.94
Y2	193.3	129.3	4.68
Y3	196.8	142.6	6.96

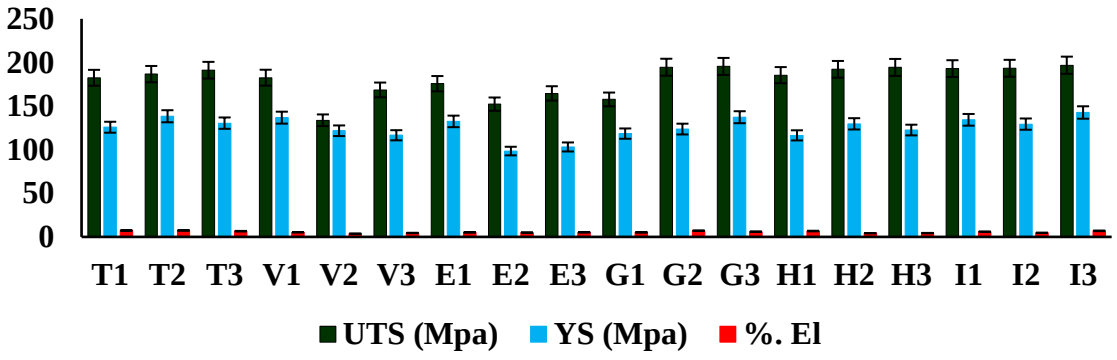

Fig. 4.62 Tensile properties of fabricated surface nanocomposites (multi groove technique) of 3 measurements.

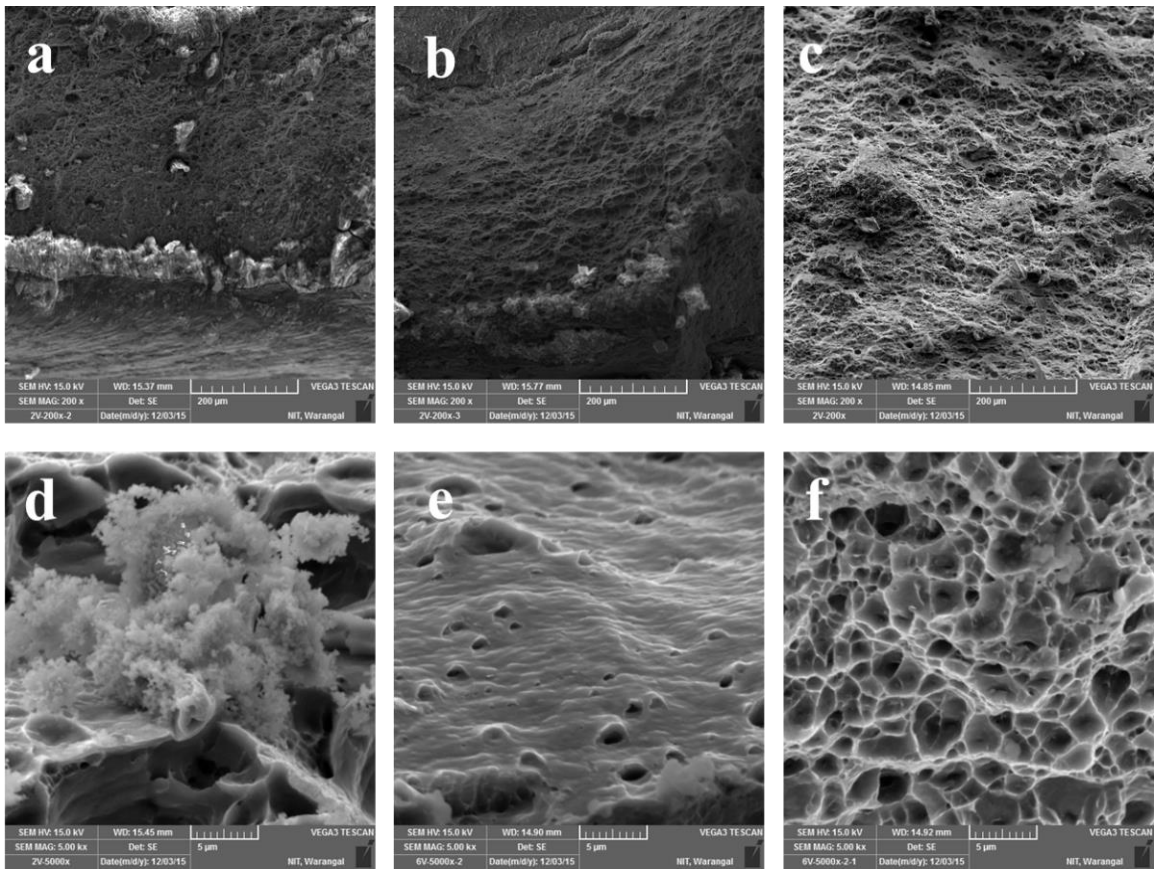

Fig. 4.63 SEM micrographs of fractured surface of composites: (a) and (d) Al/Al_2O_3 composite; (b) and (e) Al/SiC composite; (c) and (e) Al/Al_2O_3+SiC composite.

From the fractography analysis it is revealed that, the failure of the composites occurred in different manner like Al/Al_2O_3 composites failed in the form of ductile (large form of dimples were formed at failure zone), Al/SiC composites were failed in the form of brittle nature (presence of hard ceramic particles) and Al/Al_2O_3 + SiC showed brittle and ductile nature. Figs. 4.63(a) and (d) show the Al/Al_2O_3 composite fractured surfaces. Fig. 4.63(a) shows that, the failure was occurred in the form of cup shape and ductile manner. Fig.4.63(d) shows the presence of Al_2O_3 particles at the failure zone. Figs. 4.63(b) and (e) are fractography micrographs of Al/SiC composites. It is observed from the Figs. 4.63(b) and (e) that the failure happened in the form of brittle nature. Figs.4.63(c) and (f) show the hybrid composite sample fractography microstructures. The combination of Al_2O_3 and SiC improved the nature of bonding between the matrix material and the reinforcement. The failure occurred in the form of ductile nature but some regions showed brittle nature.

4.3.12 Wear

The surface contact between the rotating disk and the surface nanocomposite produces frictional heat between them. This frictional heat plasticizes the soft material (fabricated composites) and lead to material loss from the surface of the composite in terms of wear rate (mg/m). During the test, material from the sample surface is sheared along the sliding direction and seems like adhesive wear. Fig. 4.64 shows the worn surfaces of fabricated surface nanocomposite ((a) Al/Al_2O_3, (b) Al/SiC & (c) hybrid (Al/Al_2O_3 + SiC)). All the samples were wear tested under same condition even though they exhibit different surface worn out surfaces.

Fig. 4.64(a) shows larger grooves than compared with Figs. 4.64(b) and (c). The surface nanocomposites fabricated with the addition of SiC reinforcement particles shows more number of grooves on the surface than Al_2O_3 and hybrid. Here hard SiC particles act like obstacles to lose the more amount of material from the surface of the composite during the wear test. The SiC particles in the composite turn as barriers during the test and reduces the contact between the surface of the composite and rotating disk. An abrasive nature wear is observed from the Fig. 4.64(b) because of SiC particle presented in the matrix and SiC reinforcement particles performed like load bearing particles.

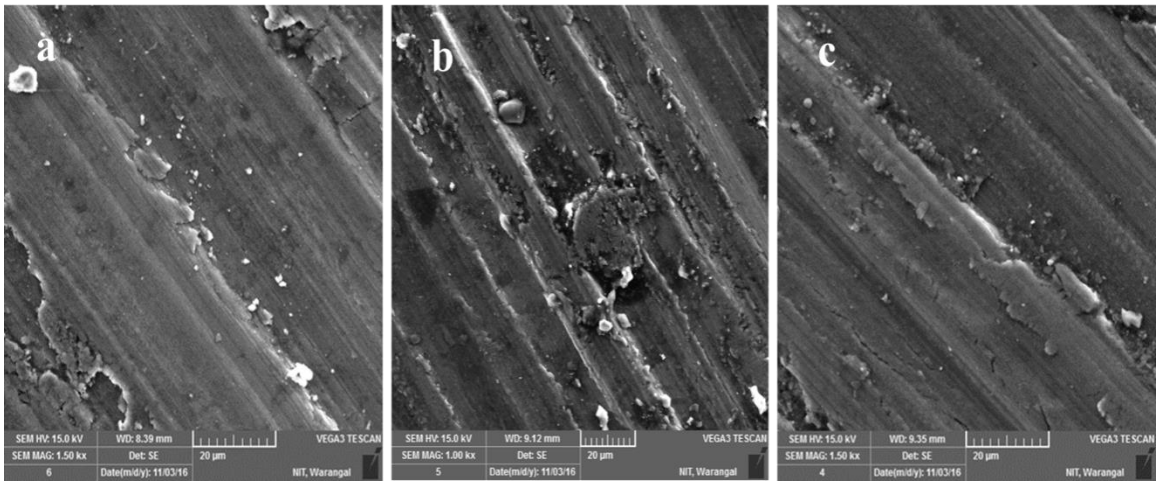

Fig. 4.64 SEM micrographs of worn surface of the composites: (a) Al/Al_2O_3, (b) Al/SiC and (C) Al/(Al_2O_3+SiC).

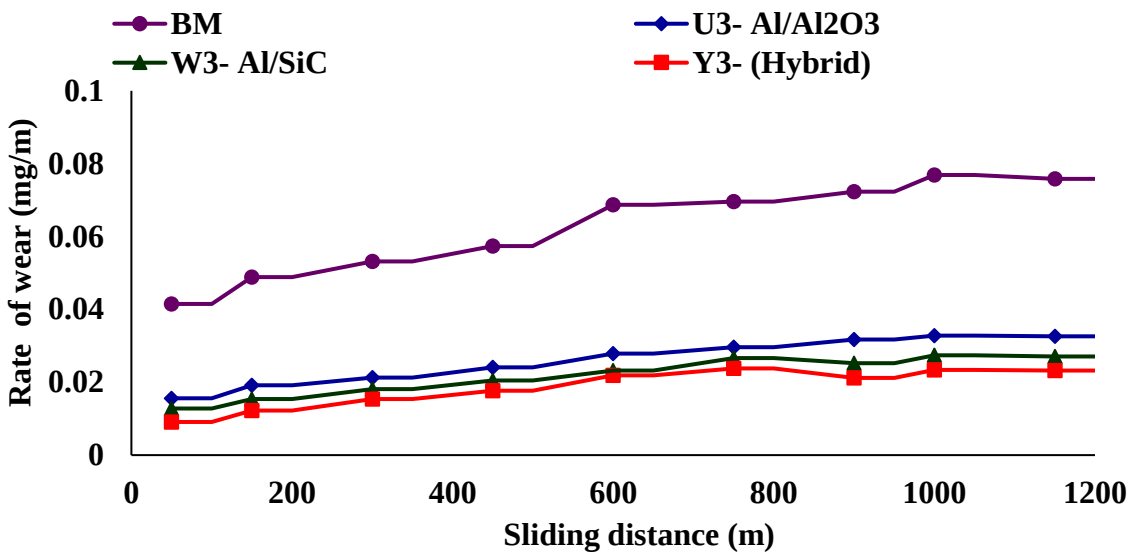

Fig. 4.65 Change in the rate of wear with sliding distance for the composites produced by multi groove technique.

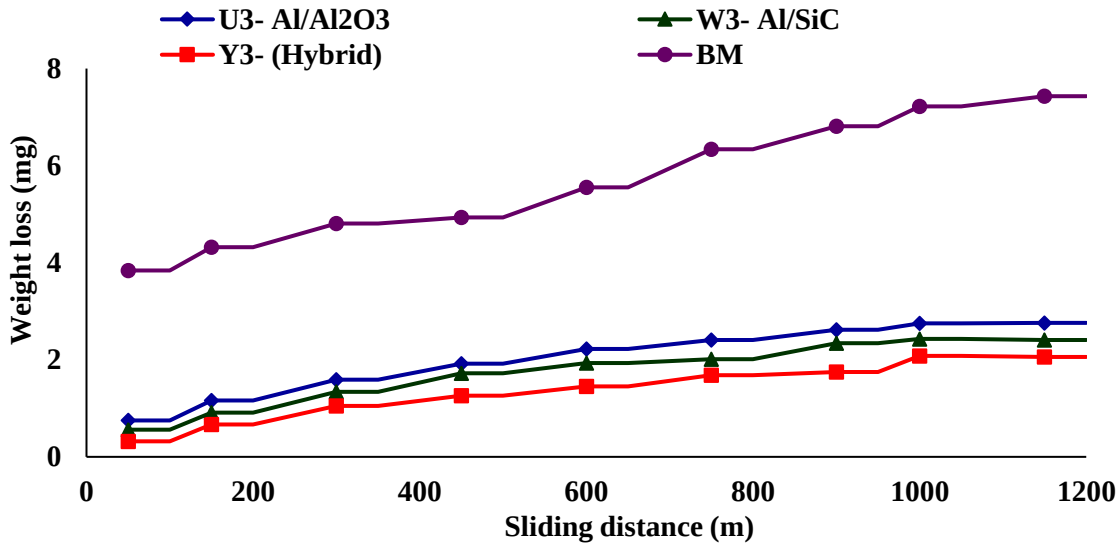

Fig. 4.66 The graphical representation of weight loss versus sliding distance.

Fig. 4.64(c) shows the worn-out surface of hybrid surface nanocomposite. A mixed (abrasive and adhesive) kind of wear is observed and shown in Fig. 4.64(c). The presence of Al_2O_3 and SiC particles are responsible for these kinds of wear properties. Here Al_2O_3 particles exhibit solid lubricating nature and SiC particles shows barrier to material removal from the hybrid surface nanocomposite.

Fig. 4.65 shows the graphical representation of rate of wear versus sliding distance drawn from the values obtained during the test of various samples (fabricated composites and base material). All the surface nanocomposite samples (U3, W3 & Y3) show less rate of wear than compared with the base material (as-received 6061-T6). From this it clearly explains that, the addition of reinforcement particles (Al_2O_3, SiC and hybrid) gives better wear resisting properties than base material. Fig. 4.65 shows the rate of wear is very less in surface composites (avg. 0.025) at varying sliding distance whereas base material wear rate is more than twice of that (avg. 0.065).

Fig. 4.66 shows the graphical representation of weight loss versus sliding distance. The fabricated surface nanocomposites show superior wear resistance properties than base material. The weight loss of the base material is more than compared with reinforced composites. With combination of Al_2O_3 and SiC particles improve the wear resistance and decreases the weight loss during the test and shown in Fig. 4.66. The sample Y3 (hybrid) shows very less wear rate than U3 (Al/Al_2O_3) and W3 (Al/SiC). The combination of Al_2O_3 and SiC reinforcement particles improves the wear resistance properties of composite (Y3) than individual composites (U3 & W3).

4.4 Comparison of mechanical and wear characteristics of surface nanocomposites using different techniques

At a constant volume percentage of nano Al_2O_3 reinforcement (i.e. 4 Vol.%), the fabricated Al/Al_2O_3 surface nano composites by applying various reinforcement techniques (Single groove, Multi hole and Multi groove technique) are compared and explained as follows.

4.4.1 Microstructure

Fig. 4.67 shows the microstructure of the fabricated sample by using various methods like single groove, multi hole and multi groove techniques. All the microstructure shows defect free but the sample fabricated with single groove technique showed defects at the processed region. A good mixing of reinforcement particles was clearly observed in all fabricated composites shown in Fig. 4.67. The samples fabricated with multi hole technique (pin region) shows better mixing of reinforcement particles and matrix material at 4 volume percentage. The sample fabricated with multi hole (pin + shoulder region) and multi groove (pin + shoulder region) exhibited good dispersion of reinforcement particle in stir region as well as in shoulder driven region.

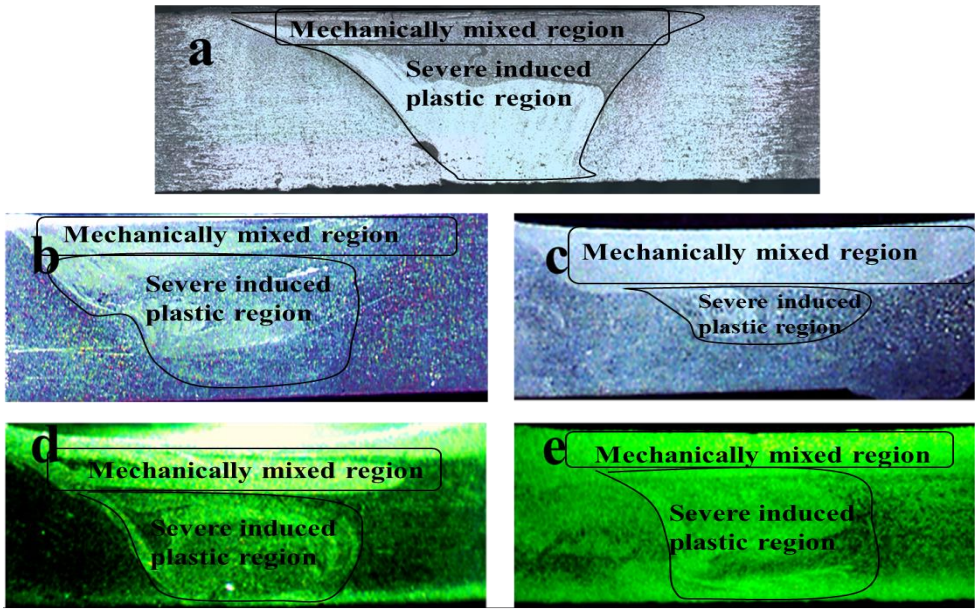

Fig.4.67 Microstructural comparison of various methods used to fabricate surface nanocomposite by FSP.

4.4.2 Microhardness

Microhardness survey of fabricated composites with various reinforcement techniques (single groove, multi hole and multi groove technique) were shown in Table 4.14 and the graphical representation was shown in Fig. 4.68. With the change in reinforcement particles and the reinforcement method the microhardness values varied with respect to the combination of matrix material and reinforcement particles.

Table 4.14 Comparison of microhardness properties.

4 Volume percentage of reinforcement	Single groove	Multi hole		Multi groove	
		Pin region	Pin + Shoulder	Pin region	Pin + Shoulder
Al/Al_2O_3	139.1	140.7	136.9	136.9	136.2
Al/SiC	144.8	143.6	140.5	146.5	142.7
Al/Al_2O_3+SiC	142.4	141.3	138.1	142.8	137.3

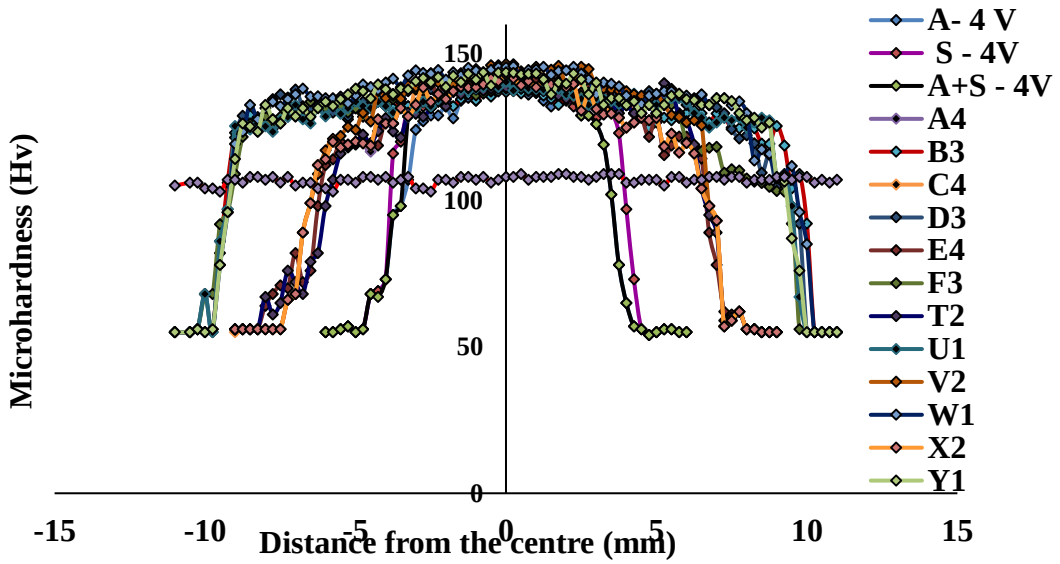

Fig. 4.68 Comparison of microhardness values of all composite fabricated at 4 vol.%.

Superior microhardness values were achieved in the all composites fabricated with SiC reinforcement. As the reinforcement method changes, the microhardness values were also changed slightly but shown higher values than Al/Al_2O_3 and Al/Al_2O_3+SiC surface nanocomposites. From the Fig. 4.68 it is clearly shown that, the microhardness values obtained from the composite fabricated with multi hole and multi groove and single groove techniques were shown superior values than as-received aluminum alloy microhardness (i.e. 108 Hv) values. Compared with all reinforcement methods and composition Al/SiC surface nanocomposite fabricated with multi groove technique (pin region) shown higher microhardness (i.e. 146.5 Hv) values than all other composites and methods.

4.4.3 Tensile properties and Fractography

Table 4.15 shows, the ultimate tensile strength (UTS) values of fabricated surface nanocomposites with various techniques by FSP. The graphical representation of obtained ultimate tensile strength values were shown in Fig. 4.69.

Table 4.15 Comparison of ultimate tensile strength (UTS in MPa) values of fabricated surface nanocomposites by FSP.

4 Volume percentage of reinforcement	**Single groove**	**Multi hole**		**Multi groove**	
		Pin region	**Pin + Shoulder**	**Pin region**	**Pin + Shoulder**
Al/Al_2O_3	188	186.3	172.1	191.1	168.5
Al/SiC	157.3	192.8	184.1	194.2	192.3
Al/Al_2O_3+SiC	182.1	198.3	186.4	194.5	193.2

The fabricated surface nanocomposites exhibit lower tensile properties than as-received aluminum alloy and it is clearly shown in the Fig. 4.69. The addition of reinforcement particles improved the microhardness and microstructural properties but simultaneously decreases the tensile properties. Compared to all the fabricated composites of Al/Al_2O_3, Al/SiC and Al/Al_2O_3 +SiC the higher ultimate tensile strength was obtained at 194.5 MPa for Al/Al_2O_3 +SiC composite.

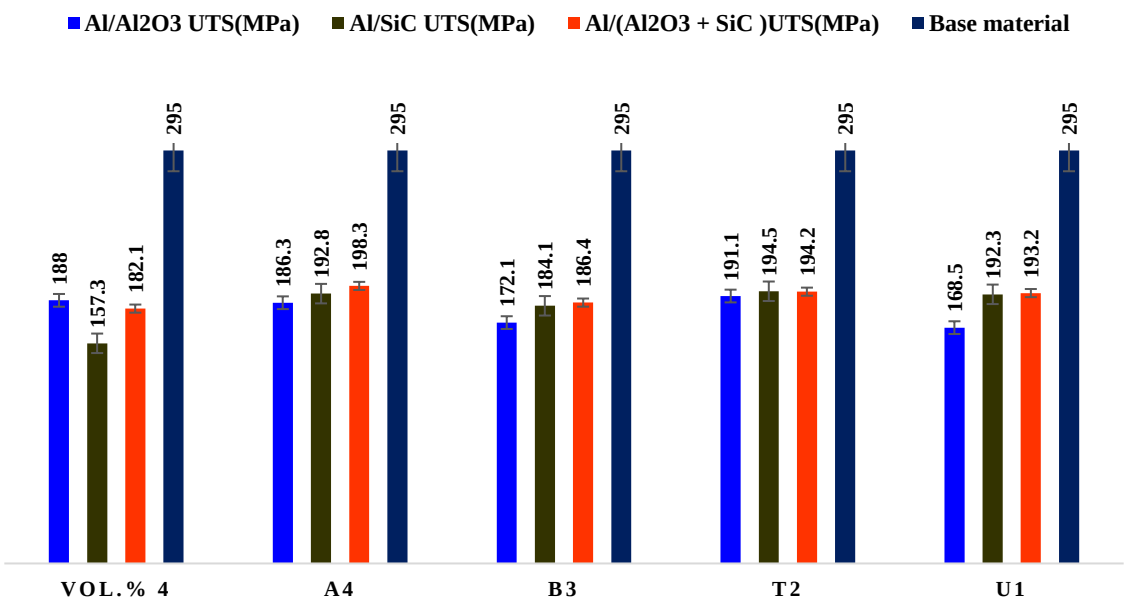

Fig. 4.69 Comparison of ultimate tensile strength (UTS) values of all the fabricated surface nanocomposites by FSP.

From the Table 4.15 and Fig. 4.69 it was observed that good tensile properties were achieved with the multi groove technique (pin region) than compared with multi hole and single groove technique at 4 volume percentage of reinforcement.

4.4.4 Wear

The main purpose of the addition of reinforcement particles into the matrix material is to improve the wear resistance properties of soft matrix material. Here Al_2O_3 and SiC nano particles were used to fabricate the Al/Al_2O_3, Al/SiC and Al/Al_2O_3+SiC surface nanocomposites.

Table. 4.16 Comparison of wear rate (mg/m) properties of fabricated surface nanocomposites.

4 Volume percentage of reinforcement	**Single groove** (mg/m)	**Multi hole** (mg/m)	**Multi groove** (mg/m)
Al/Al_2O_3	0.461	0.423	0.421
Al/SiC	0.314	0.342	0.323
Al/Al_2O_3+SiC	0.302	0.298	0.286

4 vol.%	Single groove	Multi hole technique	Multi groove technique
Al/Al_2O_3	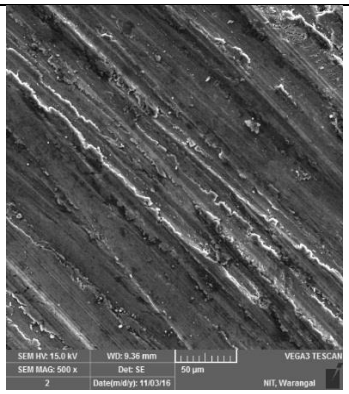	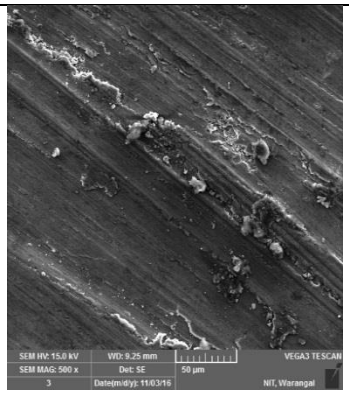	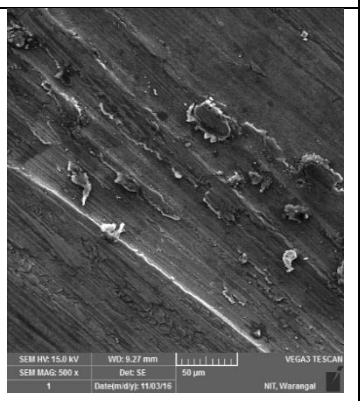
Al/SiC	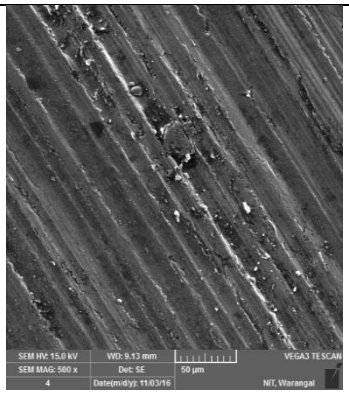	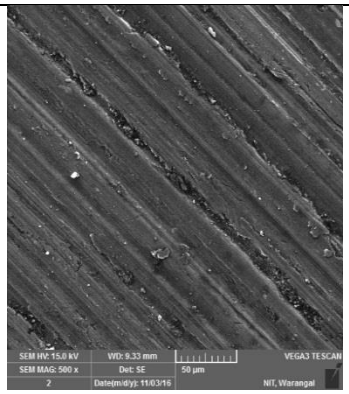	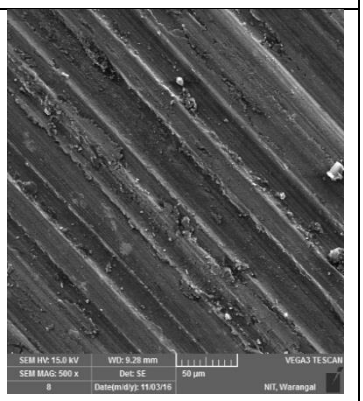
Al/Al_2O_3+SiC	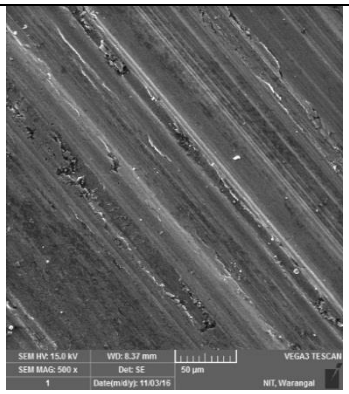	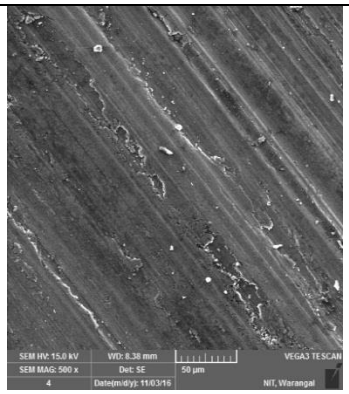	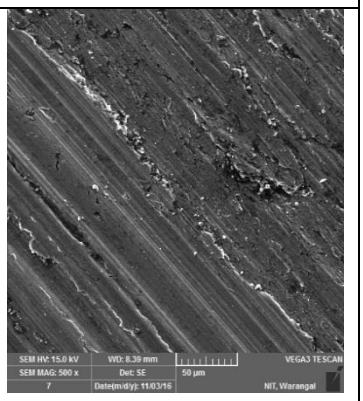

Fig. 4.70 Comparison of worn-out surfaces of fabricated surface nanocomposites with various methods by FSP.

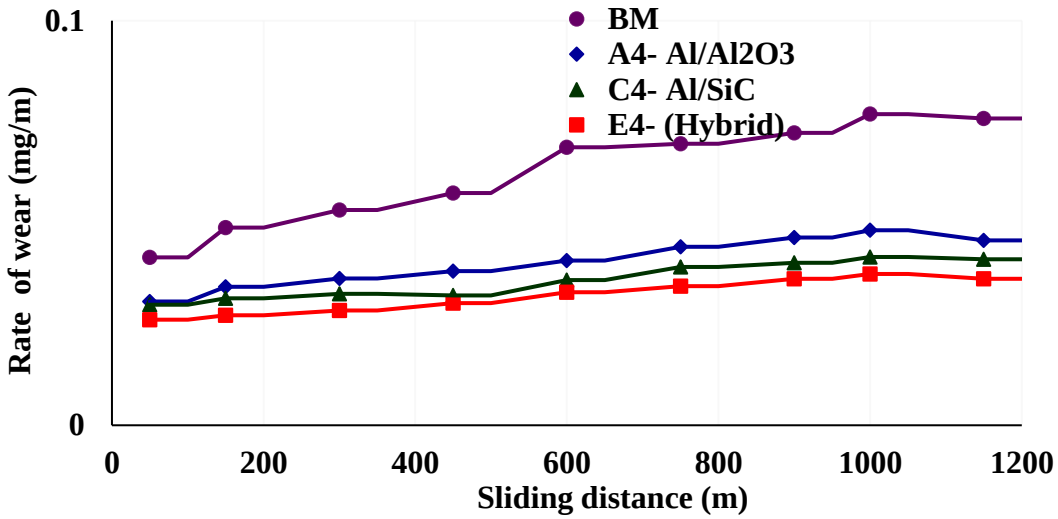

Fig. 4.71 Comparison of wear rate versus sliding distance of fabricated surface nanocomposites with various methods by FSP.

From the Fig. 4.70 shows that, the worn-out surfaces of composites fabricated with various methods by FSP and Table 4.16 represents the wear rate of samples under constant sliding distance. From the Table 4.16 it is clearly observed that the hybrid (Al/Al_2O_3 + SiC) composites shows better wear resistance properties than compared with all other composites (Al/Al_2O_3 and Al/SiC). Compared with all the fabricated methods (single groove, multi hole and multi groove) better wear resistance values were obtained from the samples fabricated with multi groove technique as per shown in Table 4.16 and it is proven from the Fig. 4.70. The composites fabricated with multi hole and multi groove techniques were shown good wear resistance properties than single groove technique. Less amount of material is removed from the surface of the composites fabricated with multi groove technique and in that hybrid (Al/Al_2O_3+SiC) composite shows best wear resistance properties than individual added reinforcements like Al/Al_2O_3 and Al/SiC and the same results were shown in Fig. 4.71.

The addition of reinforcement particles improved the wear resistance properties of fabricated surface nanocomposites (Al/Al_2O_3, Al/SiC & Al/Al_2O_3 + SiC) from an average of 0.062 mg/m (base material) to 0.025 mg/m (Al/Al_2O_3 + SiC) more than the base material shown in Fig. 4.71.

Chapter 5

CONCLUSIONS AND FUTURE SCOPE

In the current work a detailed study on fabrication and characterization of surface nano composites by adding Al_2O_3 and SiC nano reinforcement particles on the surface of AA 6061-T6 alloy through Friction stir processing is presented. The following conclusions were drawn from the results obtained.

5.1 Effect of tool rotational speed, traverse speed and tool shoulder geometry on Al/Al_2O_3 surface nanocomposite by FSP

- A defect –free surface nano composite of Al/Al_2O_3 was fabricated by applying single pass FSP.
- A defect-free surface composite was produced with concave shoulder taper threaded cylindrical tool having 24 mm shoulder diameter.
- Improved microhardness value of ~132 Hv was obtained at 1150 rpm with 15 mm/min.
- Due to sever plastic deformation and dynamic recrystallization, FSP generates a fine equiaxed grain microstructure in stir zone. Addition of Al_2O_3 particles intensifies grain refinement.
- Coefficient of friction is decreased with the addition of Al_2O_3 particles into the matrix than as received Al alloy.

5.2 Influence of Al_2O_3 and SiC nano reinforcement and its volume percentage on fabrication of surface nanocomposites

- Al/Al_2O_3 surface nano composites were successfully fabricated with 2, 4 volume percentage of Al_2O_3 and Al/SiC at 2 volume percentage of SiC reinforcement.

- Higher microhardness values were achieved with 2, 4 and 6 volume percentage of the surface nano composites than as received base material. Superior microhardness of 156 Hv was achieved at 6 volume percentage of Al/SiC surface nano composite.
- Lower tensile properties were achieved with all the fabricated surface nano composites than that of the base material.
- The rate of wear decreases with the increase of volume percentage of nano reinforcements

5.3 Influence of multi hole and multi groove techniques on the fabrication of surface nano composites

- The reinforcement particles (SiC, Al_2O_3 or their mixture) were distributed almost homogenously over the nugget zone by FSP without any defects except agglomeration of reinforcement particles.
- The average hardness of the resulted composites increased to about 160 Hv in Al/ SiC composites.
- Improved tensile properties were observed with the increase of microhardness of the nano surface composite.
- Wear characteristics of the composites were varied depending on the relative ratio of SiC and Al_2O_3.
- The hybrid surface composites exhibited superior wear resistance to other relative ratios of the Al_2O_3 and SiC particles.
- By using multi groove technique, the volume percentage of reinforcement can be increased from 4 to 7 without any defects.
- By using multi hole technique, the volume percentage of reinforcement can be increased from 4 to 5.5 without any defects.

5.4 FUTURE SCOPE OF WORK

Although the present study has helped in developing adequate understanding of the influence of process parameters, reinforcements and novel techniques (multi hole and multi groove) on wear and mechanical properties of Aluminum surface composites; a few areas emerged during the course of the present study, which needs further investigations as suggested below:

1. In this investigation, studies pertaining to influence of reinforcement particles and process parameters on other mechanical properties like fatigue crack growth rate and fracture toughness in the Aluminum surface composites are not carried out.

2. The effect of the multi pass on surface composites are not carried out.

3. The corrosion properties of Al surface composites are not studied. Extended studies in this direction would help in correlating the observed properties with microstructure and fracture behavior quantitatively.

4. The effect of the cryogenic treatment on microstructure, mechanical and wear properties of the surface composites are not studied.

5. Quantitative Metallography as well as transmission electron microscopy (TEM) studies were not studied. These studies were essential to analyze the microstructure of SZ and to identify the various phases in the SZ of surface composites.

BIBLOGRAPHY

A.B. Gurcan, T.N. Baker. Wear behaviour of AA6061 aluminium alloy and its composites. Wear 18(1995) 185–191.

A. K. Lakshminarayanan, V. Balasubramanian. Process parameters optimization for friction stir welding of RDE-40 aluminium alloy using Taguchi technique. Transaction of Nonferrous Met. Society China 18(2008) 548-554.

Bastier A, Maitournam MH, Dang Van K, Roger F. Steady state thermomechanical modelling of friction stir welding. Science and Technology of Welding and Joining, 11(2006) 278-88.

C.G. Rhodes, M.W. Mahoney, W.H. Bingel, M. Calabrese. Fine-grain evolution in friction-stir processed 7050 aluminum. Scripta Materialia, 48(2003) 1451–1455.

Charit. I., R.S. Mishra. High strain rate superplasticity in a commercial 2024 Al alloy via friction stir processing. Materials and Engineering A, 359(2003) 290-296.

Charit. I., Mishra, R.S. Low temperature superplasticity in a friction-stir processed ultrafine grained Al–Zn–Mg–Sc alloy', Acta Materialia, 53(2005) 4211-4223.

C.H. Chuang, J.C. Huang, P.J. Hsieh. Using friction stir processing to fabricate MgAlZn intermetallic alloys. Scripta Materialia, 53(2005) 1455–1460.

Choi DH, Ahn BW, Lee CY, Yeon YM, Song K, Jung SB. Effect of pin shapes on joint characteristics of friction stir spot welded AA5J32 Sheet. Materials Transactions, 51(2010) 1028–1032.

Colegrove PA, Shercliff HR. Experimental and numerical analysis of aluminium alloy 7075 T7351 friction stir welds. Science and Technology of Welding and Joining, 8(2003) 360-368.

Dawood H.I, Mohammed K.S, Rahmat A, Uday M.B. Effect of small tool pin pro-files on microstructures and mechanical properties of 6061 aluminum alloy by friction stir welding. Trans Nonferrous Met Soc China 25(2015) 2856–2865.

Dietre GE. Mechanical Metallurgy: McGraw-Hill; 1988

Douglas C. Hofmann, Kenneth S. Vecchio. Submerged friction stir processing (SFSP): An improved method for creating ultra-fine-grained bulk materials. Materials Science and Engineering A, 402(2005) 234–241.

Duma. J.A. Heat Tratment for Optimizing Mechanical and Corrosion Resisting Properties of Nickel-Aluminium Bronzes, Naval Engineers Journal, 87(1975) 45-64.

E.R.I. Mahmoud, M. Takahashi, T. Shibayanagib, K. Ikeuchi, Wear characteristics of surface-hybrid-MMCs layer fabricated on aluminum plate by friction stir processing, Wear, 268 (2010)1111–1121.

Esmaeili S, Lloyd DJ, Poole WJ. A yield strength model for the Al-Mg-SiCu alloy AA6111. Acta Materialia, 51(2003) 2243-57.

Ferrara, R.J., Caton, T.E. Review of de-alloying of cast aluminium bronze and nickel aluminium bronze alloys, Material Performance, 21(1982) 30-34.

Feng, A.H., Ma, Z.Y. Enhanced mechanical properties of Mg-Al-Zn cast alloy via friction stir processing. Scripta Materialia (2007) 397-400.

Fratini L, Buffa G, Palmeri D, Hua J, Shivpuri R. Material flow in FSW of AA7075-T6 butt joints: Numerical simulations and experimental verifications. Science and Technology of Welding and Joining, 11(2006) 412-421.

Gerlich A. Local Melting and Tool Slippage during Friction Stir Spot Welding of Aluminum Alloys. University of Toronto (2007).

Gerlich A, Su P, Yamamoto M, North TH. Material flow and intermixing during dissimilar friction stir welding. Science and Technology of Welding and Joining, 13(2008) 254-264.

Givi MKB, Asadi P. Advances in friction stir welding and processing. Woodhead Publishing (2014).

G. Liu, L.E. Murr, C-S. Niou, J.C. McClure, and F.R. Vega. Microstructural aspects of the friction-stir welding of 6061-T6 aluminum. Scripta Materialia, 37(1997) 355-361.

Historical Development of Welding (2006), available from: http://www.totalmateria.com/page.aspx?ID=CheckArticle&site=kts&NM=186.

Hu, C., Baker, T.N. C. Hu, T.N. Baker. Laser processing to creat in-situ Al-SiCp surface metal matrix composite. Journal of Materials Science, 30(1995) 891-897

Hu, C., Xin, H., Baker, T.N. Laser processing of an aluminium AA6061 alloy involving injection of SiC particulate. Journal of Materials Science, 30(1995) 5985-5990.

J.A. Schneider, A.C. Nunes Jr., Metall. Mater. Trans. B 35 (2004) 777.

Jian-Qing Su, Tracy W. Nelson, Colin J. Sterling. Friction stir processing of large-area bulk UFG aluminum alloys. Scripta Materialia, 52(2005) 135–140.

Johannes, L.B., Charit, I., Mishra, R.S., Verma, R. Enhanced superplasticity through friction stir processing in continuous cast AA5083 aluminium - I, Materials Science and Engineering A, 464(2007) 351-357.

Johannes, L.B., Mishra, R.S., Multiple passes of friction stir processing for the creation of plastic 7050 aluminium – II. Materials Science and Engineering A, 463(2007) 255-260.

J.U. Ejiofor and R.G. Reddy; "Developments in the Processing and Properties of particulate Al-Si Composites", The Journal of The Minerals, Metals & Materials Society. 11(1997) 31-37.

Jung-Moo Leea, Suk-Bong Kanga, Jianmin Han. Dry sliding wear of MAO-coated A356/20 vol.% SiCp composites in the temperature range 25–180 °C. Wear 264 (2008) 75–85

L.A. DobrzaĔski, M. Kremzer and M. Drak' Modern composite materials manufactured by pressure infiltration method, Journal of Achievements in Materials and Manufacturing Engineering, 30(2008) 121-128.

Liechty BC, Webb BW. The use of plasticine as an analog to explore material flow in friction stir welding. Journal of Materials Processing Technology 184(2007) 240-250.

Liu, F.C., Ma, Z.Y. Low-temperature superplasticity of friction stir processed Al–Zn–Mg–Cu alloy, Scripta Materialia, 58(2008) 667-670.

Lloyd DJ. Particle reinforced aluminum and magnesium matrix composites. Int. Mater Rev. 39(1994) 1–24.

Lorrain O, Favier V, Zahrouni H, Lawrjaniec D. Understanding the material flow path of friction stir welding process using unthreaded tools. Journal of Materials Processing Technology 210(2010) 603–609.

Kainer KU. Metal Matrix Composites. Wiley-VCH (2006).

K. Colligan, Material flow behavior during friction stir welding of aluminum. Welding Journal 65(1999) 229–233.

K. Kumar, Satish V. Kailas. The role of friction stir welding tool on material flow and weld formation, Materials Science and Engineering A, 485(2008) 367–374.

K. Nakata, Y.G. Kim, H. Fujii, T. Tsumura, T. Komazaki. Improvement of mechanical properties of aluminum die casting alloy by multi-pass friction stir processing. Materials Science and Engineering A, 437(2006) 274–280.

Krishnan KN. On the formation of onion rings in friction stir welds. Materials Science and Engineering A, 327(2002) 246-51.

K.V. Jata and S.L. Semiatin. Continuous dynamic recrystallization during Friction stir welding of high strength Aluminum alloys. Scripta materialia. 439(2000) 743–749.

Mahmoud ERI, Takahashib M, Shibayanagib T, Ikeuchi K. Wear characteristics of surface-hybrid-MMCs layer fabricated on aluminum plate by friction stir processing. Wear, 268(2010) 1111–1121.

Mahoney MW, Rhodes CG, Flintoff JG, Spurling RA, Bingel WH. Properties of friction-stir-welded 7075 T651 aluminum. Metallurgical and Materials Transactions A: Physical Metallurgy and Materials Science, 29(1998)1955-1964.

Mazahery A., Abdizadeh H., Baharvandi H.R. Development of high-performance A356/ nano-Al_2O_3 composites, Materials Science and Engineering A, 518(2009) 61–64

Mazen A.A. and Ahmed A.Y. Mechanical Behaviour of Al-Al_2O_3 MMC Manufactured by PM Techniques Part I'—Scheme I Processing Parameters, Journal of Materials Engineering and Performance, 7(1998) 393-401.

Ma, Z.Y., Mishra, R.S., Mahoney, M.W. Superplastic deformation behaviour of friction stir processed 7075Al alloy, Acta Materialia, 50(2002) 4419-4430.

Ma. Z. Y., R.S. Mishra. Cavitation in superplastic 7075Al alloys prepared via friction stir processing. Acta Materialia, 51(2003) 3551–3569.

Ma, Z.Y., Mishra, R.S., Mahoney, M.W., Grimes, R. High strain rate superplasticity in friction stir processed Al-Mg-Zr alloy', Materials Science and Engineering A, 351(2003) 148-153.

Ma. Z. Y., R.S. Mishra. Development of ultrafine-grained microstructure and low temperature (0.48 Tm) superplasticity in friction stir processed Al–Mg–Zr. Scripta Materialia, 53(2005) 75–80.

Ma, Z.Y., Sharma, S.R., Mishra, R.S. Effect of multiple-pass friction stir processing on microstructure and tensile properties of a cast aluminium-silicon alloy – II. Scripta Materialia 54(2006) 1623-1626.

Ma ZY. Friction stir processing technology: A review. Metallurgical and Materials Transactions A: Physical Metallurgy and Materials Science A, 39(2008) 642-58.

Ma, Z.Y., Pilchak, A.L., Juhas, M.C., Williams, J.C. Microstructural refinement and property enhancement of cast light alloys via friction stir processing, Scripta Materialia, 58(2008) 361-366.

M. Guerra, C. Schmidt, J.C. McClure, L.E. Murr, A.C. Nunes, Mater. Charact. 49 (2003) 95.

M. Gui, S.B. Kang, Aluminum hybrid composite coatings containing SiC and graphite particles by plasma spraying, Mater. Lett. 51 (2001) 396–401.

Mishra R S, Ma Z Y, Charit I. Friction stir processing: a novel technique for fabrication of surface composites. Material Science Engineering A 341(2003) 307–310.

Mishra. R.S and Ma, Z.Y. Friction stir welding and processing, Materials Science and Engineering R, 50(2005) 1 – 78.

Mishra RS and Mahoney MW. Friction stir welding and processing. ASM International (2007).

M.K. Surappa. Aluminium matrix composites: challenges and opportunities. Sadhana, 28 (2003) 319-334.

M.L. Santella, T. Engstrom, D. Storjohann, T.-Y. Pan. Effects of friction stir processing on mechanical properties of the cast aluminum alloys A319 and A356. Scripta Materialia, 53(2005) 201–206.

Mohanty HK, Mahapatra MM, Kumar P, Biswas P, Mandal NR. Effect of tool shoulder and pin probe profiles on friction stirred aluminum welds — a comparative study. Journal of Marine Science and Application, 11(2012) 200–7.

Moreira, P. M. G. P., Jesus, A. M. P. de, Ribeiro, A. S., Castro, P. M. S. T. de. Fatigue Crack Growth in Friction Stir Welds of 6082-T6 and 6061-T6 Aluminium Alloys: A comparison Theoretical and Applied Fracture Mechanics, 50(2008) 81 – 91.

Morisada, Y., Fujii, H., Nagaoka, T., Fukusumi, M. MWCNTs/AZ31 surface composites fabricated by friction stir processing, Materials Science and Engineering A, 419(2006) 344-348.

Morisada Y, Fujii H, Kawahito Y, Nakata K, Tanaka M. Three-dimensional visualization of material flow during friction stir welding by two pairs of X-ray transmission systems. Scripta Materialia, 65(2011) 1085-8.

M. Salehi, M. Saadatmand, J. Aghazadeh Mohandesi, Optimization of process parameters for producing AA6061/SiC nanocomposites by friction stir processing. Trans. Nonferrous Met. Soc. China. 22(2012) 1055-1063.

M. Sharifitabar, A. Sarani, S. Khorshahian, M. Shafiee Afarani. Fabrication of 5052Al/Al_2O_3 nanoceramic particle reinforced composite via friction stir processing route, Materials and Design, 32(2011) 4164–4172.

M. Sharifitabar, A. Sarani, S. Khorshahian, M. Shafiee Afarani, Fabrication of 5052 Al/Al_2O_3 nanoceramic particle reinforced composite via friction stir processing route, Mat. Des. 32 (2011) 4164–4172.

Mukherjee S, Ghosh AK. Flow visualization and estimation of strain and strain-rate during friction stir process. Materials Science and Engineering A, 527(2010) 5130-5135.

Nandan R, Roy GG, Debroy T. Numerical simulation of three-dimensional heat transfer and plastic flow during friction stir welding. Metallurgical and Materials Transactions A: Physical Metallurgy and Materials Science, 37(2006) 1247-1259.

Nandan R, DebRoy T, Bhadeshia HKDH. Recent advances in friction-stir welding - Process, weldment structure and properties. Progress in Materials Science, 53(2008) 980-1023.

Oh-ishi, K., McNelley, T.R. Microstructural Modification of As-Cast NiAl Bronze by Friction Stir Processing', Metallurgical and Materials transactions A, 35(2004) 2951-2961.

Oh-ishi, K., McNelley, T.R. The Influence of Friction Stir Processing Parameters on Microstructure of As-Cast NiAl Bronze, Metallurgical and Materials transactions A, 36(2005) 1575-1585.

Ouyang JH, Kovacevic R. Material flow and microstructure in the friction stir butt welds of the same and dissimilar aluminum alloys. J of Materi Eng and Perform, 11(2002) 51-63.

Park, H.S., Kimura, T., Murakami, T., Nagano, Y., Nakata, K., Ushio, M. Microstructures and mechanical properties of friction stir welds of 60% Cu-40% copper alloy, Materials Science and Engineering A, 371(2004) 160-169.

Park, S.H.C., Sato, Y.S., Kokawa, H. Effect of micro-texture on fracture location in friction stir weld of Mg alloy AZ61 during tensile test, Scripta Materialia, 49(2003) 161-166.

Park, S.H.C., Sato, Y.S., Kokawa, H., Okamoto, K., Hirano, S., Inagaki, M. Rapid formation of the sigma phase in 304 stainless steel during friction stir weldin. Scripta Materialia, 49(2003) 1175-1180.

Patrick B. Berbon, William H. Bingel, Rajiv S. Mishra, Clifford C. Bampton and Murray W. Mahoney. Friction stir processing: a tool to homogenize Nanocomposite aluminum alloys. Scripta materiala. 44(2001) 61–66.

P. Cavalierea, A. Squillace. High temperature deformation of friction stir processed 7075 aluminium alloy. Materials Characterization, 55(2005) 136– 142.

P. Heurtier, M.J. Jones, C. Desrayaud, J.H. Driver, F. Montheillet, D.J. Allehaux, Mater. Process. Technol. 171(2006) 348

P J. Haagensen, O.T. Midling, M Rane. Fatigue performance of friction stir butt welds in a 6000-series aluminum alloy. Transactions on Engineering Sciences, 8(1995) 225-237.

Przydatek J. A ship classification view on friction stir welding. In: Proceedings of the 1st international friction stir welding symposium, Oaks (CA, USA), 14–16 June, 1999.

P.S. Pao, S.J. Gill, C.R. Feng and K. K. Sankaran. Corrosion-fatigue crack growth in friction stir welded Al 7050. Scripta Materialia 45(2001) 605-612.

Rai R, De A, Bhadeshia Hkdh, DebRoy T. Review: friction stir welding tools. Science and Technology of Welding and Joining, 16(2011) 325–42.

R.A. Prado, L.E. Murr, D. J Sindo, and K.F.Soto. Tool wear in friction stir welding of aluminum alloy 6061 + 20% Al_2O_3: A preliminary study. Scripta Materialia, 45 (2001) 75-80.

R.A. Saravanan, J. Lee, S. Kang, Dry sliding wear behavior of A356-15 Pet SiCp composites under controlled atmospheric conditions. Metall. Mater. Trans A, 30(1999) 2523–2538.

Reynolds, A.P., Hood, E., Tang, W. Texture in friction stir welds of Timetal 21S. Scripta Materialia, 52(2005) 491-494.

R. Palanivel, P. Koshy Mathews, N. Murugan , I. Dinaharan, Effect of tool rotational speed and pin profile on microstructure and tensile strength of dissimilar friction stir welded AA5083-H111 and AA6351-T6 aluminum alloys, Materials and Design, 40 (2012) 7–16.

Ruifeng, L., Zhuguo, L., Yanyan, Z. and Lei, R. A comparative study of laser beam welding and laser-MIG hybrid welding of To-Al-Zr titanium alloy, Materials Science and Engineering A, 528(2011) 1138 – 42.

S.A. Alidokht, A.A. Zadeh, S. Soleymani, H. Assadi, Microstructure and tribological performance of an aluminium alloy based hybrid composite produced by friction stir processing, Materials Design 32 (2011) 2727–2733.

S.A. Sajjadi , H.R. Ezatpour, M. Torabi Parizi' Comparison of microstructure and mechanical properties of A356 aluminum alloy/Al_2O_3 composites fabricated by stir and compo-casting processes, Materials and Design, 34(2012) 106–111.

Sato, Y.S., Sasaki, A., Sugimoto, A., Honda, A., Kokawa, H. Enhancement of265 Formability in Magnesium Alloy AZ31B via Friction Stir Processing, Materials Science Forum, 539-543(2007) 3775-3789.

Schneider JA, Nunes Jr AC. Characterization of plastic flow and resulting microtextures in a friction stir weld. Metallurgical and Materials Transactions B: Process Metallurgy and Materials Processing Science, 35(2004) 777-83.

S.C. Tjong, K.C. Lau, S.Q. Wu, Wear of Al-based hybrid composites containing BN and SiC particulates, Metall. Mater. Trans. A 30(1999) 2551–2555.

Seidel TU, Reynolds AP. Visualization of the material flow in AA2195 friction-stir welds using a marker insert technique. Metallurgical and Materials Transactions A: Physical Metallurgy and Materials Science, 32(2001) 2879-2884.

Shafiei-Zarghani, A., Kashani-Bozorg, S.F., Zarei-Hanzaki, A. Microstructures and mechanical properties of Al/Al2O3 surface nano-composite layer produced by friction stir processing' Materials Science and Engineering A, 500(2009) 84-89.

Shamsipur Ali, Kashani-Bozorg Seyed Farshid, Zarei-Hanzaki Abbas. Surf Coat Technol. 206(2011) 1372–1378.

Sinclair I, Gregson PJ. Structural performance of discontinuous metal matrix composites. Materials Science and Technology, 13(1997) 709-26.

S. Soleymani, A.A. Zadeh, S.A. Alidokht, Microstructural and Tribological Properties of Al5083 based Surface Hybrid Composite Produced by Friction Stir Processing, Wear 278–279 (2012) 41–47.

SU P, Gerlich AP, North TH, Bendzsak GJ. Intermixing in Dissimilar Friction Stir Spot Welds. Metallurgical and Materials Transactions A, 38(2007) 584 - 595.

Sutton MA, Yang B, Reynolds AP, Taylor R. Microstructural studies of friction stir welds in 2024-T3 aluminum. Materials Science and Engineering A, 323(2002) 160-166.

Tachai Luangvaranunt, Lerlert Tamrongpoowadon and Katsuyoshi Kondoh' Fabrication of Al/Al_2O_3 composite by powder forging of aluminium powders and manganise oxide powders, 16^{th} International Conference on Composite Materials. Kyoto Japan. May 16, 2007.

Threadgilll PL, Leonard AJ, Shercliff HR, Withers PJ. Friction stir welding of aluminium alloys. International Materials Reviews, 54(2009) 49-93.

Thomas, W. M., Nicholas, E. D., Needham, J. C., Church, M. G., Templesmith, P., Dawes, C. J.., Friction Stir Butt Welding, International Patent Application PCT/GB92/02203 and G.B. Patent Application 9125978.8, Dec 1991.

Thomas WM. Friction stir welding. UK Patent Application 2(1996) 306 – 366.

T.U. Seidel, A.P. Reynolds. Visualization of the material flow in AA2195 friction-stir welds using a marker insert technique. Metallurgical and Materials Transactions A, 32(2001) 2879–2887.

Valiev, R.Z., Islamgaliev, R.K., Alexandrov, I.V. Bulk nanostructured materials from severe plastic deformation, Progress in Materials Science, 45(2000) 103-189.

W. M. Thomas U, E. D. Nicholas. Friction stir welding for the transportation industries, Materials & Design, 18(1997) 269-273.

Xiaopeng Hou, Xinqi Yang, Lei Cui, Guang Zhou. Influences of joint geometry on defects and mechanical properties of friction stir welded AA6061-T4 T-joints, Materials and Design 53 (2014) 106–117.

Xu S, Deng X, Reynolds AP, Seidel TU. Finite element simulation of material flow in friction stir welding. Science and Technology of Welding and Joining, 6(2001)191-193.

Yang Q, Mironov S, Sato YS, Okamoto K. Material flow during friction stir spot welding. Materials Science and Engineering A, 527(2010) 4389-4398.

Yin YH, Sun N, North TH, Hu SS. Microstructures and mechanical properties in dissimilar AZ91/AZ31 spot welds. Materials Characterization, 61(2010) 1018-28.

Y.J. Kwon, I. Shigematsu, N. Saito. Mechanical properties of fine-grained aluminum alloy produced by friction stir process. Scripta Materialia, 49 (2003) 785–789.

Yi, L., Jinhe, L. and Hong, Y. Bubble flow and the formation of cavity defect in weld pool of vacuum electron beam welding, Vacuum, 86(2011) 11 – 17.

Y. Morisada, H. Fujii, T. Nagaoka, M. Fukusumi.Effect of friction stir processing with SiC particles on microstructure and hardness of AZ31. Materials Science and Engineering A, 433(2006) 50–54.

Yutaka S. Soto, Mitsunori Urata, Hiroyuki Kokawa, Keisuke Ikeda and Masatoshi Enomoto. Retention of fine grained microstructure of equal channel angular pressed aluminum alloy 1050 by friction stir welding. Scripta Materialia, 45(2001) 109-114.

Zhang, D., Suzuki, M., Maruyama, K. Microstructure evolution of a heatresistant magnesium alloy due to friction stir welding, Scripta Materialia, 52(2005) 899-903.

Zhao, Y.H., Liao, X.Z., Jin, Z., Valiev, R.Z., Zhu, Y.T. Microstructures and mechanical properties of ultrafine grained 7075 Al alloy processed by ECAP and their evolutions during annealing, Acta Materialia, 52(2004) 4589-4599.